Universiteit Utrecht
Faculty of Geosciences
Royal Netherlands Institute for Sea Research

Eastern Scheldt foreshore stability: towards hybrid flood protection strategies in the future

-An indicative field study of the Eastern Scheldt, SW-Netherlands-

Fleur Elena van Gool

Utrecht - April 2019

Eastern Scheldt foreshore stability: towards hybrid flood protection strategies in the future

-An indicative field study of the Eastern Scheldt, SW-Netherlands-

---

GEO4-1520

Author:

Fleur Elena van Gool

Student number:

4030656

Contact details:

f.e.vangool@students.uu.nl

+31646003859

Supervision

Asociate Prof Dr. Esther Stouthamer – UU
Prof. Dr. Tjeerd Bouma – NIOZ & UU

Bas Knaake – Msc, PhD student UU

Framework:

MSc thesis for the Master Program of "Marine Sciences" at Utrecht University

Credits:

37.5 ECTS

Version:

2

Date:

April 9th, 2019

Preface

This study was performed as a graduation research accounting as final piece of the Master Program 'Marine Sciences' at Utrecht University. The topic of this research has established as a result of the common interest into foreshores and its stability by both the faculty of Geography, Utrecht University and the Royal Netherlands Institute of Sea Research (NIOZ). Together with my supervisors Esther Stouthamer (UU) and Tjeerd Bouma (NIOZ) this interest was transformed in a research plan consisting of field, lab and modelling work.

Due to the elaborate character of this self- made project, quite some time was needed to execute and finalize all steps. During this process some delays and personal motivation set- backs were experienced. However within this year long project, I have learned incredibly much, for which I am really grateful. Firstly, I improved my scientific thinking and skills by working in different aspects of the scientific field. Furthermore I learned how set up a research project independently and how to plan and organize with different scientific parties involved. Therefore I would like to thank both NIOZ and Utrecht University for giving me the opportunity to work on this project.

I would like to thank both of my supervisors Esther Stouthamer (UU) and Tjeerd Bouma (NIOZ) for thinking outside of the box with me and motivating me in times I could not foresee the next step. Also, I would like to thank Bas Knaake for the additional support and directions on the more regular basis. During the field campaign in Zeeland a whole team was assembled in assisting me during cold winter days collecting shallow and deep cores within the Eastern Scheldt. Thereto, I would firstly like to express my gratitude to Lennart van Ijzerloo who has helped me so patiently during all my days spend at NIOZ, Yerseke and all the other staff members making me feel welcome. Furthermore, I would like to thank my field team members; Bas Knaake, Sergej Seepma, Marieke Laengner, Corinne Böhm and Mark Eijkelboom. Furthermore, I would like to thank Rudi Heijmen and Hans Venema (Rijkswaterstaat, Helpdesk water) for making the model D-Flow Slide 18.1.1 available. Also, I would like to thank Geeralt van den Ham (Deltares) for helping me interpret the results of D-Flow Slide.

During the last phase of processing my data and writing up my results, I had great help from my friend Berkcan Gökce in modelling whom I would like to thank for all his help. Additionally, I had an elaborate support team of friends and family motivating me in finishing the job. Special thanks to my great parents for thinking along in the process, and my mother Janneke Ottens and Corinne for reviewing my report. Also thank you, Julia, Mathijs, Eva, Leah, Janna, Tamara, Rosan, Joëlle, Emmi, Marjolein, Marije and Marieke for all the support along the way.

Executive summary

Since the 1970's the perspective on ideal coastal management has changed in the Netherlands. A shift occurred to more eco-system based management with a focus on the implementation of the so called soft measures. Tidal mudflat and salt marshes are known for their functioning towards enhanced flood protection. In this study research has been conducted on the role of the foreshore in the Scheldt estuary. The foreshore includes mudflats and salt marshes between dike and waterfront. Stability of these systems has mostly been studied for shallow subsurface processes and to a lesser extent for deep subsurface stability. In this master thesis the stability of foreshores in de Eastern Scheldt has been studied coupling both shallow and deep subsurface stability.

Subsurface characteristics were studied for 3 locations with different energetic conditions. Characteristics such as lithology, disturbance layers and bulk density were used to assess the stability on 2 different scales; shallow subsurface (0-30 cm) and deeper subsurface (0-max. channel depth~15 m). Additionally, it was tested, whether foreshore stability could relate to an important failure mechanism of water defences shown within the Eastern Scheldt; the occurrence of so-called "flow slides".

The stability in both the lateral and vertical stretch of tidal salt marshes and mudflats of all 3 locations in terms of erosion resistance was not to be related directly. The same holds for the probability of flow slides. Erosion resistance was influenced mainly by soil strengthening factors in the top-layer such as sediment density, moisture content and the presence of roots and shells. Based on this study, probability of flow slides is mainly influenced by the degree of consolidation of deeper lain sand layers and the total geometry of the channel to dike foreshore system.

Within the scope of a better understanding of foreshore stability, more research is needed on the relation of soil characteristics with stability and erosion resistance.
Moreover, boundary conditions for foreshores with different deeper subsurface characteristics should be tested on their sensitivity for flow slides.

Table of Contents

1. Introduction

Worldwide flood protection measures have been implemented in coastal regions to prevent flooding events and to guarantee a safe living environment. Since the 10^{th} century, so called hard flood protection measures have been implemented within the Dutch delta (Wesselink et al., 2015). Since their implementation, these measures known as the typical Dutch dikes have to be heightened and strengthened continuously. This is more so since the coastal land level slowly lowered due to a combination of human-induced subsidence and a lack of re-sedimentation from the rivers through construction of dikes (Wesselink et al, 2015). This vicious cycle of implementing more technical solutions with time to keep the water out, while the polders are continuously subsiding, is known as a 'technological lock in'. However, the relative advanced coastal protection was not sufficient to overcome the worst-case scenario flooding event in 1953 (Wesselink et al, 2015). This triggered the design of a large delta program in which estuaries were closed off by dams and dikes were strengthened, while harbours remained accessible (Bannink & ten Brinke, 2008).

In the 1970s however, a turning point towards eco-engineering was reached within the objective of Dutch water management (Wesselink et al, 2015). Due to societal pressure and doubts concerning the impacts of large scale engineering onto the environment the last estuary was to be kept open, hereafter referred to as the Eastern Scheldt (Bijker, 2002; Disco, 2002). Consequently, a storm surge barrier was implemented, providing both flood protection when needed and an open system status for the maintenance of existing ecosystem dynamics. Within recent coastal management plans, the focus shifted to more ecosystem based strategies. The typical Dutch hard flood protection measures benefit nowadays being supported by existing ecosystem dynamics, the so called soft measures (De Vriend et al., 2015; Wesselink et al, 2015).

Worldwide tidal mudflats and salt marshes are increasingly recognized for their function as a soft measure reducing flood risk (Keryn et al., 2012). In the estuary of the Scheldt research has been conducted on the role of the foreshore dynamics as response to wave and tidal exposure. The studied area of the foreshore includes mudflats and salt marshes between dike and waterfront. Moreover, alternative stability parameters were assessed to verify their functioning towards flood protection (Bouma et al., 2016; Hu et al., 2017; Li et al., 2017; Stark et al., 2016; Wang et al., 2017). Stark et al. (2016), studied the flood protection potential of the combined nature-based and engineering approach of foreshore and adjacent dikes in the Eastern Scheldt, by modelling the effect of foreshore geometry on wave attenuation.

However, in-situ characteristics of shallow and deeper subsurface of foreshores and their effect on the stability of Dutch dikes towards flood protection were not included in former research. Only the probability of hydraulic failure (overtopping and wave scour), processes which play a role in the surface stability of water defences, were addressed (TAW, 1999; Vrouwenvelder & Steenberger, 2003A).

To enhance the understanding of foreshore functioning favouring enhanced flood protection, foreshore subsurface characteristics are to be studied in relation to foreshore stability. Based on existing literature (Chapter 2, Background) it can be stated, that the stability of foreshores in the Eastern Scheldt is dependent on the composition and processes in both the topsoil layer and the deeper lain subsoil. Different sediment types such as sand, silt, clay and peat, deposited under different environmental conditions exert different strength to the subsoil (section 2.1 & 2.2).

Furthermore, the presence of organic material such as reed, halophyte plant species and inorganic material like shells affect the erodibility and thereby the stability of the topsoil layer (section 2.2). The rapidly shifting coastlines in Zeeland's' geological past have left the deeper subsurface with an alternation of loosely packed sands and silts with clay and peat layers (section 2.1). This makes the subsurface susceptible to instability and possible occurrence of flow slides (section 2.3). However, the causes of foreshore stability, integrated over different scales both lateral and vertical, have not been assessed to a broad extent.

Therefore, in this study both lateral and vertical, subsurface characteristics are investigated in relation to foreshore stability. Therefore, 3 locations in the Eastern Scheldt area with different energetic conditions and susceptibility to the occurrence of flow slides were studied for various sub-environments within the foreshore. These subsurface characteristics were used to interpret the stability for the 3 different foreshores on 2 different scales; the shallow subsurface (0 to 30 cm) and the deeper subsurface (0 to maximum channel depth, approximately 15 m). Additionally, it was tested whether foreshore stability can be related to an important failure mechanism of water defences within the Eastern Scheldt; the occurrence of flow slides. (Stoutjesdijk et al., 1995; TAW, 1999; Vrouwenvelder & Steenbergen, 2003A; Kanning, 2012).

Specific research questions were addressed in this study:

(1) Which parameters determine the stability of the foreshore (salt marsh and mudflat) subsurface in terms of erosion resistance and probability of flow slides?

(2) What are lithological characteristics for tidal salt marshes, mudflats with different morphological and ecological settings for the 3 selected locations regarding the first 30 cm and deeper depth profiles(0-max. channel depth ~15 m)?

(3) How can lithological cross-sections, obtained from shallow and deeper profiles with the existing subsurface data be related to lateral and vertical stability of the 3 foreshore systems?

(4) Are the selected foreshore systems of Krabbendijke, within the Eastern Scheldt prone to the occurrence of flow slides?

The significance of this study lies in its potential of broadening our understanding and recognition of the ecosystem service of the foreshore in the Eastern Scheldt therewith enhancing the safety of our water defences in the nearby future.

2. Background

The three foreshore systems Krabbendijke, Dortsman Zuid and the Krabbenkreek are situated along the Eastern Scheldt estuary in the southwestern part of the Netherlands, province of Zeeland. The Eastern Scheldt is part of an active estuary/ tidal system landscape (Figure 1) and it has a broad geological and cultural history that has led to its present shape. In this study both shallow and deep geology of the 3 foreshores are of interest. In section 2.1 the hydraulic and a geomorphological setting of the Eastern Scheldt region is described as well as its geological history. In section 2.2 a short geographic history and future prospect is given for the foreshore systems of locations Krabbendijke, Dortsman Zuid and Krabbenkreek. In section 2.3 the failure mechanism of flow slides is explained together with a method to determine the probability of occurrence of flow slides.

Figure 1: Distribution of active estuary /tidal system landscape within the Netherlands.
Source: http://www.geologievannederland.nl/landschap/landschappen/zeekleilandschap

2.1 General geology, geomorphological and hydrological setting Eastern Scheldt

2.1.1 Hydrological and geomorphological setting Eastern Scheldt

The Eastern Scheldt is an elongated tidal basin, comprising 50 km in length. The estuary covers a surface area of 350 km^2 since the closure by the back barrier dams built in the sixties, called the Grevelingendam and the Volkerakdam (Fig. 2 (3 & 4); Nienhuis & Smaal, 1994). The current inlet lies within the two former islands Schouwen & North Beveland and consists of 3 main channels divided by shoals (Eelkema et al., 2013). The Eastern Scheldt lies within the reach of a semidiurnal tide entering the southern part of the North Sea both from the north around Scotland and from the southwest through the English Channel. The tidal wave propagates from the southwest to the northeast as a progressive wave with a mean tidal range of 2.9 meter at the inlet of the Eastern Scheldt. With spring tide this tidal range increases to approximately 3.5 meters and decreases to 2.3 meters at neap tide (Eelkema et al., 2013; Eelkema et al., 2012).

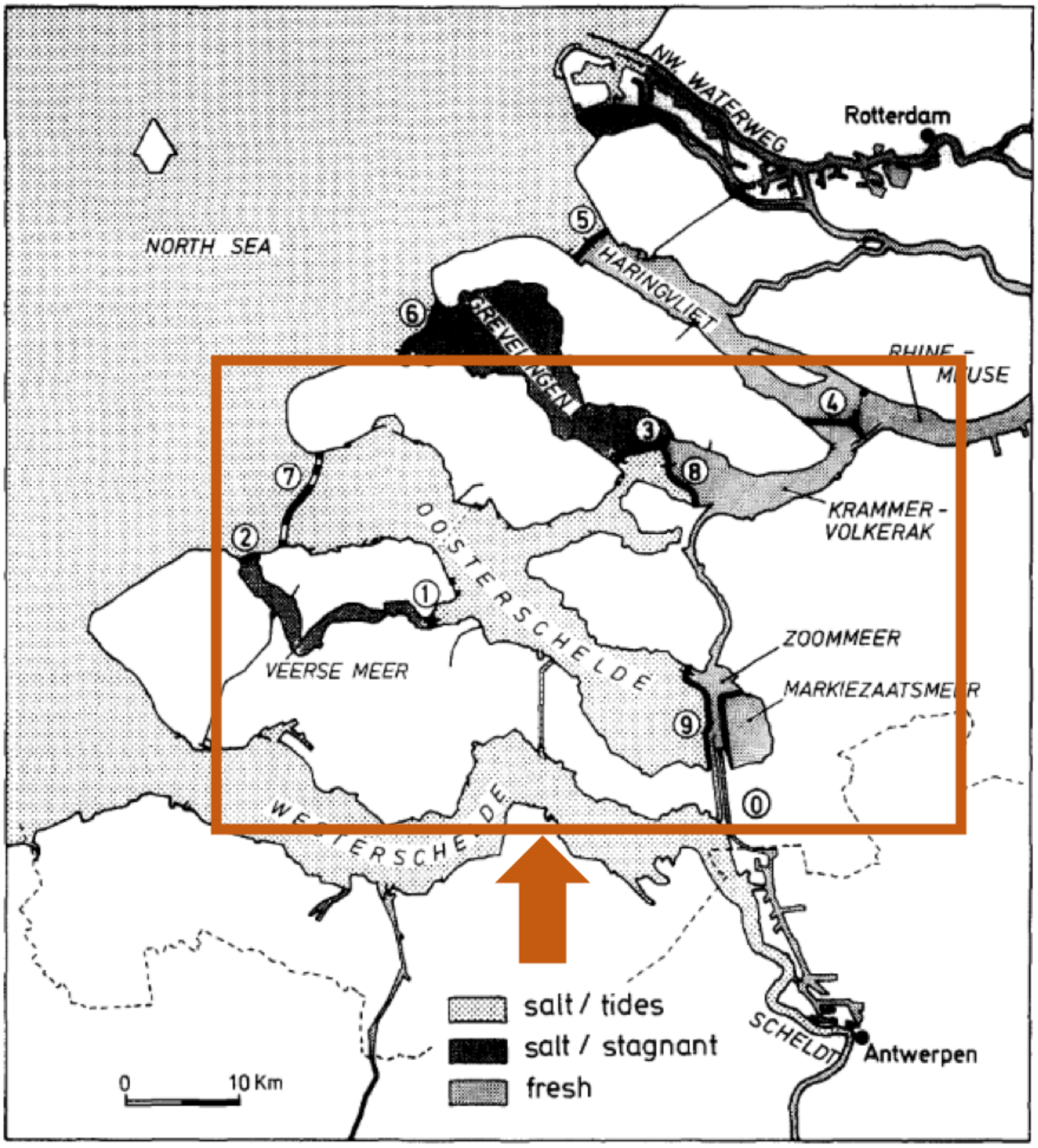

Figure 2: Location of the Eastern Scheldt estuary and mapping of the Delta Works series within the delta area of the Rhine, Meuse and Scheldt rivers in southwest Netherlands. 0= Kreekrakdam, 1867; 1=Zandkreekdam, 1960; 2=Veersegatdam, 1961; 3=Grevelingendam, 1964; 4= Volkerakdam, 1969; 5=Haringvlietdam, 1970; 6=Brouwersdam, 1971; 7=Oosterschelde storm-surge barrier,1986; 8=Philipsdam, 1987; 9= Oesterdam,1986. The Markiezaatsdam has closed of the Markiezaatsmeer from the Zoommeer in 1983 (adapted from: Nienhuis & Smaal, 1994).

The tidal prism passing through the inlet has decreased by roughly 25% from 1200 million m^3 to around 900 million m^3 ,because of the construction of barriers and dams. Simultaneously, the flow velocities in the western part have reduced by the same percentage (Eelkema et al., 2013).

Wave records over the last decades show significant averaged wave heights from the prevailing SW-NW winds decreasing from 0.4 m at the inlet to 0.1 m in the landward part of the Eastern Scheldt (Figure 3c). Most of the short waves are wind-induced waves with a minor contribution of swell. The dominant wave energy flux originates from the southwest (Figure3d) (Louters, van den Berg, & Mulder, 1998).

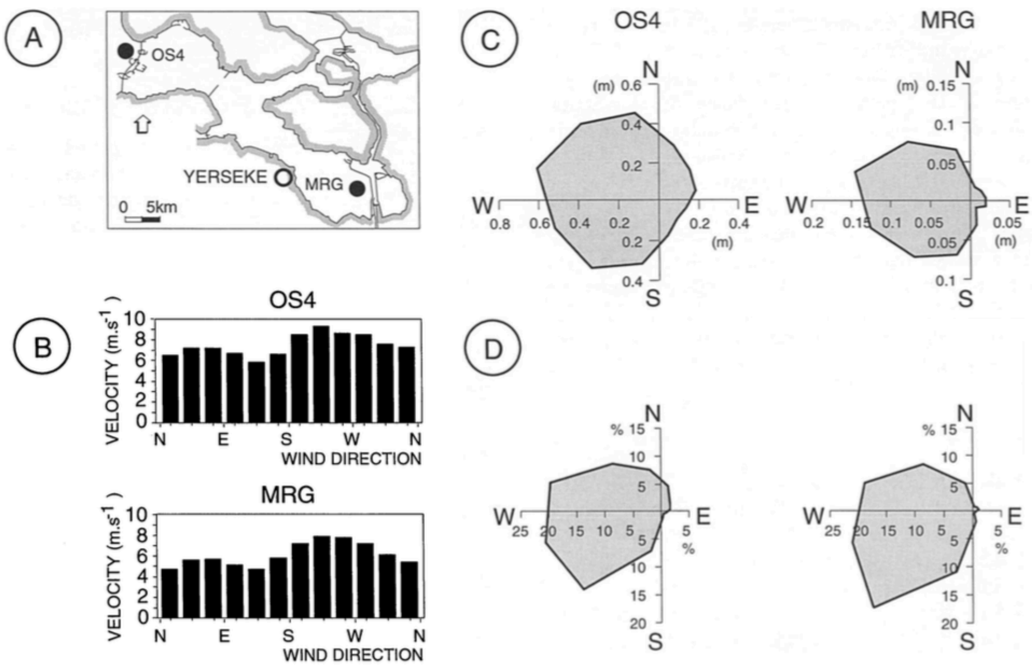

Figure 3: Wave and wind characteristics of the Eastern Scheldt tidal basin observed over the last decade (1977-1990): (a) location of wave stations OS4 and MRG; (b) average wind velocity; (c) average significant wave height (m); (d) proportional wave energy distribution for different wind directions (Louters et al., 1998).

The geomorphology of the Eastern Scheldt tidal basin features a complex interplay of intersecting tidal shoals, mudflats and salt marshes, whereby ebb dominated channels are generally deeper than flood dominated channels (Louters et al., 1998). Channel depth decreases in eastern direction varying from approx. -30 m Amsterdam ordnance Datum (AOD) to -10 m AOD (Louters et al., 1998). The height of individual shoals increases in eastern direction to a maximum of roughly +1 AOD (Louters et al., 1998).

2.1.2 Geological history, Pleistocene deposits

The subsurface of Zeeland relevant to this study has developed over the last 2.6 million years (2.6 Ma). Its geological past is characterized by rapidly shifting coastlines that can be associated with coastal sediments alternated with peat deposits. Due to rapid deposition rates, the medium (fine) sand deposits of the first 30 meters of Holocene sediments are loosely packed (van den Ham et al., 2014). With variations of tidal currents, an alternation of thin clay layers is found in between the thicker sand layers. This coastal sediment succession is underlain with deeper lain fluvial, periglacial and aeolian deposits from the former periods dating back to the Pleistocene.

The Zeeland high is part of the Neogene North Sea Basin, which has been subsiding since 201 million years (Jura) because of plate tectonic movements. This subsidence has increased over time due to the fill of sediment loading (Stouthamer et al., 2015).
At the end of the Pliocene and start of the Pleistocene (2.6 Ma – 11.7 ka) the North Sea retreated and sediments originating from the Northern Eridanos river system (Peize Formation (Fm.)) and from the Rhine- Meuse delta (Waarle Formation (Fm.)) were deposited (Westerhoff & Weerts, 2003). This showed that both river systems were expanding at the same time. Both formations, which are found at a depth of -20 m and deeper, are characterized by sand and silts of varying grain size. These represent fluvial as well as estuarine deposits of both river systems (Bosch, 2003; Westerhoff & Weerts, 2003).

With alternating glacial and interglacial periods throughout the Pleistocene, the depositional environment in Zeeland altered between coastal/ marine dominated, to fluvial and periglacial/ Aeolian dominated.
From the Elsterien (475 - 420 ka) onwards to the Holocene period, aeolian sand with fine grainsizes was deposited in Zeeland; rivers were absent. These deposits belong to the Boxtel Fm. and are found between -5 and -10 m depth (Stouthamer et al., 2015; Schokker et al., 2005). The Boxtel Fm. also includes cover sands and löss, together with river dune sands and reworked riverbed deposits.
This Boxtel Fm. is intertwined with the Eem Fm., which was deposited during the previous interglacial (Eemian, 130 - 115 ka) and is currently occurring at -7.5 to 25 m in Zeeland (Stouthamer et al., 2015). This sediment succession shows a transition of shallow fresh to brackish to full marine environment of deposition (Bosch et al., 2003). During the Weichselian (115 – 11.7 ka), the last glacial of the Pleistocene, a periglacial climate dominated the surface in the south of the Netherlands.

During this period the rivers Meuse and Rhine had a braided pattern and deposited mostly gravel and coarse sands that belong to the Kreftenheye Fm. Deposits in Zeeland originating from the Late-Weichselian are considered as the Kreftenheye -6 Member of the Formation (Fig.4) and these can be found at -7,5 to -25 meters depth (Stouthamer et al., 2015).

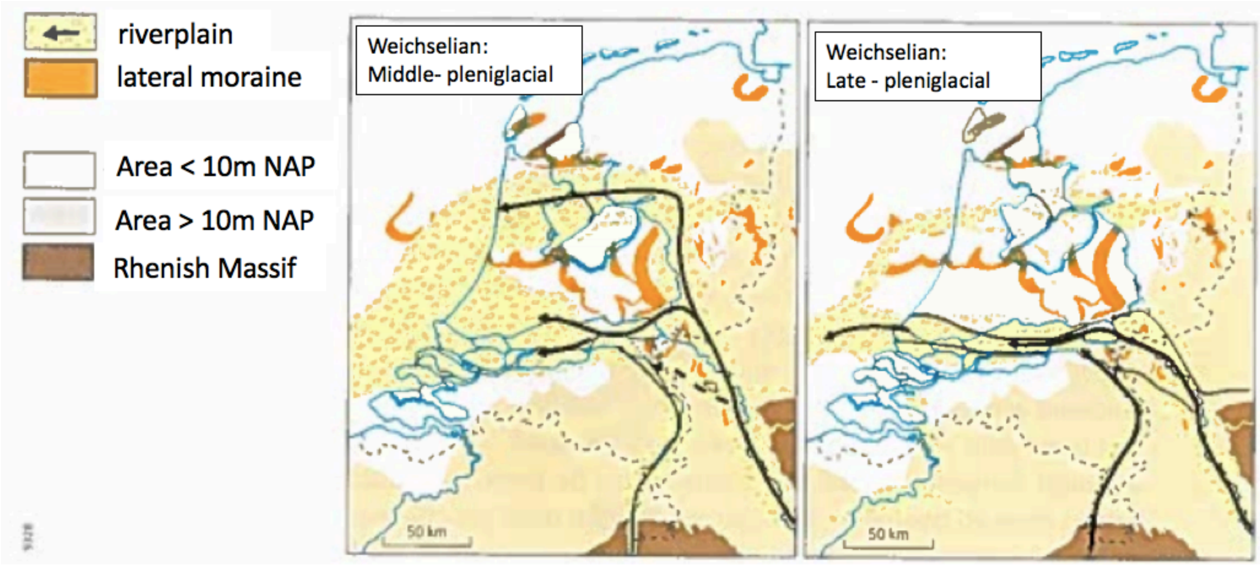

Figure 4: Braided pattern of Rhine and Meuse during the Middle-Pleniglacial (left) and the Late-Pleniglacial during the Weichselian (right). What do you see? The figure needs to be clear with one look, without reading the text. I would briefly explain the legend and what you see on the figure (adapted from Stouthamer et al., 2015).

2.1.3 Geological history, Holocene development and anthropogenic influence

At the end of the Weichselian temperature increased, which continued during the Holocene (0 - 11.7 ka). The increased temperature resulted in the melting of continental ice sheets and subsequently sea-level rise (Vos, 2015). This affected the subsurface of Zeeland from the Atlanticum (5.6 - 9.2 ka) onwards, when groundwater levels in the coastal area followed global sea level rise (Stouthamer et al., 2015).

The global sea level rise led to the formation of the Basal peat, which is the Basisveen Member belonging to the Nieuwkoop Fm., on top of Pleistocene deposits (Weerts & Busschers, 2003). Between 7400 and 6300 years ago the precursor of the Eastern Scheldt developed (Figure 5). An important tidal inlet flooded the lowest lain northern part of what is now known as the island Tholen and connected with the river Scheldt. The Scheldt started following a northern flow path flowing into the North Sea close to the present location of the Haringvliet (Kiden, 2006; Province of Zeeland 2013).

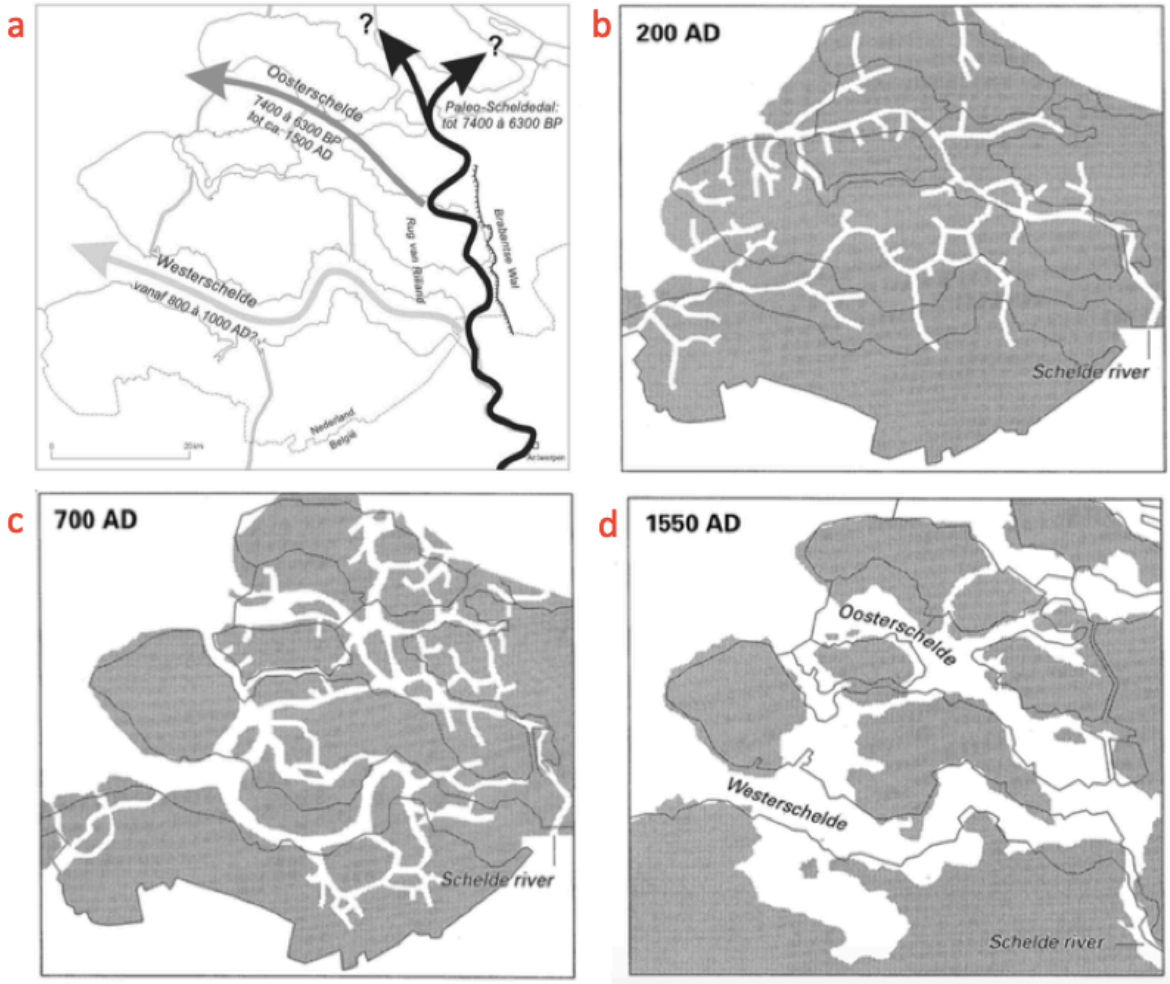

Figure 5: a) possible different courses of the river Scheldt down stream of Antwerp since the last ice age. Ages BP are calendar years before present (Kiden 2013). b, c & d) The evolution of the Eastern Scheldt basin since 200 AD, 700 AD and 1550 AD. (after Vos & van Heeringen, 1993)

Shortly after, the river Scheldt avulsed to the shorter northwestern path and the northern course slowly filled up with clay and peat over the following time period. During the Mid-Holocene (4.2 - 8.2 Ka), the North Sea became a shallow sea. With wave action and sufficient sand available, sandy islands formed several kilometres off the coast along the Dutch coast. Behind this coastal barrier sandy tidal- and silty mudflat sediments were deposited on top of the Basal peat layer, which belongs to the Wormer Member of the Naaldwijk Fm. (Stouthamer et al., 2015).

The coastal barrier closed off as a consequence of reduced sea-level rise and continuous sediment supply. A fresh water environment slowly developed through the Subboreal period (2.6 - 5.7 ka) through water provided by the Scheldt river and connected little streams. In this environment with shallow depths, peat developed, forming the Holland peat layer, which is the Hollandveen Member, belonging to the Fm. of Nieuwkoop, which lays on top of the Wormer Member.

The Scheldt river meandered through this peat landscape with almost no tidal influence. The occasional flooding of the floodplain gave the Holland peat layer a clayey character (Kiden, 2006). The Holland peat layer can be found at a depth of -5 to -10 m in Zeeland and it is covered by the Walcheren Member of the Naaldwijk Fm., consisting of sandy inlet fills and silty clayey salt marsh deposits, that originate from the last 2000 to 3000 years. The median grain size within the ebb tidal delta is shown to be between 150 and 200 µm on the shoals and between 200 and 300 µm in the channels (Eelkema et al., 2012). Generally, sediments of mudflats and salt marshes have a median grainsize of less the 150 µm (Louters et al., 1998).

These deposits are the result of a regressive trend of the coastline from the last 2500 years (Stouthamer et al., 2015) due to anthropogenic interference, postglacial subsidence, glacio-eustatic sea level rise and increased influence of tidal currents on the peat area. Since the arrival of the Romans approximately 2000 years ago, dewatering techniques were introduced to manage the arable land (Province of Zeeland, 2013).

Through this dewatering, peat was oxidized and land started to subside, making the landscape more susceptible to influence of the sea. Little dug channels became larger tidal inlets and by 350 AD, most of the peaty landscape became uninhabitable. At the same time a diverse landscape of salt marshes, tidal channels and little streams developed. Also, the precursor of the Western Scheldt, the Honte, developed at the start of this period with an initial connection to the North Sea estimated around 800 to 1100 AD (Vos & van Heeringen, 1997). With time the tidal inlet grew larger and after the storm floods of 1530-1532 AD the river Scheldt shifted its course to the present Western Scheldt estuary (Kiden, 2006; Province of Zeeland 2013). Sandy channel belt deposits within the Eastern Scheldt became the higher ridges within the landscape, as surrounding peat and clay consolidated through its own weight and dewatering (Province of Zeeland, 2018; Stouthamer et al., 2015). These ridges became appropriate to the re-inhabitancy of Zeeland as they were protected from the influence of the sea by the implementation of the typical Dutch dikes. A geological cross section through Schouwen-Duivenland (west) and Tholen (eastward of channel) of the coastal Holocene deposits is shown in 6 & 7.

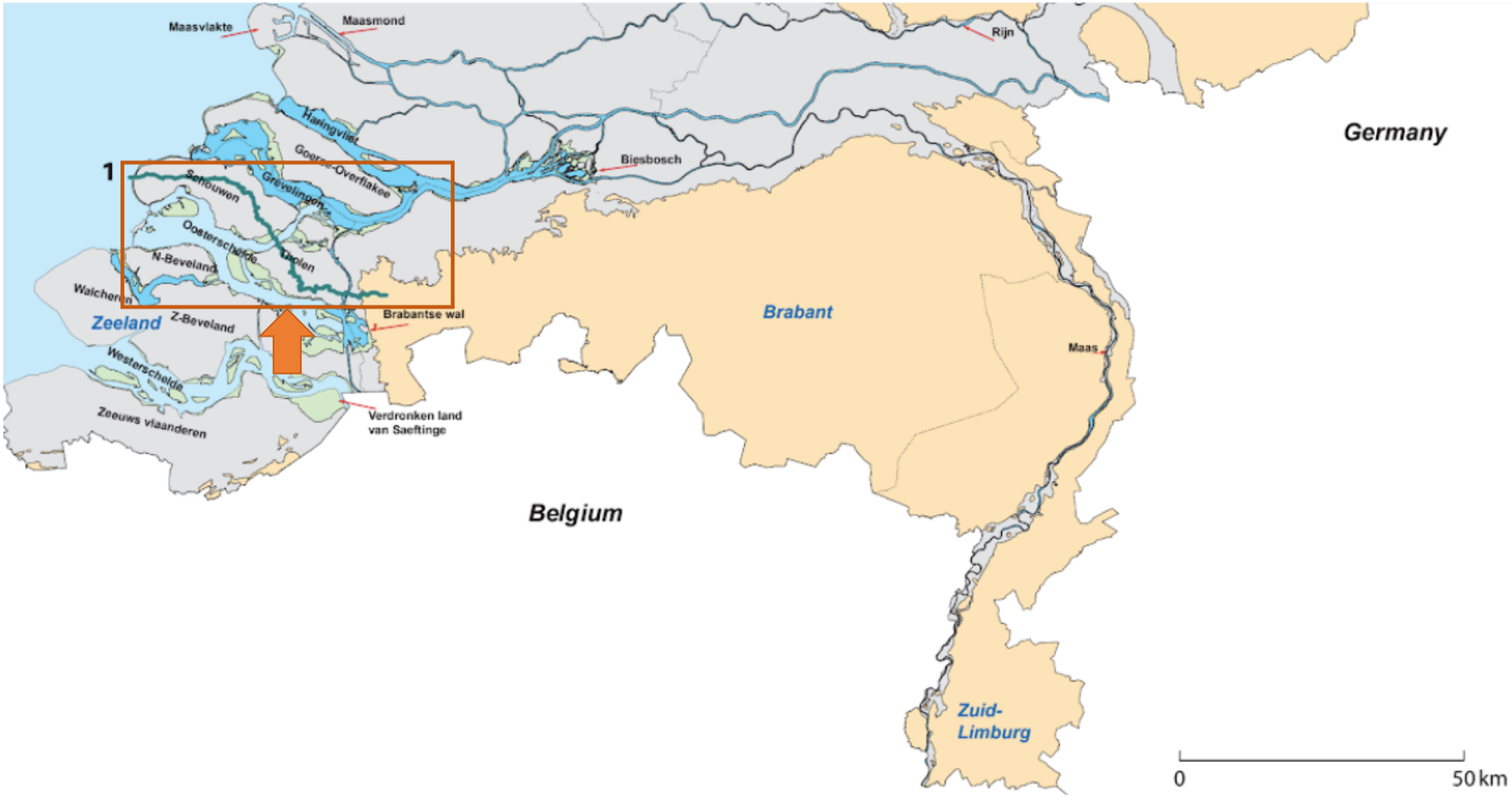

Figure 6: Location of geological cross-section(indicated with square and arrow) of the Holocene deposits found in the Province of Zeeland (adapted from; Vos 2015)

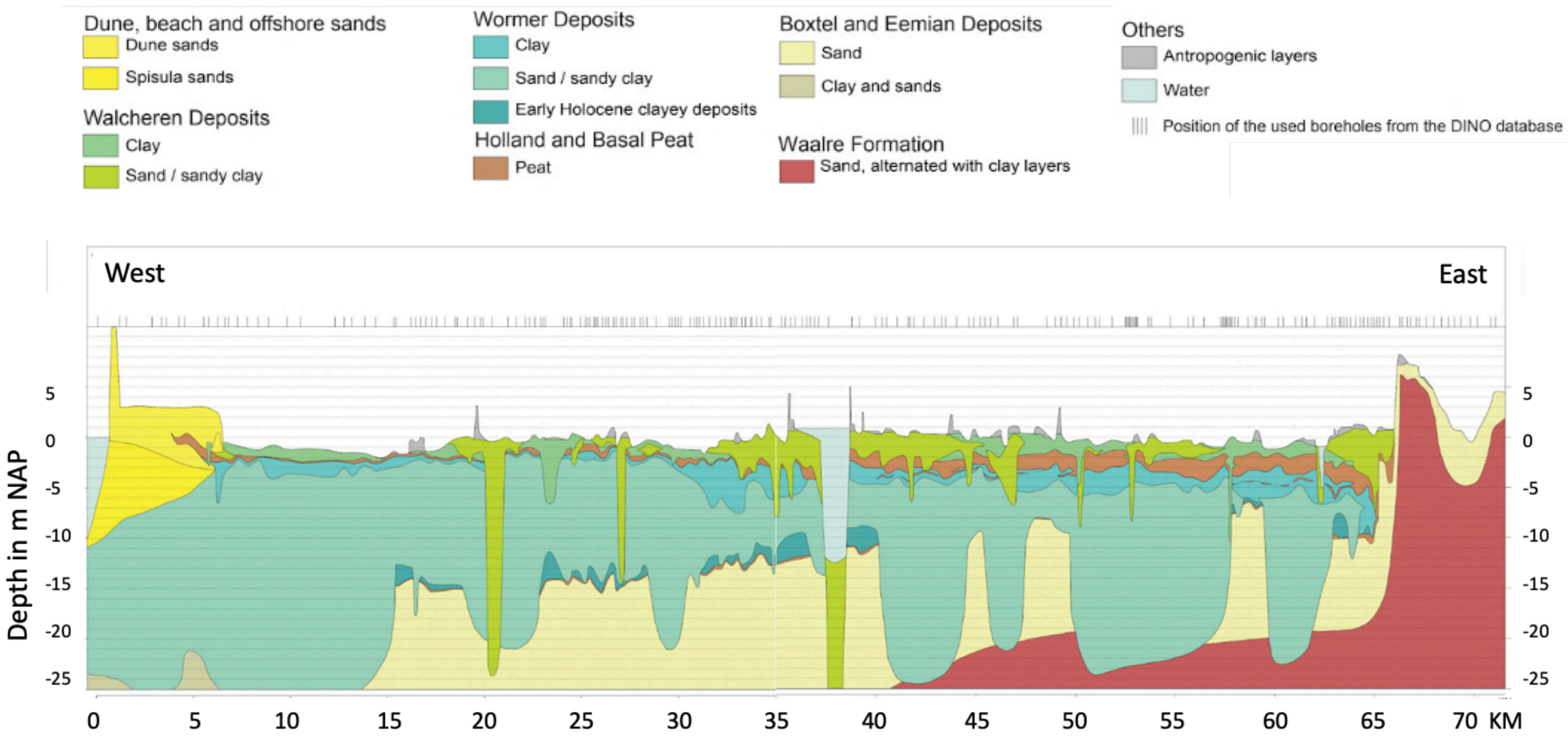

Figure 7: Geological cross-section of the Holocene deposits found in the Province of Zeeland (Vos 2015), In the legend geologically different stratigraphic layers are indicated by different colours used in the transect.

2.1.4 Delta works development

Since the 10th century, dikes have been implemented in Dutch deltas functioning as hard measures against flooding. However, through continuous human induced subsidence, a lack of new sediment supply and increased water levels during spring tides and storms (Fig. 8; Kiden, 2006), this coastal protection could not overcome the flooding event of 1953 (Wesselink et al., 2015).

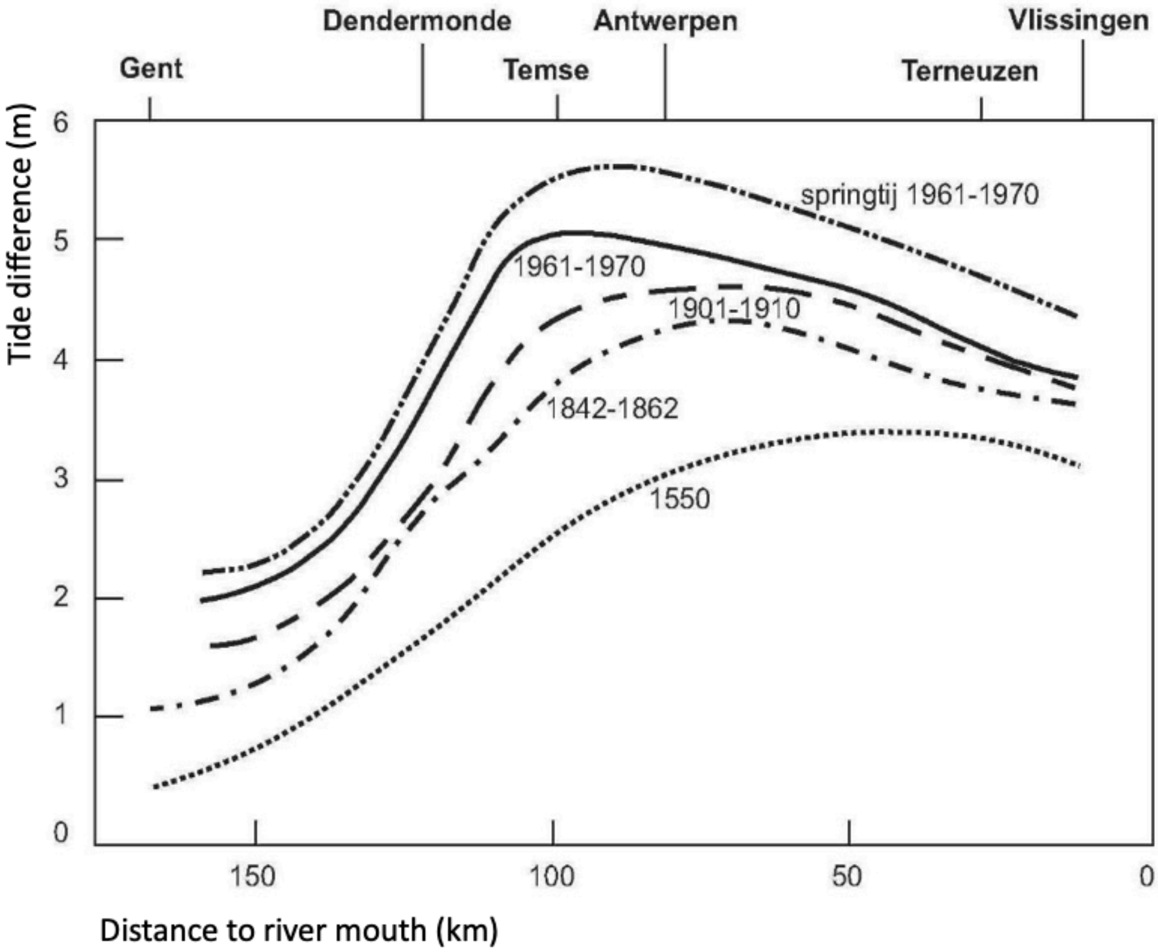

Figure 8: Increase of water levels during storms and spring tides due to reduced space for water within the Eastern Scheldt estuary due to fixed estuary boundaries (Kiden, 2006).

Within the greater Delta Plan, in which estuaries were closed off by dams and dikes were strengthened, the Eastern Scheldt was closed off by a storm surge barrier (Bannink & ten Brinke, 2008). However, this flood protection measure differed from the default solution. As a result of societal pressure and doubts concerning the impacts of large scale engineering onto the environment, the Eastern Scheldt was not closed off completely (Bijker, 2002; Disco, 2002). This adapted solution had to account for maintenance of excising ecosystem dynamics through its open system status.

However, the storm barrier changed the ecosystem dynamics, resulting in coastal squeeze of the salt marshes and mudflats in the Eastern Scheldt (Balke et al., 2016). Within more recent coastal management plans, focus lies on strategies in which excising ecosystems support typical Dutch hard flood protection measures (De Vriend et al., 2015).

Since the Middle ages, land was reclaimed by the Dutch, which led to a gradual separation between the Eastern Scheldt and the Western Scheldt (Cozzoli et al., 2017). The Eastern Scheldt was already separated from the fresh water input of the Scheldt river in 1867 with the construction of the Kreekrakdam (Nienhuis & Smaal, 1994). As a response to the North Sea flood of 1953, a substantial system of coastal defence was implemented (Delta Works, 1959-1987). The Eastern Scheldt was then separated from the other connecting basins by the construction of two back-barrier dams, the Grevelingendam (Fig. 2 (3) in 1964 and the Volkerakdam in 1969 (Fig. 2 (4); (Nienhuis & Smaal, 1994).

This reduced freshwater input from the Rhine river to the Eastern Scheldt from 70 $m^3 s^{-1}$ to almost 0 m^3s^{-1} (Nienhuis & Smaal, 1994). In the following years, the Eastern Scheldt storm surge barrier was constructed and finalised in 1986, which closed the basin partially off from the sea. The storm surge barrier is located within the two islands of Schouwen-Duiveland and NoorFlBeveland, has a total length of 9 km and is the longest of all 13 dams comprising the Delta Works series (Cozzoli et al., 2017). During calm weather conditions, the Eastern Scheldt storm surge barrier is kept open and therefore allows tidal influence and tolerates marine life and shellfisheries. However, the barrier can be closed to prevent storm surges flooding the hinterland (Cozzoli et al., 2017).

In contrast to the relative open character, the tidal prism (i.e. the water volumes brought in and out by the tide) within the Eastern Scheldt has been reduced by almost 30%. Tidal and wave current velocities have respectively decreased by 20 to 40% (Louters, van den Berg, & Mulder, 1998a). This dissipated initial tidal energy and the development of secondary currents in the Eastern Scheldt hinders the sand exchange with the North Sea through the barrier.

Due to the reduction of tidal prism and the channels being relatively too large for the reduced stream velocities, sedimentation occurs within the channels. As sand cannot be supplied from outside the tidal basin, an amplified erosive sand transport occurs from the tidal flats into the channels (Eelkema et al., 2012). With continuation of this erosive process a total disappearance of the tidal salt marshes and mudflats is predicted within less than a century (Jongeling, 2007).

For the Western Scheldt a different situation applies, since an open connection to the sea and the river Scheldt still exists and the estuary has a full salinity gradient. However, since the beginning of the last century, dredging activity is applied and strongly intensified after 1960 due to the growth of ship transit and draft to Antwerp harbour (Cozzoli et al., 2017) In order to maintain the shipping lane, approximately 6.5 to 7 million m^3 of sediment is dredged annually. The removed sediment is not permanently extracted as it is mostly re-deposited within the estuary. Due to the deepening of dredged channels, the tidal range has subsequently increased, which hassled to an enlargement in tidal currents of approximately 30% since 1955. Furthermore, altered mixing patterns evolved between fresh and salt water (Cozzoli et al., 2017).

2.2 Mudflats and salt marshes in the Eastern Scheldt

The present day salt marshes and mudflats within the Eastern Scheldt have developed during the last 2000 years. Since the anthropogenic influence of the Romans, the sea increasingly affected the present state of the tidal basin. Tidal channels became deeper and the levee and floodplain deposits slowly rose above sea level, generating mudflats, which are considered being part of the intra tidal zone. Slowly the mudflats rose above mean high water level and were solely flooded with extreme high water levels and storm floods. Therefore they developed to vegetated salt marshes, known as supra tidal zones (Fig. 9) (Stouthamer et al., 2015; Province of Zeeland, 2013). Consequently, salt tolerant vegetation could establish, known as halophytes such as the *Spartina* spp (Lo et al., 2017).

Mudflats and salt marshes provide valuable ecosystem services and include habitats supporting biodiversity, primary production, water purification, carbon sequestration and coastal protection (Bouma et al., 2014; Craft et al., 2009; Fourqurean et al., 2012). Tidal mudflats and salt marshes are however threatened by sea-level rise and coastal squeeze (Gedan, Silliman, & Bertness, 2009). Coastal squeeze is defined as the intertidal habitual loss due to the high water boundary being determined by a sea defense and the low water boundary moving landwards in response to sea level rise. Coastal squeeze in the Eastern Scheldt occurs due to the constructed dikes, which prevent the foreshore systems (tidal mudflats and salt marshes) to move land-inward with predicted sea-level rise (Feagin et al., 2009; Francalanci et al., 2013). Simultaneously, dikes obstruct sufficient sediment supply (Feagin et al., 2009; Francalanci et al., 2013).

These stressors could ultimately lead to the disappearance of mudflats and salt marshes in tidal basins of the Netherlands, which would decline its functioning towards the ecosystem services including coastal protection.

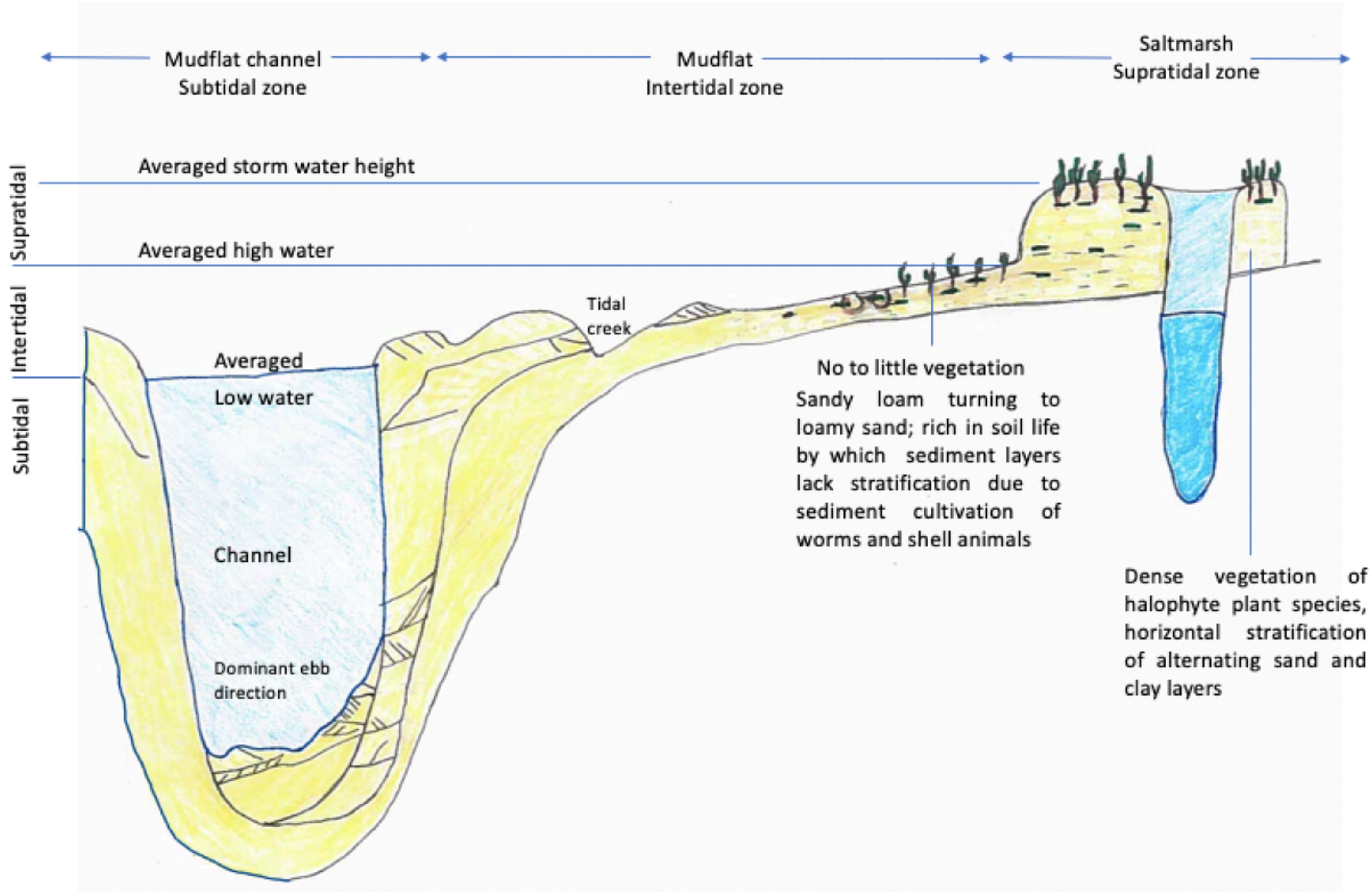

Figure 9: Sketch of depositional environments on mudflats and salt marshes (adapted from Stouthamer et al., 2015).

2.2.1 Coastal protection of salt marshes and mudflats – in perspective

Foreshores, comprising both tidal mudflats and salt marshes, are increasingly recognized worldwide, functioning as a soft measure reducing flood risk (e.g., Gedan et al., 2010; Temmerman et al., 2013). Studies in the Scheldt so far focussed on the role of foreshore (mudflats and salt marshes) dynamics as response to wave and tide exposure to verify its functioning towards flood protection (Hu et al., 2017; Bouma et al., 2016; Li et al., 2017; Wang et al., 2017 & Stark et al., 2015). Stark et al. (2016) studied the flood protection potential of the combined nature-based and engineering approach of foreshore and adjacent dikes in the Eastern Scheldt, by modelling the effect of foreshore geometry on wave attenuation. Here it was shown that limitations in storage area or salt marsh extent have a significant impact on storm surge attenuation and may drastically reduce attenuation rates. It increases the wave forcing on the hard flood protection dikes in the hinterland. However, in-situ characteristics of tidal salt marshes and mudflats and their effect on the stability of Dutch dikes towards flood protection, were not included. The study of Wang et al. (2017) showed that both extrinsic and intrinsic factors affect salt marsh edge erosion across different scales (Figure 10) and thereby denoted the importance of internal salt marsh structure and geomorphological setting.

Lo et al., (2017) investigated lateral erosion control modified by the presence of *Spartina* spp. vegetation, sediment grain size, and nutrient status of salt marshes of the Italian Northern Adriatic coastline. The presence of *Spartina* spp reduced erosion across the salt marsh area by 80 % volume loss for sandy soils and 17 % volume loss for silty soils. Moreover, the *Spartina* biomass in the upper 30 cm soil layer enhanced erosion resistance. When vegetation was absent, resistance of erosion was amplified by silt content with mean lateral erosion being 72 % lower for the volume loss in silty vs sandy soils (Lo et al., 2017).

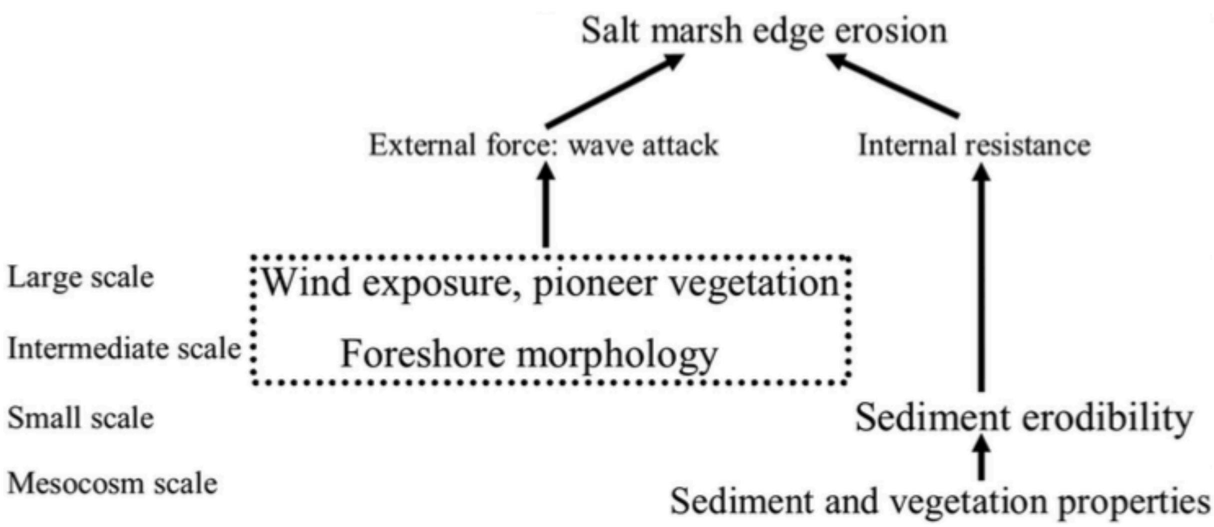

Figure 10: A schematic view of extrinsic and intrinsic factors affecting salt marsh edge erosion across different scales, with the arrows indicating the flow of influence. (Wang et al., 2017).

Coupling extrinsic and intrinsic factors to the ecosystem service of coastal protection is key in understanding the flood protection potential of combined nature-based and engineering approach of foreshore and the adjacent dikes in the Eastern Scheldt for decades to come.

2.2.2 Krabbendijke, Dortsman – Zuid en Krabbenkreek

Since the implementation of the Delta works, the proportion of total channel space within the Eastern Scheldt and its tidal prism has been disturbed (Jacobse et al., 2008). Growing to equilibrium, channels within the basin are filled with sediments originating from the mudflats and saltmarshes. This effect is clearly present for the basin of the Eastern Scheldt from which the sediment volume was reduced from 1990 to 2007 with 10 Mm^3. The eroded sediment is subsequently deposited at the channel edges and in the intertidal shallow water areas with an elevation of -5 m NAP or lower (Jacobse et al., 2008). In the next century, loss of intertidal area will continue by approximately 4000 hectares (Jacobse et al., 2008). In the Eastern Scheldt both governmental and private institutions have been deployed to monitor and predict the extent of the salt marshes during next decades. This will grow insight in the extent of coastal squeeze of mudflats and salt marshes (Hordijk, 2007; Jacobse et al., 2008). Smoothening of mudflats and salt marsh edges is expected, whereby lower parts of the basin are filled with sediment originating from higher erosive parts of the basin.

However, time plays a significant role in this newly formed equilibrium, as without sediment supply of higher parts, lower areas will also experience erosion. Within a future prospect for the Eastern Scheldt, mudflats will decrease in height by 50 cm to 1 meter within the coming century (Jacobse et al., 2008). For foreshores within the Eastern Scheldt a redistribution of sediment is expected leading to slackening of foreshore profiles (Jacobse et al., 2008). For the salt marshes of Krabbendijke, Dortsman- Zuid and Krabbenkreek a prediction was made for changing salt marsh edges over time (Figure 11; Jacobse et al., 2008; Fig. 12; Hordijk, 2007).

For the year 2060, it is expected that for Krabbendijke only 60 % of the present salt marsh area will remain. For Dortsman- Zuid it is expected, that the whole salt marsh area will disappear by 2060 and for Krabbenkreek 80-90 % is expected to still exist by 2060. With the decrease of foreshore areas, wave load to adjacent dikes will increase and foreshore surface and deeper subsoil will become more prone to destabilization.

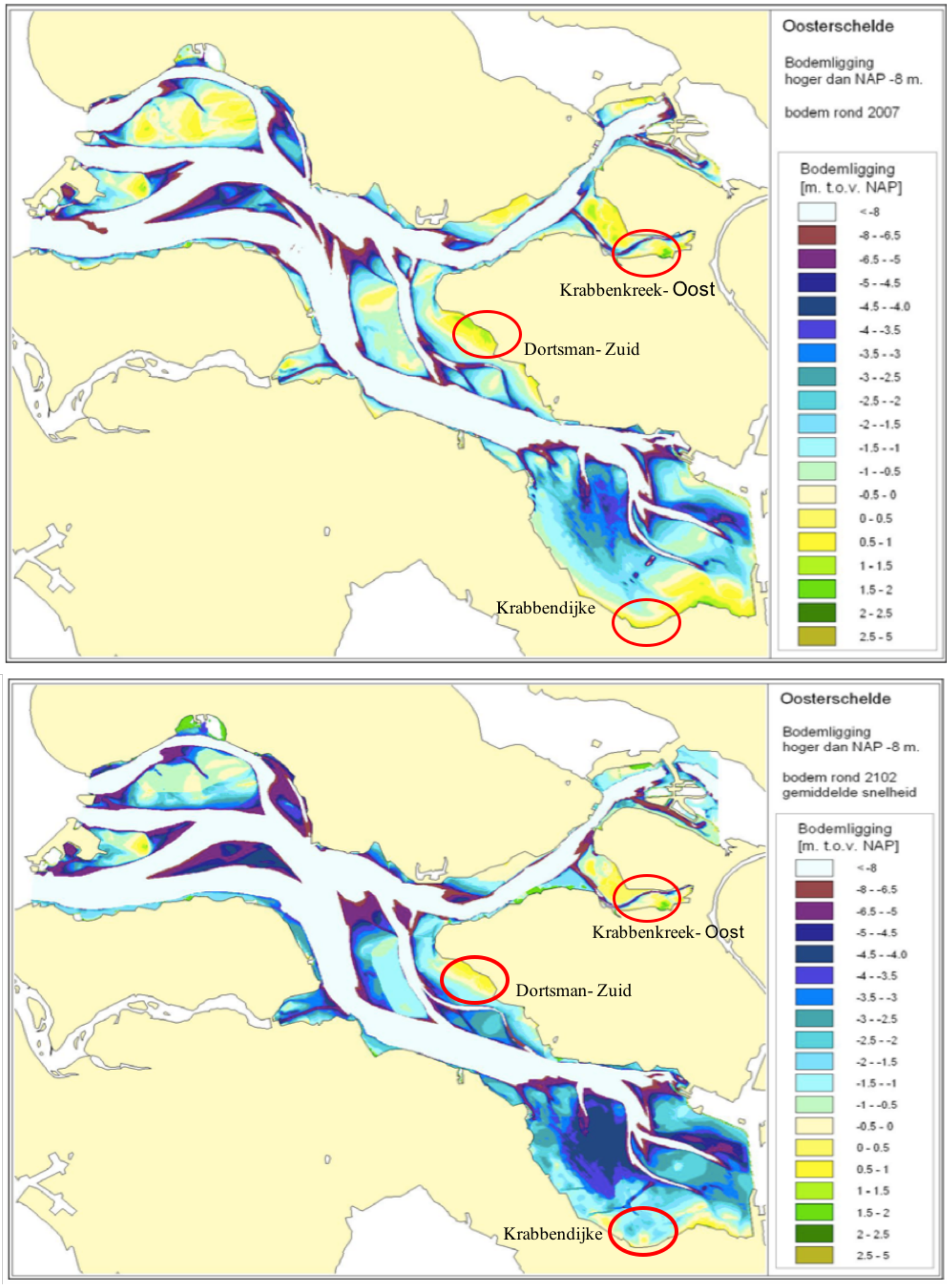

Figure 11: Bed elevation modelled for beds within the Eastern Scheldt higher than -8 meters NAP compared for the years 2007 and 2102 respectively (Jacobse et al., 2008). The red circles indicate the three locations of the study sites.

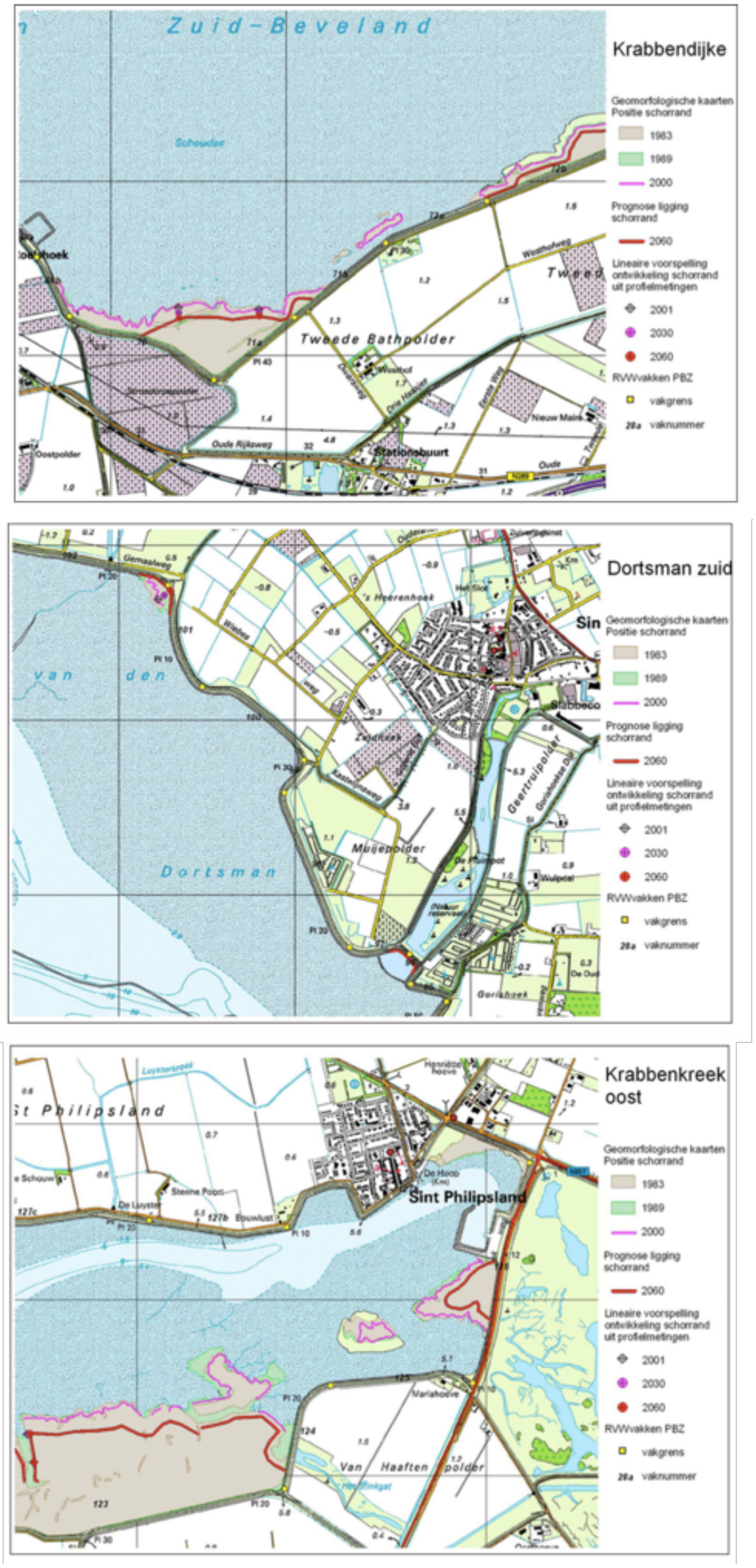

Figure 12: Model prediction of the location of salt marsh edges based on parameterization of existing data including height and horizontal extent of the salt marsh edge. The red line indicates the expected location for 2060 (Hordijk, 2007).

2.3 The mechanism of flow slides

The combination of loose packing of sand intertwined with clay and peat layers, which determines dissipation of excessive pore pressures, makes soils within the Eastern Scheldt sensitive to liquefaction (Hicks & Onisiphorou, 2007; van den Ham et al., 2014). Liquefaction results in the occurrence of flow slides in submerged slopes in the non-lithified sand and silt sized sediments along estuary coastlines (van den Ham et al., 2014). Therefore, it forms a potential threat to flood defences (van den Ham et al., 2014). Flow slides may cause serious damage to foreshores and dikes. Additionally, measures taken to prevent, mitigate or repair flow slide damage is costly (van den Ham et al., 2014).

Two important mechanisms can be distinguished; static soil liquefaction and breaching. These mechanisms lead to similar results. Firstly, a flowing sand water mixture develops, which with time redeposits under a gentle slope. This complicates recognition of different mechanisms within the analysis of historical flowslides. The in-situ properties and state variables of subsurface materials determine if the zone is sensitive to flow slides. Furthermore, external processes such as; changes in geometry, erosion, changes in water-level or other triggers can stimulate the occurrence of a flow slide. With a change of geometry of a local submerged slope, this can lead to breaching. If the zone of static liquefaction and reduced shear stress is large enough, a retrogression of the slope can occur. Both liquefaction and breaching lead to a failure of the levee and thus flooding (Fig. 13; Deltares).

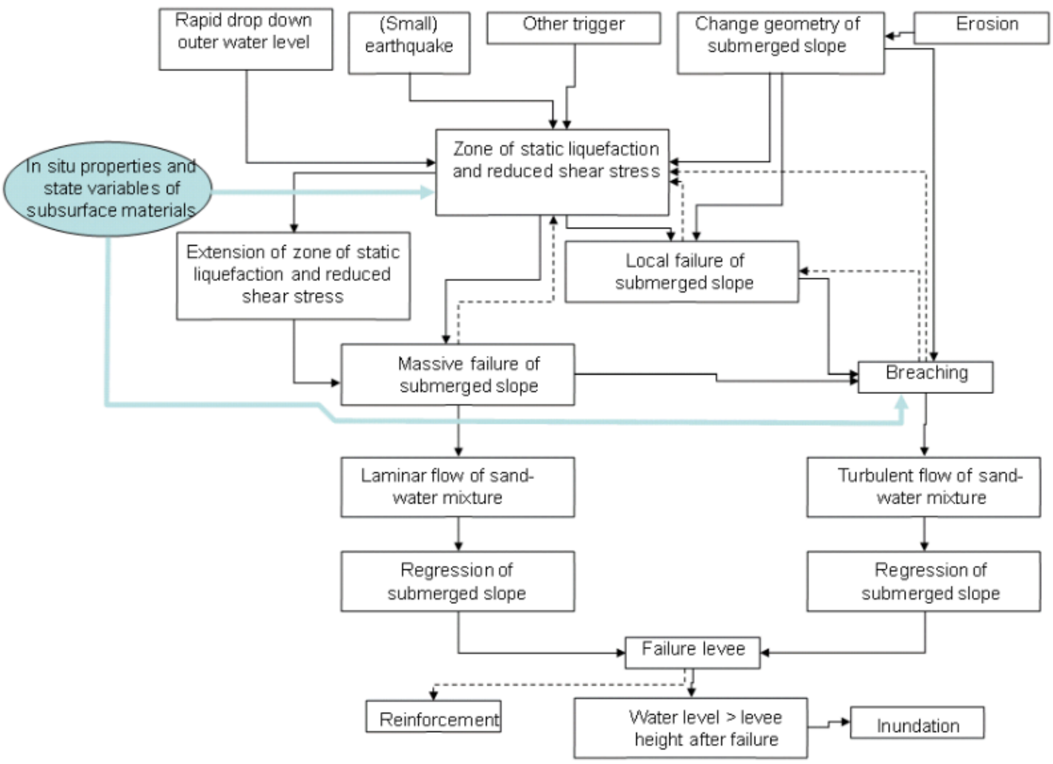

Figure 13: Processes involved with the occurrence of flow slides (Deltares, 2017).

2.3.1 Static liquefation

The mechanism of static soil liquefaction encompasses the sudden loss of strength and collapse of a body of loosely packed sands and silts being saturated with water. This body of sand then flows laminar like a viscous fluid in a liquefaction flow slide. This is different from the ordinary slope failure, where sediment bodies often slide along a clear rupture surface and stay more or less intact (van den Ham, 2014).

Towards the occurrence of static liquefaction the following criteria are to be met, (1) a sufficiently thick succesion of loosely packed and water-saturated sands and silts should be present; (2) the stress state of the individual sand particles has to approximate the metastability point, known as the intermediate maximum in the stress path and (3) a trigger should be present (i.e a load change to the foreshore). The intermediate maximum in the stress path is shown in Figure 15. This intermediate maximum is reached with sufficiently high and steep slopes where grain and deviator stress are sufficiently large.

For a saturated sand body the volume cannot change under applied stress. Instead a water overpressure is being generated, by which the soil skeleton experiences both contraction and dilatancy averaging out to a zero-volume change. This principle can be understood through the following equation:

$$p = p' + u \quad \text{or} \quad p' = p - u \ [\text{kN/m}^2 \text{ or kPa}] \tag{1}$$

Here, water pressure (u) is the difference between the total stress of the soil (p) and isotropic grain stress (p'). Soil stress increases with growing external deviator stress (q). Grain stress (p') shows a contrary signal and first decreases after which it increases to the critical/ steady state value.

A special phenomenon occurs within the shear trajectory of loosely packed sand, as deviator stress (q) reaches an intermediate maximum indicated with the red star. From this maximum, it decreases to a moment of maximum contraction ('phase transformation'), which is indicated with a 0 and then reduced to negative values. Here shear strain (γ) is still small, but deviator stress has almost reached its maximum. This proportion of contraction and dilatancy is strongly related to both density and stress state of the soil structure.

When comparing the path of deviator stress with different sand body densities, it appears that for denser soil structures this intermediate maximum is no longer reached. The moment of this intermediate maximum is called the wet critical density. Soils with a higher initial soil stress (p) or a low initial density (Fig. 14 & 15) often lie beneath the distinction line of the wet critical density, indicated with the discontinued red line in Figure 14. These soils are therefore sensitive to liquefaction.

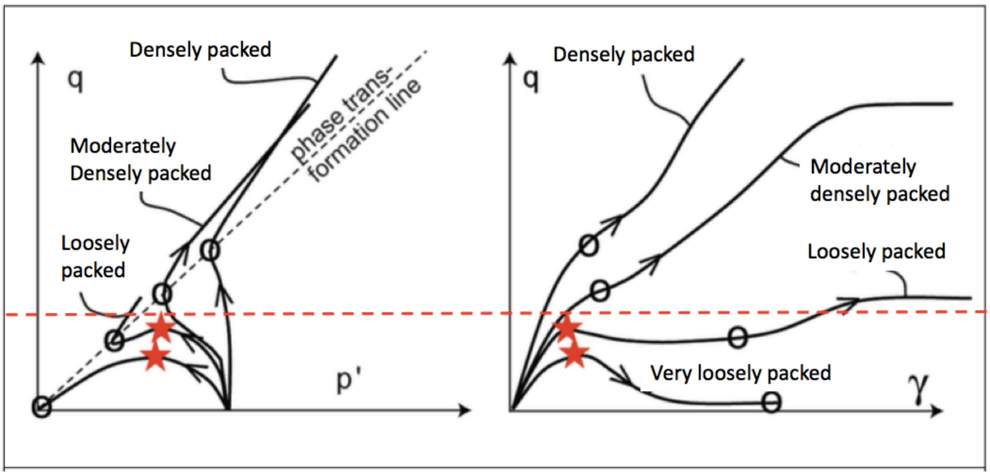

Figure 14: The intermediate maximum of deviator stress(q) for loosely packed sand (indicated with the red star), decreases to a moment of maximum contraction ('phase transformation') indicated with a 0 and boundary of wet critical density (indicated with the dashed red line) for increasing shear strain (γ) (adapted from: de Groot et al., 2007*).*

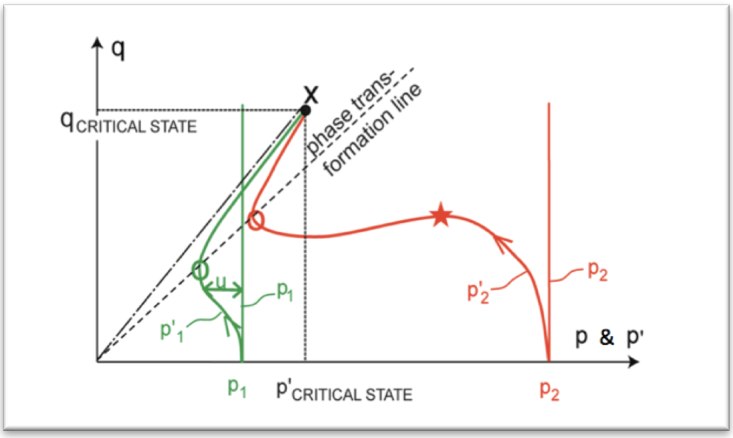

*Figure 15: A higher initial ground stress(p_2 , red line) for versus lower initial ground stress (p_1, green line) indicated on the x-axis results in a density below the wet critical density. This triggers the existence of the intermediate maximum (red star) of deviator stress (q) on the y-axis. (*adapted from: de Groot et al., 2007*).*

For every type of sand a unique relation exists between the density of the sand body/void ratio and critical state values of deviator stress (q) and grain stress (p'). This relation is called the critical state line (de Groot et al.,2007) and is illustrated in Figure 16 with stress trajectories of Figure 15.

The difference between the in-situ void ratio and the void ratio at the steady state/critical state is named the state parameter (ψ) (Been & Jefferies, 1986). The larger the state parameter (positive value), the more sensitive the sand is for static liquefaction.

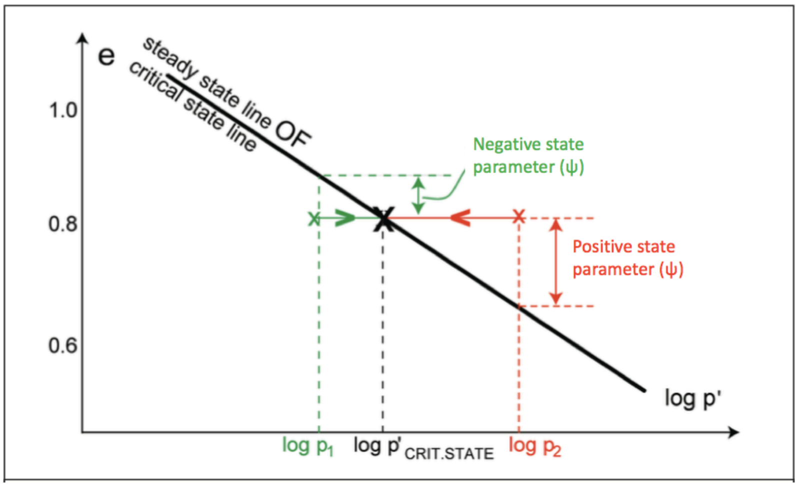

Figure 16: The difference to the in-situ void ratio and the void ratio at the steady state/ critical state is known as the state parameter(ψ). A positive value for ψ implies sensitivity to liquefaction (adapted from: de Groot et al.,2007).

With a high ground stress (p), the grain stress (p') should subsequently decrease to the steady/ critical state. This implies a generation of water overpressure (u) causing instability of the sand. The body of sand is not in a balanced state at the intermediate maximum of q at point A and jumps to a new state at point B (Fig. 17; de Groot et al., 2007). As the net ground stress p is unchanged and p' decreases, water overpressure develops in the same split second accompanied with high shear strain causing instability. At point A, known as the meta- stability point of the soil, only a small trigger could lead to liquefaction.

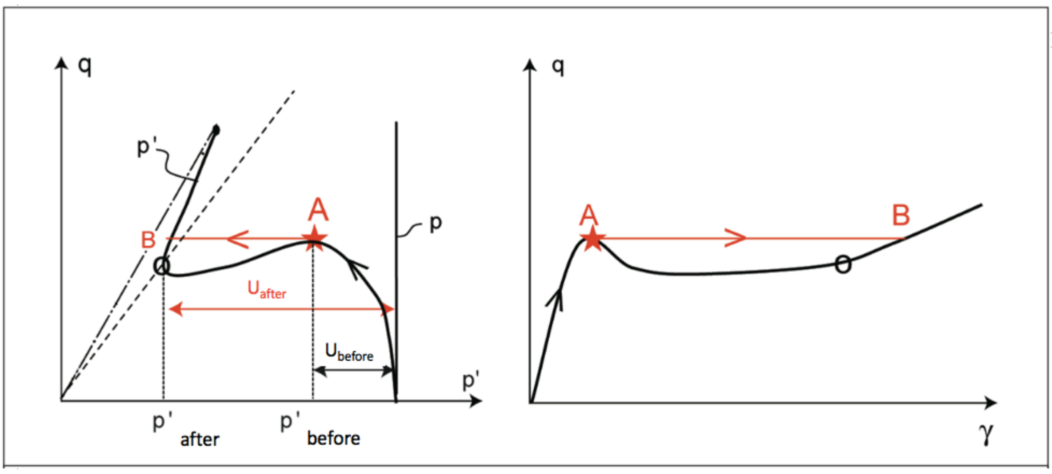

Figure 17: A sudden shift from the point of metastability (A) to the point of phase transformation (B) illustrating to the sudden instability due the water overpressure u and the high shear strain (γ) (adapted from: de Groot et al.,2007).

A more elaborate explanation of the soil liquefaction mechanism can be found in Appendix 1.

2.3.2 Breaching

The second mechanism involved in the occurrence of flow slides, breaching, only takes place at the sand surface of the slope. By the emergence of the so-called breach, a tempestuous mixture of sand and water flows downslope over the sand surface causing an retrogressive erosional trend (Fig. 18). With a slope steep enough and the initial disturbance of the slope triggers a sufficiently high velocity stream carrying a fair amount of sand, velocity and magnitude of this turbulent flow increases over time. (van den Ham et al., 2012). This mechanism takes more time to occur (several hours), as the retrogression velocity of the initial breach is relatively small compared to the time span in which static liquefaction occurs (several minutes). For a breach flow slide to take place in an under-water slope the following conditions have to be met: (a) sufficiently large zone of sand / silt present (b) a proportional high and steep slope and (c) a local slope instability causing a small but very steep slope section (breach) (van den Ham et al., 2012). The slope instabilities that start as a breach flow sometimes trigger a phase of static liquefaction. This changeover of processes also occurs in the opposite direction, where flow, that developed with static liquefaction, degenerates into a breach flow. This causes uncertainty in determining which sub mechanism was initially responsible for historic flow slides.

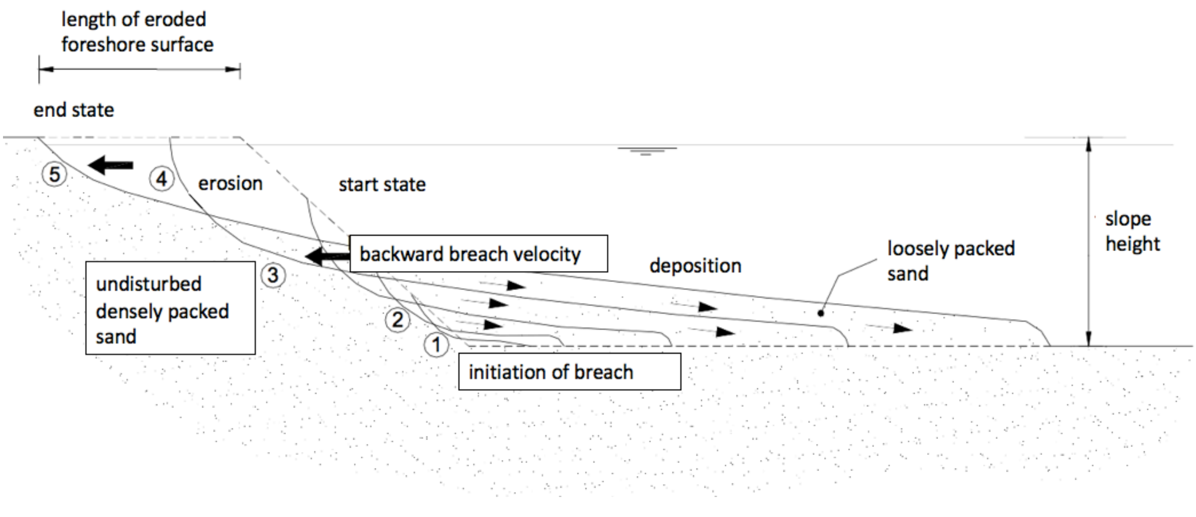

Figure 18: The process of breach flow. With (a) sufficiently large zone of sand / silt available (b) a proportional high and steep slope and (c) a local slope instability causing a small but very steep slope section (breach) (adapted from : van den Ham et al., 2012).

2.3.3 Historic flow slides in the Netherlands and semi- empirical relations

Along the estuary banks of Zeeland, between 1800 and 1978, approximately 710 flow slides were recorded by Wilderom (1979). Most of these slides have probably been the result of static liquefaction as they mostly occurred in areas with thick layers of loosely packed sand. However, from descriptions it can also be deducted, that some of the flow slides occurred over a time window of several hours to even roughly a time record of a full day. This indicates that the mechanism of breaching often played a similarly important role. Wilderom (1979) documented specific parameters of underwater slope geometry prior to occurrence of flow slides, general local soil conditions and triggers for various bank stretches along the shores of Zeeland (van den Ham et al., 2014). In Figure 19 the influence of subsurface deposits is shown. The frequency of flow slides seems to be related to deposit age and has the tendency to occur less with increasing age of the deposits. However, among the different bank stretches a large variability is visible in sensitivity to flow slides, where some stretches even show opposite tendency regarding subsurface lithology (van den Ham et al., 2014). This underlines the importance of other factors than solely the lithology related to geological history. Regarding the slope angle, again large variability can be observed (Fig. 20). From all the data Wilderom (1979) collected and described, averaged site properties were deducted. These site properties can be related to an average flow slide probability based on the total length of susceptible estuary banks. Moreover, these properties can be related to the frequency of occurrence of flow slides. The average frequency of flow slides in Zeeland was found to be 0.02/km/year (van den Ham et al., 2014) with a total estuary bank length of approximately 190 km. Averaged site properties are summarized in Table 1.

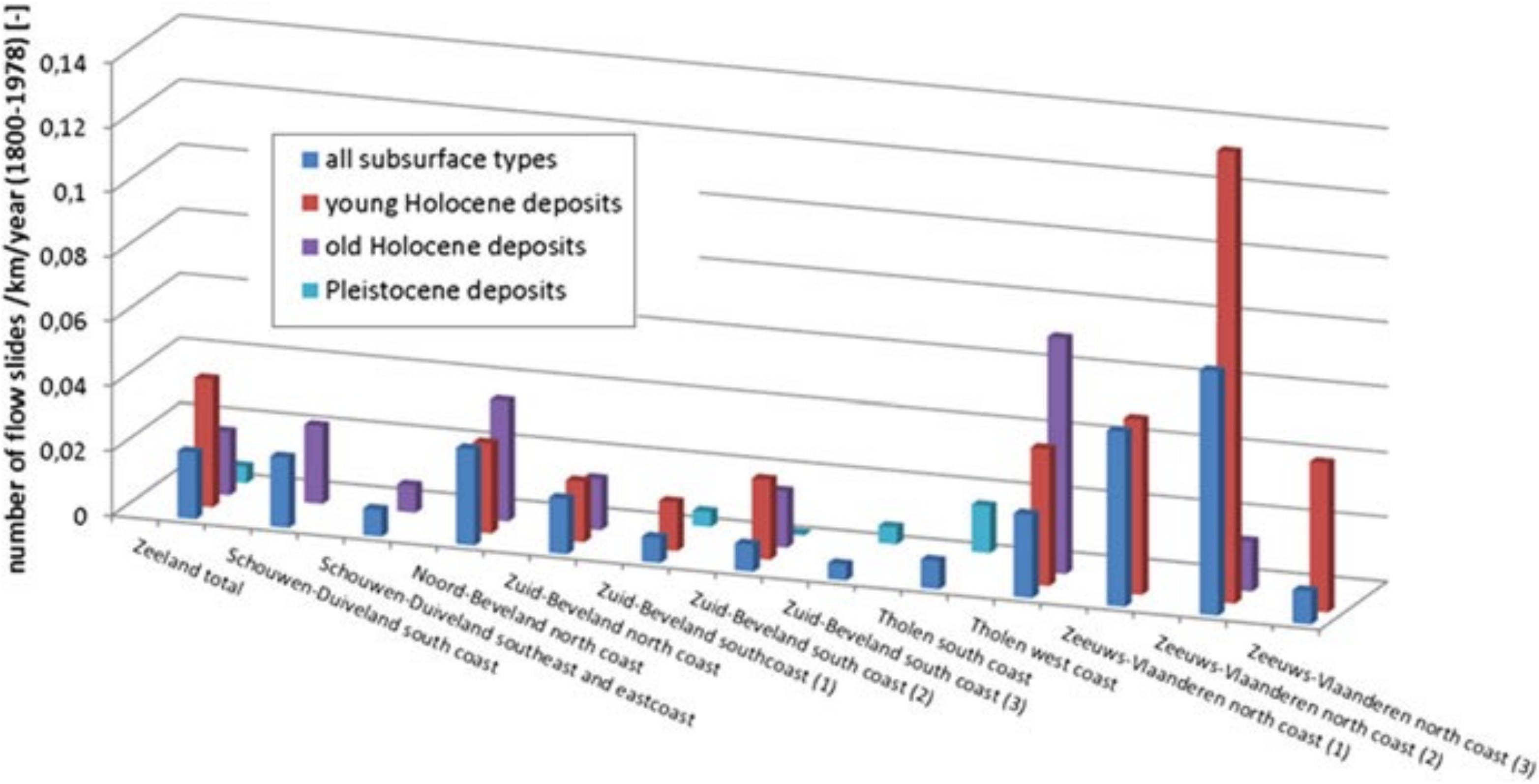

Figure 19: Frequency of flow slides for all estuary banks as a function of geology within Zeeland documented by Wilderom, 1979).

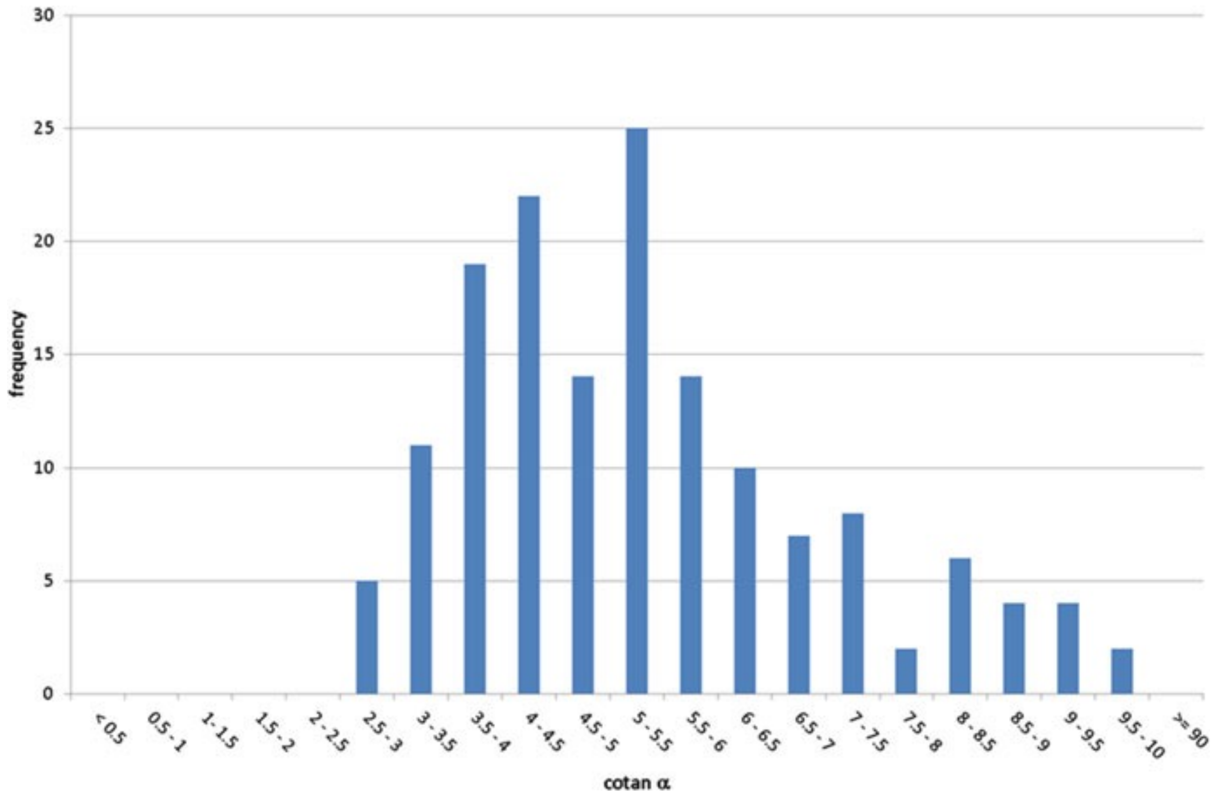

Figure 20: Cotangent of average slope angle (α) for flow slides in Zeeland documented by Wilderom (1979).

Table 1: Averaged site properties based on empirical data from flow slides in Zeeland.

Parameter	Averaged value
mean slope height (H_R)	24 m
mean slope angle	1:5
mean relative density	30 %
state parameter (ψ) (van Duinen et al. 2013)	-0.05
mean median grain size	200 µm

2.3.4 Testing for flow slides

In present day, probability of flow- slides for the Dutch estuary and river banks are tested through application of a standardized safety protocol based on a step by step safety assessment (Deltares, 2017; Rijkswaterstaat, 2017, 2016; van den Ham et al., 2012). The safety assessment is supported by modelling programs, such as D-Flow Slide (Deltares, 2018). Based on empirical data from historical cases a semi empirical method has been developed to quantify the influence of site characteristics on flow slide probability (Rijkswaterstaat, 2016; van den Ham et al., 2012; van den Ham et al., 2015; van Den Ham et al., 2014). This method tweaks the flow slide probability with a mean slope as starting point and quantifies the influence of local deviations using empirical data. As most flow slides encompass both mechanisms of static liquefaction and breaching the probability of flow slides can be written as:

$$P(ZV) = \left(\frac{5}{(\mathrm{cotan}\alpha_{\mathrm{R}})}\right)^{5.7} \left\{0.5 \cdot \left(\frac{(H_R)}{24}\right)^{2.5} \cdot \left(\frac{1}{10}\right)^{-10(0.05+\psi)} + 0.5 \cdot \left(\frac{(H_R)}{24}\right)^{5} \left(\frac{2\cdot 10^{-4}}{D_{50}}\right)^{5} \cdot Fcohesivelayers\right\} \cdot L_{vak} \cdot \frac{Vlocally}{VZeeland} \cdot 0.025\, km^{-1} \cdot year^{-1} \tag{2}$$

Within this equation, the occurrence of liquefaction is dependent on (1) stress state, expressed by the fictitious slope height, H_R (Fig. 22; Deltares 2017). The height of the above water part of the slope is also included with the average of the underwater slope and slope angle (cotanα_R) to simulate the most un-favourable situation of water overpressure during the assessment.

Furthermore, probability of liquefaction depends on (2) packing of the liquefiable layer expressed in relative density (I_D) of the subsoil or state parameter (ψ). Thickness of the layer is set to be 5 meters as this is the minimal thickness of a layer to be vulnerable to liquefaction. For the occurrence of breach flow, medium grain size (D_{50}), presence of clay layers (F cohesive layers) and presence of disturbing layers, such as peat, are included as important parameters too (van den Ham et al., 2014). F may vary from 1/3 (no clay layers) to 3 (many clay layers). For Zeeland's alternation of clay layers within the sand successions of young Holocene depositional age, F=1 representing the median. Furthermore, the equation was extended with movability of foreshore, $\frac{Vlocally}{VZeeland}$ and length of the dike section, L_{vak} in km.

Further explanation on the above stated formula can be found in Appendix 2.

As flow slides can lead to instability of the foreshore, a displacement of a metastable sand body can occur. Within the D-Flow Slide therefore, displacement area and corresponding retrogression length for the inserted foreshore profile is determined through an iterative probabilistic calculation (Fig. 21; Deltares 2018). Within a flow slide, sediments will partly displace to the sides of the profile resulting in displaced sediment volume, which is a factor 1:4 greater for area 1 compared to area 2. Furthermore, 2 different slopes apply in the displacement profile with a steep slope for the upper part and a more gentle slope in the lower part.

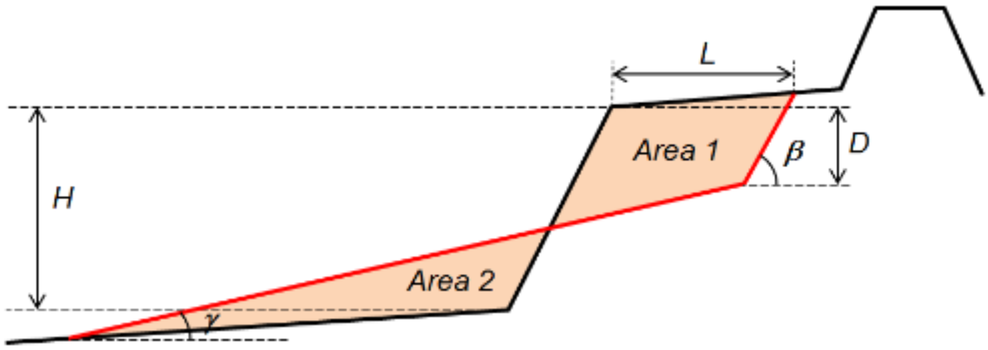

Figure 21: Displacement of a sediment area during a flow slide, and the retrogression length L. Where D represents the steepest part of the damage profile for the dike, H is the water level (m) and β, and γ represent the slope angles of the different area's(Deltares, 2018)

Depending on inserted parameters, for each foreshore situation a retrogression length can then subsequently be determined through probabilistic calculation. To test if sediment displacement influences dikes in the hinterland, retrogression is compared to the allowed retrogression length for that particular dike – foreland area to determine if displacement of sediment would damage the excising profile (Equation 3; Deltares 2018).

$$Z = L_{allowed} - L \tag{3}$$

In this equation $L_{allowed}$ is a value representing a typical safety zone around dikes and L is the calculated retrogression length for the inserted parameters in D-Flow Slide.

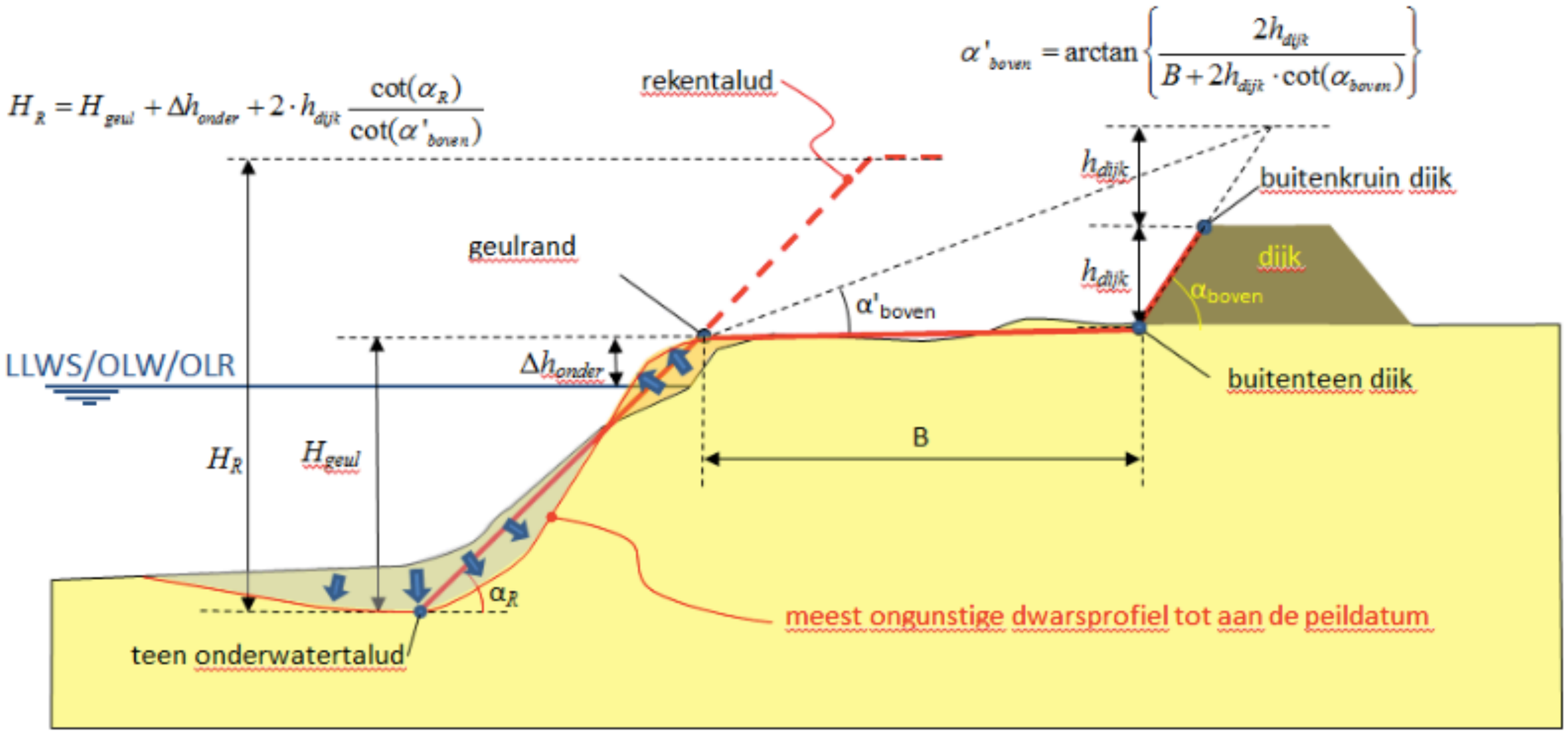

Figure 22: determination of H_R in its most unfavourable situation during the assessment period. In this figure: Hgeul is depth of the channel [m], Δh_{onder} is the height of the slope above the water level during extreme low water: "niveau van geulrand" – "niveau LLWS/OLW/OLR" [m], h_{dijk} height of the levee with respect to the outer toe of the levee [m], B is the width of the foreland. In case of a so-called "schaardijk", B = 0 [m], cot(α) is the cotangent of the slope α [-], α_R is the slope angle of the schematized fictitious under water profile [degrees], α_{boven} is the slope of the outer slope of the levee [degrees] and α'_{boven} is the slope between incision of channel and the fictitious outer crest of the levee with a height of $2.h_{dijk}$ In case of a "schaardijk", α'boven = αboven [degrees] (Deltares 2017).

3. Methodology

In this combined literature, fieldwork and modelling study the stability of 3 foreshore systems (salt marsh and mudflats) for 3 locations within the Eastern Scheldt were studied from a combined lateral and vertical perspective. Firstly, three different foreshore systems, were selected based on literature review. This was coupled with an analysis of aerial photographs and Google-Earth images for locations with different energetic conditions and for which cone penetration data were available. Then locations for sampling cross-sections were selected, including 1) a salt marsh 2) a mudflat and 3) a sea connected channel.

Furthermore, for every location a reference cross-section was selected, where only tidal mudflat is present in front of the adjacent dike. This reference cross section was sampled to identify different stability characteristics depending on 1) location with reference to the dike, and with or without presence of salt marshes (section 3.1). The lithological succession of these pre-selected cross-sections were subsequently studied and sampled for two different scales in the field; (1) lithology of top sediments (shallow sediment cores, 0-30 cm below surface) and (2) lithology of deeper sediments (deeper sediment coring up to 5 meters) (section 3.2).
Additionally, penetration resistance was determined for each of the surface sampling sites as a measure of load bearing capacity. Also, undrained shear stress (shear vane), representing the upper soil erosion probability, was measured for each of the surface sampling sites (section 3.2).

In the laboratory of NIOZ, at Yerseke, bulk density of the surface and deeper lithology was determined. For surface lithology, also presence of organic and inorganic material (root and shell density) and moisture content were obtained (section 3.3). Lithological profiles and analytical results were subsequently related to the degree of stability for the foreshore systems of the 3 locations for various depths. Focusing on bulk density, grain size distribution, presence of (an)organic matter and moisture content, results were mapped in a vertical and lateral perspective using Excel and Matlab. Furthermore, based on the lithological characteristics found for deeper sediments related to the geological background, a global and detailed test was executed for probability of flow slide (section 3.4) and tested for multiple theoretical scenario's.

3.1 Pre-analysis studied area

Firstly, the 3 locations of the studied foreshores were chosen meeting the following criteria by using available data (Table 2):

- Visual estimate of varying energetic conditions within the estuary.
- Susceptibility to soil liquefaction (Kanning, 2012; Stoutjesdijk, de Groot, & Lindenberg, 1995; TAW, 1999)
- Each location contains three sub-environments, 1) a salt marsh 2) a tidal mudflat and 3) a sea connected channel and a stretch of tidal mudflat without a salt marsh present in between dike and waterfront.
- The foreshore systems chosen, are at a convenient distance to the NIOZ Laboratory at Yerseke and can be easily reached by car.
- Cone penetration test (CPT) data is available from GSN-TNO, DINOloket close to the chosen locations.
- No foreshore strengthening in the form of a revetment is present at chosen locations.

To this goal, the following data and software were used:

Table 2: Software and data used with choosing three locations within the Eastern Scheldt.

Software and data
RWS - webmappingservice; Aerial photography of the Netherlands, 1996 to 2014
EWJ Aerial photography of the Netherlands, 2016
GSN-TNO, DINOloket; cone penetration data of the Eastern Scheldt
GOOGLE EARTH Pro (2018)

This resulted in the selection of three foreshore systems: 1)Krabbendijke; 2)Dortsman-Zuid and 3)Krabbenkreek (Fig. 23 & 24). The most energetic location of these three foreshore systems is Dortsman-Zuid followed by Krabbendijke and Krabbenkreek. Transects were drawn perpendicular to the dike toe with the help of Google Earth. For each location one transect was drawn through the salt marsh and the adjacent mud-flat bordering the channel margin. The total length of this transect was chosen to be twice the width of the tidal salt marsh projected over the mudflat. A second transect was drawn on the mudflat, where no salt marsh was present between dike and channel margin. The length of this transect was set to be once the length of the tidal salt marsh to scale the vertical stretch of the obtained core and sample data from both transects.

Figure 23: (upper) Location of the Eastern Scheldt from a global and Dutch perspective. (lower) Location of the three tidal salt marsh- mudflat units within the Eastern Scheldt. (GOOGLE EARTH Pro, 2019; https://en.wikipedia.org/wiki/Netherlands#/media/File:EU-Netherlands.svg)

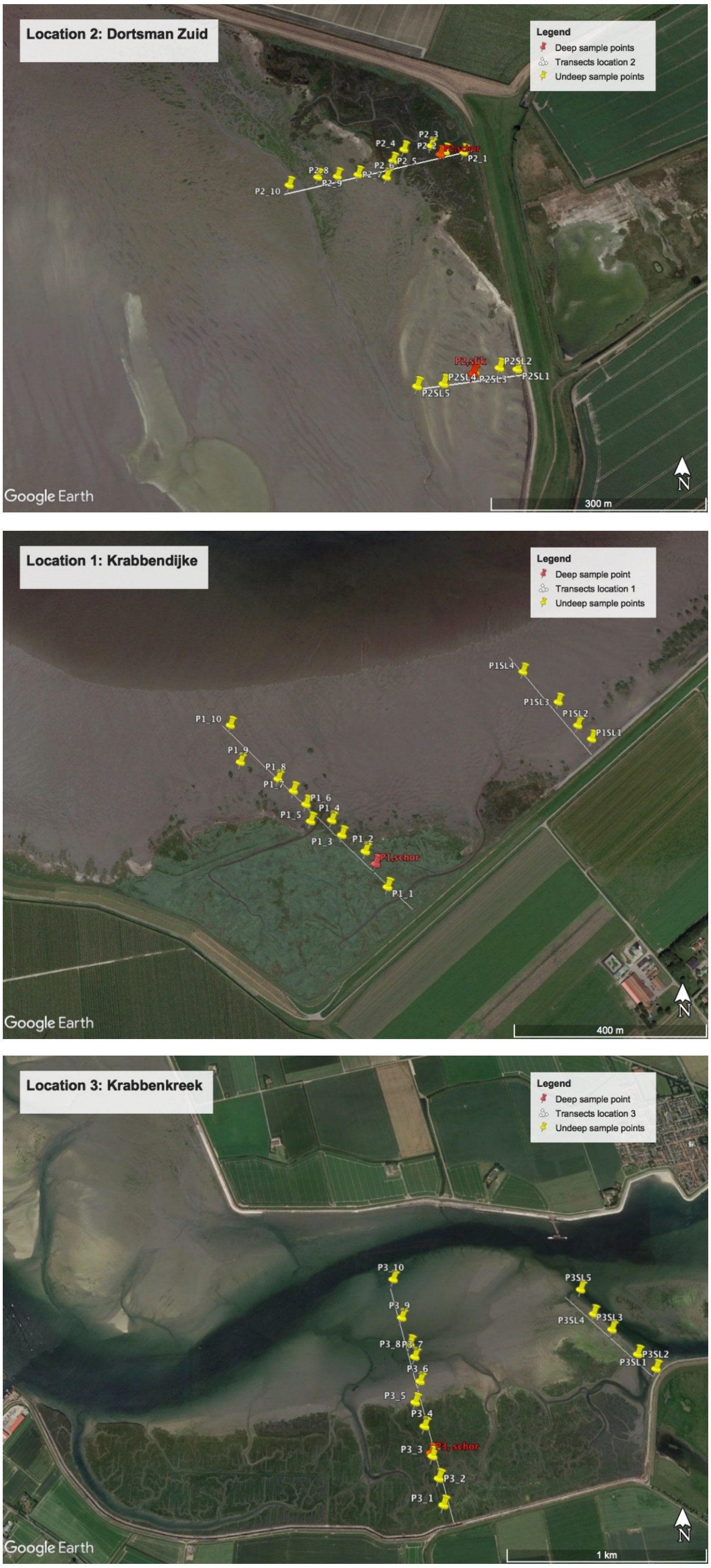

Figure 24: The three foreshore locations (upper) Krabbendijke, (middle), Dortsman-Zuid and (lower) Krabbenkreek with one transect drawn for the salt marsh and the adjacent mud-flat bordering the channel margin and a second transect drawn for the mudflat where no salt marsh is present between the dike and the channel margin.

3.2 Fieldwork

3.2.1 Lithological succession

During the fieldwork in the Eastern Scheldt, lithological succession of pre-selected cross-sections were subsequently studied on two scales:
(1) Shallow sediment cores (0-30 cm below the surface) and according reference cores were taken for all sections and were subsequently analysed at NIOZ (Yerseke) for its bulk density and presence of organic material (root density) and lithology.
(2) Deeper sediment cores were taken to a depth of 3 to 5 meters below surface. The succession was visually described and lithological properties; grain size and presence of organic material, were determined in the field. Samples of deeper cores were analysed at NIOZ, Yerseke for its bulk density.
The lithological characteristics were obtained by different sediment coring techniques.

Properties, grain size and presence of organic material, were described in the field using paper sounding charts with the USDA soil classification (Soil Survey Staff (SSS), 2010) and processed digitally with the program LLG (Cohen, 2018). Regarding the surface sediment coring of 30 cm depth, 10 points were sampled along transects perpendicular to the adjacent dike for the 3foreshore systems of the 3 locations. Coordinates of sampling points were first selected through use of Google Earth and at locations with clear morphological features visible and a slight higher density around the transition of saltmarsh and mudflat (overview shown in Fig. 23 & 24).

Another reference transect containing 5 points for locations Krabbenkreek and Dortsman- Zuid and 4 points for location Krabbendijke was sampled, where the salt marsh was absent and only a mudflat lied in between the waterfront and the adjacent dike.

Surface sediment samples were collected using PVC soil cores of 30 cm in length with a diameter of 5.2 cm. For each of sample point on the salt marshes 2 cores were obtained versus 1 core per sample point on the mudflat. Concerning content of the 2 cores taken per salt marsh sample point, 1 core was used to determine volume and weight of root and shell material for correcting bulk density of collected samples. The content of the second core (salt marsh sampling point) was used to determine bulk density (design shown in Fig. 25).

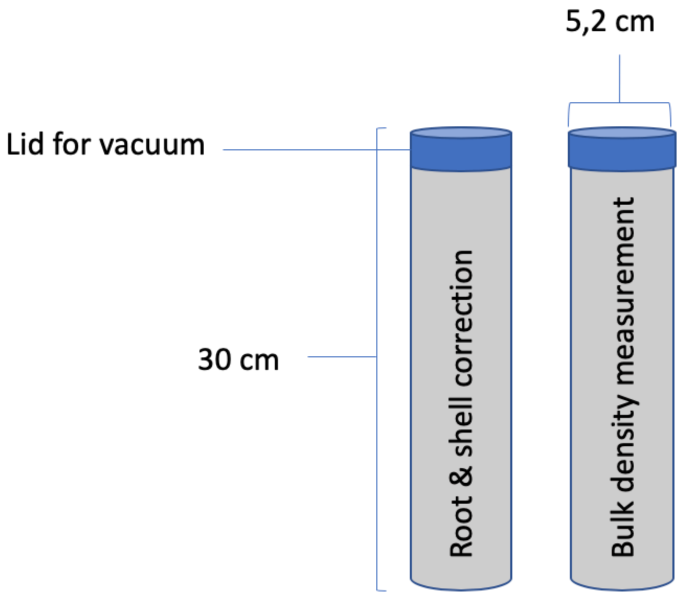

Figure 25; Design of 2 PVC tubes for the topsoil coring and sampling with air tight lids bring vacuum during coring by which the sediment is retained in the PVC tubes. One core is to determine the bulk density. The second core is used to correct for root and shell content.

For each of the 3 locations, 1 deeper core was taken in the salt marsh environment. For the upper layer (until the groundwater level) of this deeper drilling, the so-called Edelman corer (Berendsen, 2005a) was used. Then, the so called 'gouge' was used for the more clayey layers and a Staay suction corer for the predominantly sandy layers below groundwater (van de Meene, E. A., Van der Staaij, J. Teoh, 1979).

For these samples, a soil sample was obtained for every 5-cm depth with a predetermined fixed volume cuvette of 5 x 1 x 1 cm and collected in labelled 40 ml containers for further analysis at NIOZ, Yerseke.

3.2.2 Topsoil stability and erosion probability

Penetration resistance of the top 50 cm of soil was studied as a measure of load bearing capacity using a penetrologger with GPS (Eijkelkamp Agrisearch Equipment, 2010), which is shown in Figure 26. Hereby penetration resistance in Mega Pascal (MPa) is measured. This measurement is repeated 3 times per location to lower the degree of error within the measurement. The cone type used was 3.3 cm^2/ 60 degrees and the averaged penetration speed of 2 cm/s was applied. As a measure of topsoil erosion probability, the shearvane (kPa/kN m^{-2}) was measured using a Pocket vane tester (Fig. 26; Eijkelkamp Agrisearch Equipment, 2010; 2011). This measurement was replicated three times on relatively clear soil surface. The vane used was equipped with a measuring range, MR_{max} of 0.007575 (kg/cm^2).

$$\tau = \frac{RO}{10} \cdot MR_{max} \cdot 100 \quad (4)$$

Figure 26: The penetrologger (right) and the pocket shear vane tester (left) for testing the topsoil penetration strength and the topsoil erodibility (Eijkelkamp Agrisearch Equipment, 2010;2011)

Calculation of shear strength (τ) for the top soil was done by converting movement per reading (RO, read out), (value of 1 to 10), which represents 1/10 part of the complete revolution to a total kPa/ kN m-2 value. Here the maximum measuring range MRmax was included and a multiplying factor of 100 to obtain the value in kPa/ kN m-2 (Equation 4).

3.3 Laboratorial analysis – root and bulk density

3.3.1 Shallow cores

To determine bulk- and root density of the subsurface soil for shallow cores, each core was sliced in the lab to known volumes. For the first 5 cm, cores were sliced every 2,5 cm and sliced every 5 cm for the remaining sample. This resulted in 2 samples of 53 ml and 5 samples of 106 ml per core (Fig. 27).

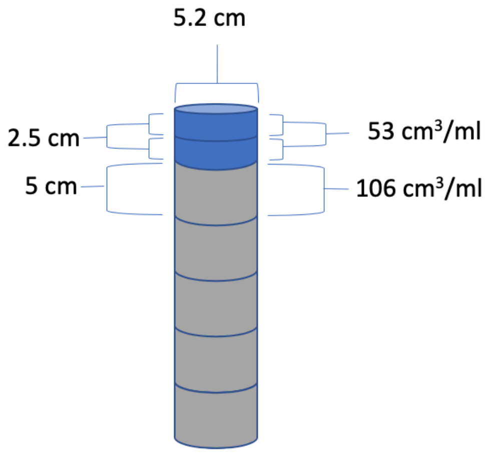

Figure 27; Slices and volume division for each 30 cm core

The samples were then collected in large zip lock bags and they were labelled with date of sampling, type of environment (salt marsh or mudflat) and depth. After collecting the samples in the bags, wet weight of the samples including corresponding bags was determined with an electronic scale (precision of 0.001 gr) and dried in a freeze dryer at the NIOZ Laboratory for a minimum of 72 hours. After freeze-drying the dry weight of each sample was determined with an electronic scale (precision of 0.001 gr). In the processing of the data the sample weight was corrected for the weight of the bags to determine the wet bulk density (ρ_b, Equation 5; Dadey et al., 2006), dry bulk density (ρ_t, see Equation 6; Dadey et al., 2006).

$$\rho_b = \frac{M_S}{V_t} \tag{5}$$

$$\rho_t = \frac{M_t}{V_T} \tag{6}$$

In the formulas mentioned above M_S represents the mass of the soil in wet state. Mt is mass of freeze dried soil corrected for organic matter and shell content (see section 3.3.2 & 3.3.3). Vt represents the corrected volume over which the bulk density is determined.

3.3.2 Correction for organic matter

For each of the salt marsh samples the dry weight bulk density had to be corrected for roots in the sample. To this aim, roots present in one of the two salt marsh cores were washed and collected from the sample with a 500-micrometer sieve and collected in 40 ml plastic containers. These plastic containers where labelled with the specific sample location and depth. The weight of wet roots together with the containers was determined with an electronic scale.

After weighing the volume of wet roots for each slice was determined with an indicative method based on the law of Archimedes, where root volume was assumed to equal the amount of water being displaced by the roots. To this method, milliQ water was brought to a temperature of 20 degrees in a water bath (with a known density of 0.9982 $g/cm^3/ml$) and the density was evened off to a value of 1 g/ml for simplicity during these measurements.

Weighing the glass jar with water and correcting for the weight of the jar determined the volume of a glass jar with lid solely filled with water. As density of the water has a value of approx. 1 g/ml, we can assume that this weight is equal to the volume of water. This volume measurement was then carried out for a glass jar filled with roots and water for each sampled core slice and corrected for the weight of the jars and the water.

After these volume measurements, roots were dried in an oven at 60 °C. After drying the weight of both dry roots was determined with an electronic scale (precision of 0.0001 gr).
The obtained ratio of dry root mass and root volume was used to correct the bulk density values of non-washed out samples. Furthermore, values of weight and volume were used to determine the percentage of organic matter in samples.

3.3.3 Correction for shells

After slicing and freeze-drying mudflat samples, it became apparent, that many samples were inhomogeneous, caused by the presence of large shells, stones and wood pieces, thereby disturbing calculations for sediment bulk density. To overcome this error, calibration curves were obtained for the dry weight/wet volume of the shells. Firstly, all mudflat samples were visually scanned for larger fragmented shell pieces or whole shells present (greater than 1000 µ); smaller materials were accounted for as original of bulk density.

Samples were sieved after freeze-drying with a 1000 µ sieve and sediment and shells were recollected separately. Shells were collected in small zip lock bags. The weight of shells and adjoining bag was determined in wet and dry state and corrected for the weight of the bags afterwards. Volume of shells was determined with the same method as described for the determination of root volume. With dry weight and wet volume of the material> 1000 mu, calibration curves for shells and other material >1000 mu were made for all three locations (Fig. 28, 29, 30).

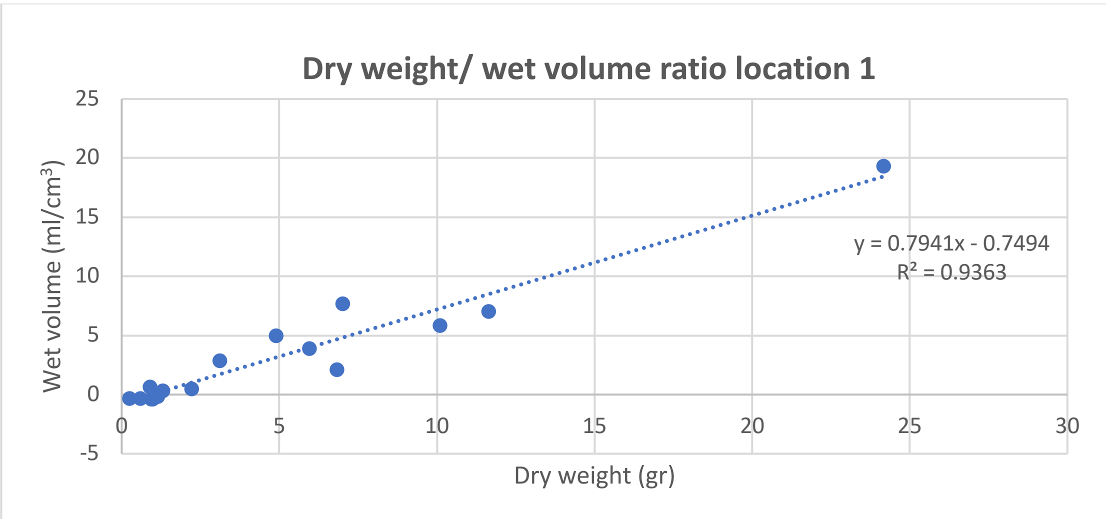

Figure 28: Calibration line for the shells dry weight and wet volume for location 1; Krabbendijke

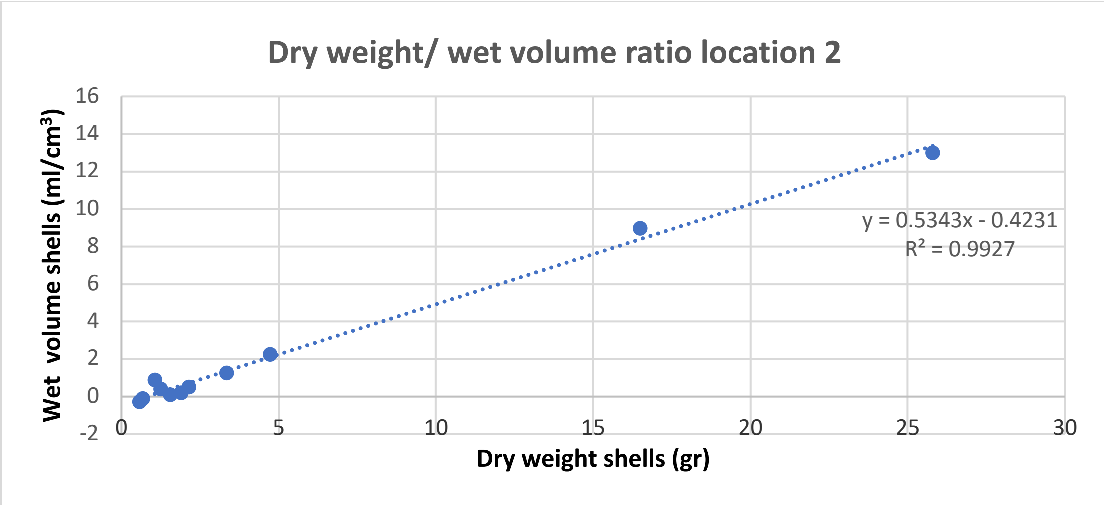

Figure 29: Calibration line for the shells dry weight and wet volume for location 2; Dortsman- Zuid

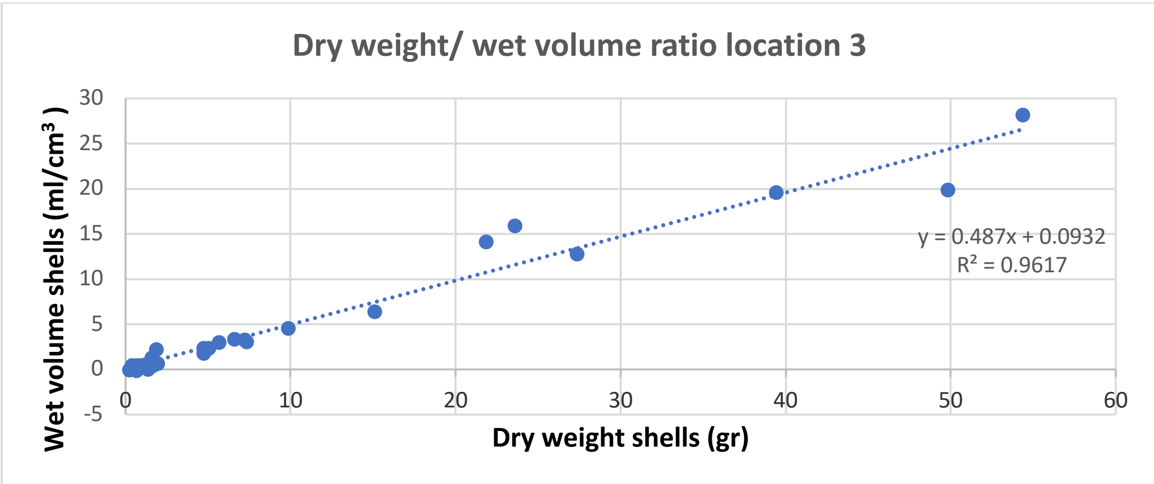

Figure 30: Calibration line for the shells dry weight and wet volume for location 3; Krabbenkreek

As these calibration lines share a value of R^2 higher than 0.9, the corresponding equations shown in the plot area were used to determine the volume matching the dry weight of the shells, thus correcting the bulk density of the sediments. Also, the dry weight/volume ratio was used to determine the percentage of shell material >1000 mu within the sediment.

Additionally the gravimetric moisture content within the sample also (Clarke Topp et al., 2010;Hendriks, 2010):

$$u = \frac{(Mw - Md)}{Mw} * 100\ \% \quad (7)$$

Where u is the moisture content, Mw is wet weight of the sample and Md is dry weight of the sample.

3.3.4 Deep Cores

For deep samples also, dry bulk density was determined for every 5- cm core. Therefore wet- and dry weight (Mw & Wd) were subsequently measured. Afterwards, wet bulk density (ρ_b, see Equation 5), dry bulk density (ρ_t, see Equation 6) and moisture content (see Equation 7) of each soil sample were determined.

3.3.5 Laboratory analysis – grain size distribution

For all samples, sediment particle sizes were determined by laser diffraction (Malvern Master sizer) with a detection range of; 0,02 – 2000 µm. Before measuring, samples were sieved over a 1 mm sieve. Organic matter and carbonate were not removed prior to the analysis of the laser diffraction. During this analysis, various sediment parameters were determined, summarized in Table 3 together with their application in this study:

Table 3: Parameters obtained by the Mavern Master sizer, and application in study per parameter.

Parameters obtained Malvern Master sizer	Application in study
10% percentage (10% smaller then…µm)	Extrapolated to value of D15, D -Flow slide
90% percentage (90% smaller then …µm)	-
Median grainsize D50 (µm)	Lithological description, D - Flow slide
Median grainsize D50 (PHI)	-
Silt % < 63 µm	Used in lithological description, shallow cores
Very Fine sand fraction (PHI 3–4, 62.5-125 µm	-
Fine sand fraction PHI 2-3, 125-250 µm	-
Medium sand fraction PHI 1-2, 250-500 µm	-
Coarse sand fraction PHI 0-1, 500-1000 µm	-
Modus grainsize in µm	Used in lithological description, shallow cores

3.4 Determining the probability of flow-slides

In this study, the software tool D-Flow Slide of Deltares was proposed to be used, in which a step by step safety assessment is being supported (Deltares, 2017, 2018). The first step in this assessment, known as the global assessment method (APPENDIX 3a), entails the examination of the geometry only for the area of interest and its sensitivity to flow slides. An important factor to diminish the possible risk of flow slides occurring is the presence of slope protection such as a revetment. With a revetment, erosion at the channel margin is not possible and the initiation of a flow slide will not occur. For the 3 locations chosen within the Eastern Scheldt, no revetments are found to be present (APPENDIX 4).

With soil data available, a second step of the assessment can be performed, named the detailed check (APPENDIX 3b). In this second part of the assessment, the probability to flow slides is tested for both its geometry and soil parameters. Furthermore, the chance is determined of exceeding the acceptable length taken from the channel margin over which the foreshore is being eroded; $Z = L_{acceptable} - L$. Also in the D-Flow Slide program a third step of analysis is possible if the detailed check is not passed, applying the advanced models SLIQ2D and HMBreach (Deltares, 2018). In this study this third step in the assessment could not be included due to insufficient input data.

3.4.1 D-Flow Slide, input parameters

For the execution of the global assessment (APPENDIX 3a) a surface line with ascending x- value from the channel side of the embankment to the dike top at the polder side was inserted in the program D-Flow Slide (Deltares, 2017, 2018). The five following characteristic points are mandatory in D-Flow Slide with increasing x- and varying z-value:

Bottom river channel(B)

Insert River channel (C)

Dike toe at river (D)

Dike top at river (G)

Dike top at polder (J)

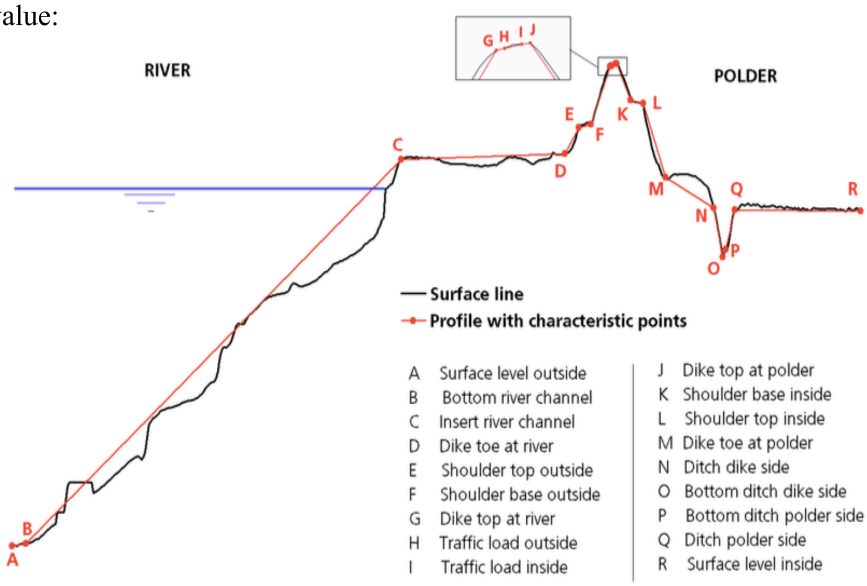

Figure 31: Surface line to be inserted in D Flow Slide with characteristic surface points. Points B, C,D,G and J are mandatory (Deltares, 2018)

Points were selected from the bathymetry and topography for the 3 locations based on laser altimetry and multibeam data of Rijkswaterstaat (vaklodingen, year 2016) and data of AHN 3 (Actueel Hoogtebestand Nederland, 2014). Within ArcGis different theoretical scenarios were created by selection of varying characteristic points (B,C,D,G,J) along one profile line for each location. Hereby all parameters were kept constant and insight was obtained in flow slide probability for different scenario's, where:

- Either both a mudflat and salt marsh were present vs solely the presence of a mudflat
- The location of the channel changes along the profile line

Furthermore, a soil profile for the subsurface of the considered tidal salt marsh mudflat units was required. For different lithological layers a description was to be included considering colour, lithology, standard deviation of D_{15} (particle diameter representing the 15% cumulative percentile value in µm) and standard deviation of D_{50} (particle diameter representing the 50% cumulative percentile value). Lithology data obtained in the field (until an averaged depth of 5 meters) were combined with lithology data from the subsurface model GeoTOP v1.3 (GSN-TNO, Dinoloket 2018) to a depth of 35 meters. The depth of 35 meters as lower boundary was based on the advised influence depth of 0.5 *H_R (Fig. 23; Rijkswaterstaat, 2016; van den Ham, G A de Groot & van der Ruyt, 2012; van den Ham, Geeralt A. van der Ruyt, 2009; G A van den Ham et al., 2015).

For grainsizes of sandy subsurface layers, D_{50} and D_{15} values were based on the minimum and maximum values of the 'medium fine sand' category given in D-Flow Slide (Deltares, 2018), as shown in the Table below (Table 4). The 'medium fine sand' category was chosen, as no outcome was produced for the category 'very fine sand', for calculating the chance of breach flow within the global and detailed check. Only the category 'very fine sand' could be used, when including more parameters and executing the advanced models. For the non- sandy layers D_{50} and D_{15} were based on the deep core D_{50} and D_{10} determination of the Malvern master sizer. D50 values were averaged for each lithological soil type over the obtained 5 meter depth. The D_{15} was obtained through multiplication of the D_{10} values with a factor of 1.5, for each lithological soil type. However, the program accepts a ranging value for grainsize of 30-2000 µm. A great part of the D_{50} and D_{15} values for non- sandy layers turned out to be smaller than 30 µm. Therefore, values of D_{50} and D_{15} with lower value then 30 µm were based on example values as presented in the D-Flow Slide manual (Deltares, 2018).

Table 4: Texture, description and D50 value of the different types of sand used to describe the grain sizes of the different lithological classes within D-Flow Slide (Deltares, 2018).

Description	
Very fine sand	D50 < 200 µm and D15 < 100 µm
Medium fine sand	200 < D50 < 500 µm and 100 < D15 < 250 µm
Coarse sand and gravel	D_{50} > 500 µm and D_{15} > 250 µm

An example of the surface line, soil table and soil profile as shown in D-Flow Slide is shown in Figure 32.

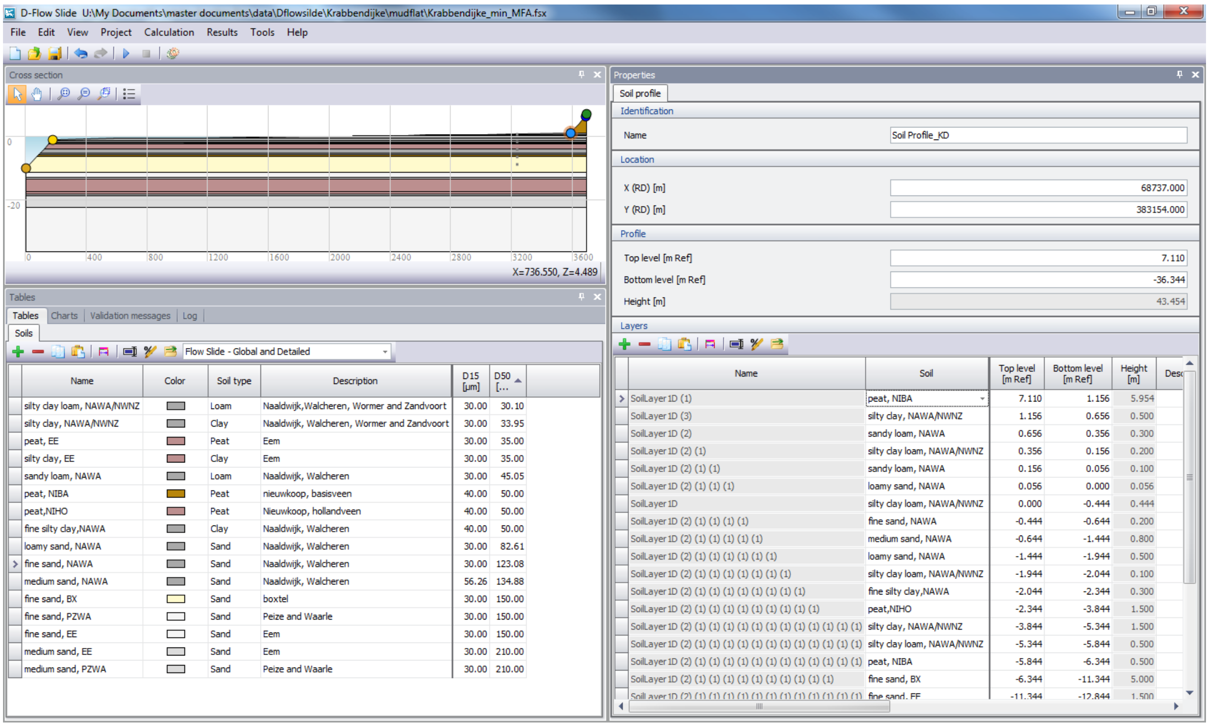

Figure 32. Overview of surface line (top right), soil table (bottom left) and soil profile (bottom left) in D-Flow Slide.

For the detailed check, the following parameters were inserted additionally, which concerns water, revetment, foreland, soil and influence zone characteristics, summarized in Table 5. These parameters were kept constant for the 3 locations. For the water level, the default averaged level of 0 m was chosen and for the unit weight water [kN/m^3] 9.81 was taken. For the top revetment length (part of concrete strengthening between dike and dike side of the salt marsh) an averaged value of 5 meters was inserted. The width of the top revetment was based on the width measurements of this concrete part for the three locations with ArcMap from the topography data of Rijkswaterstaat, vaklodingen, year 2016.

No bottom revetment is present at the 3 locations (Fig. 33 & Appendix 4). As the x-value for the first characteristic point ‘Bottom river channel (B)’ had to be set to a value greater than zero to be valid in the program, ‘B’ was set to 5 m. The parameter ‘x start bottom revetment’ was inserted to an equal value as for ‘B’ to the starting point of the of 5 meters to overcome the following program error of D-Flow Slide: *‘RX start of the bottom revetment cannot be defined outside the surface line’*.

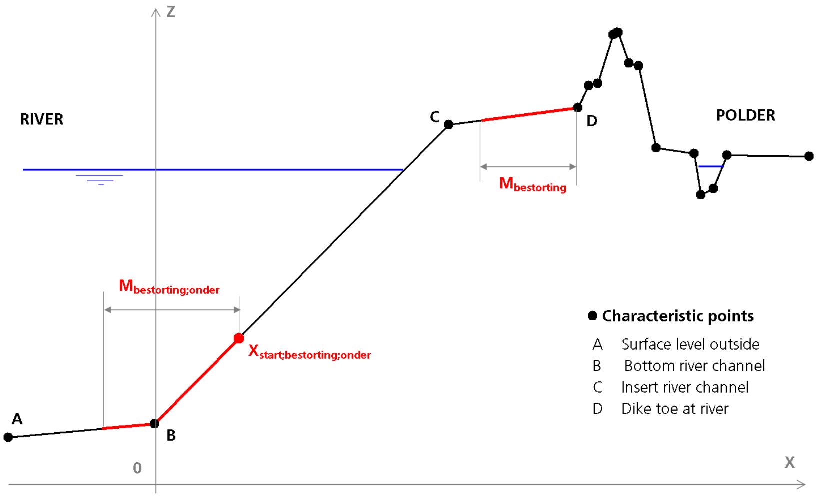

Figure 33: Definition of the revetment parameters (Deltares, 2018).

As no artificial foreland is present for the three locations ‘no’ is inserted within the foreland theme. For the theme of soil, a value of -0.05 is inserted and for the state parameter over 5 meters thickness, which is based on the averaged value for Zeeland (Rijkswaterstaat, 2016; Geeralt A. van Den Ham et al., 2014; van Duinen, Bezuijen, van den Ham & Hopman, 2014). For the sand class (particle size) one of the three default descriptions was chosen, ‘medium fine sand’ with 200<D50≤500 µm and 100<D15≤250 µm. Based on the embankment management plan 2016-2020 (Waterschap Scheldestromen, 2016) the influence zone of three dike segments was set to be 350 meters, in which protection zone A and B were taken together (Fig. 34). These zones contribute both technically as physically to the stability of the dike. Therefore, an effect of flow slides within this zone could have a damaging impact on the dike. Further explanation of these dike protection zones can be found in Appendix 5 (in Dutch).

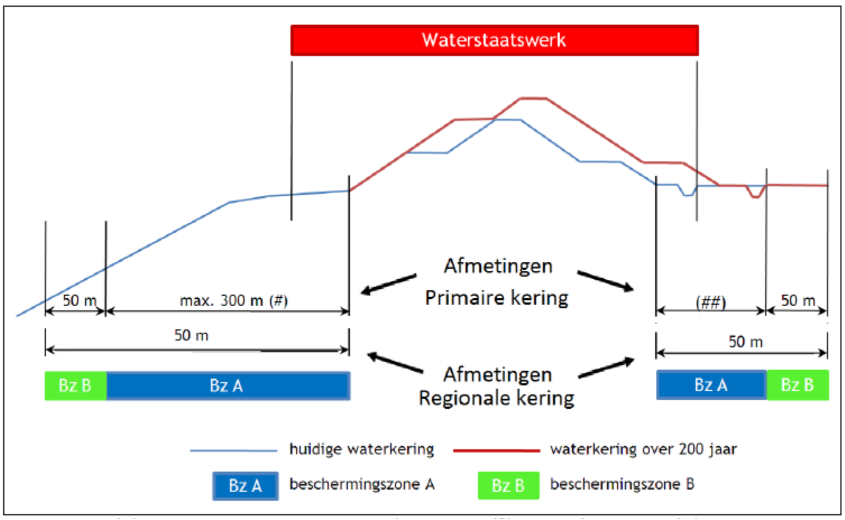

Figure 34: Mapping of safety zones for primary flood control measures within the responsible area of Waterboard Scheldestromen (Waterschap Scheldestromen, 2016).

Table 5: Overview of general parameters to be inserted for the execution of the detailed check within D-Flow Slide.

Water	Inserted values
Water level [m]	0 m
Unit weight water [kN/m^3]	9.81
Revetment	
Top revetment length [m]	5 m
X start bottom revetment [m]	5 m
X start bottom revetment [m]	-
Foreland	
Is artificial foreland [yes/no]	no
Soil	
State parameter Psi 5 m [-]	-0.05
Sand type (particle size)	medium fine sand
Influence zone	
Distance dike toe/influence zone [m]	350 m

Furthermore, the second step of the assessment, the detailed check, following parameters had to be inserted (Table 6). For the 'Area ratio', the default value of 1.4 was used, which represents the displacement ratio of area 1 and 2 (Fig. 21; Deltares 2018). This value was based on the Manual of D-Flow Slide (Deltares, 2017, 2018). For the parameter 'considered dike length' the value of 1000 meters was chosen as the probability of flow slides was calculated per *km (1000 m)* per year (Geeralt A., van den Ham et al., 2014). The 'migration velocity' of 10 m/yr was based on a generalized value mentioned in the Flow-Slide manuals (Rijkswaterstaat, 2016; van den Ham, G. A. de Groot & van der Ruyt, 2012). In case mm thick clay layers are present, as is frequent in the supra tidal deposits in Zeeland, the 'cohesive layer's factor' holds 1. This factor may vary between 1/3 (no clay layers) to 3 (many clay layers) (van den Ham et al., 2014).

Table 6: Additional parameters

Parameters detailed assessment	
Area ratio [-]	1.40
Considered dike length	1000 meters
Migration velocity foreshore [m/year]	1
Cohesive layers factor [-]	1

3.4.2 D-Flow Slide scenarios

To refine the knowledge of factors impacting the probability of flow-slide within the Eastern Scheldt for the 3 study sites several theoretical scenarios were worked out for the program D-Flow Slide. Within these scenarios, 3 parameters were altered leading to changing values of the flow-slide probability:

- characteristic point D (dike toe at the river side) of the surface line representing the presence of the salt marsh.
- All characteristic points of the surface line, representing 3 scenarios of different channel locations with reference to the dike.
- Alternation of the minimum to maximum grainsize for the deeper sand layers.

The first parameter to change, was the z value (height) of the characteristic point 'D' of the surface line, with its x value (distance from channel) remaining unchanged. This change of point 'D' represents based on hypothetical presence or no presence of a salt marsh in the profile. With salt marsh present, point D was assigned the height of the salt marsh obtained from ArcMap. Without salt marsh, point D was assigned the height of the mudflat, obtained from ArcMap.

The second parameters to be changed were x and z values of all remaining characteristic points (B, C, G, J) of the surface line representing 3 different location scenarios of the deepest channel found for the 3 bathymetry profiles with and without the presence of the salt marsh (first parameter changed). The data of these different characteristic points for the locations Krabbendijke, Dortsman- Zuid and Krabbenkreek is summarized in APPENDIX 6. (Fig. 35, 36 & 37).

The third parameter to be altered was the minimum to maximum grainsize for the deeper sand layers based on the sand class range shown in Table 4.

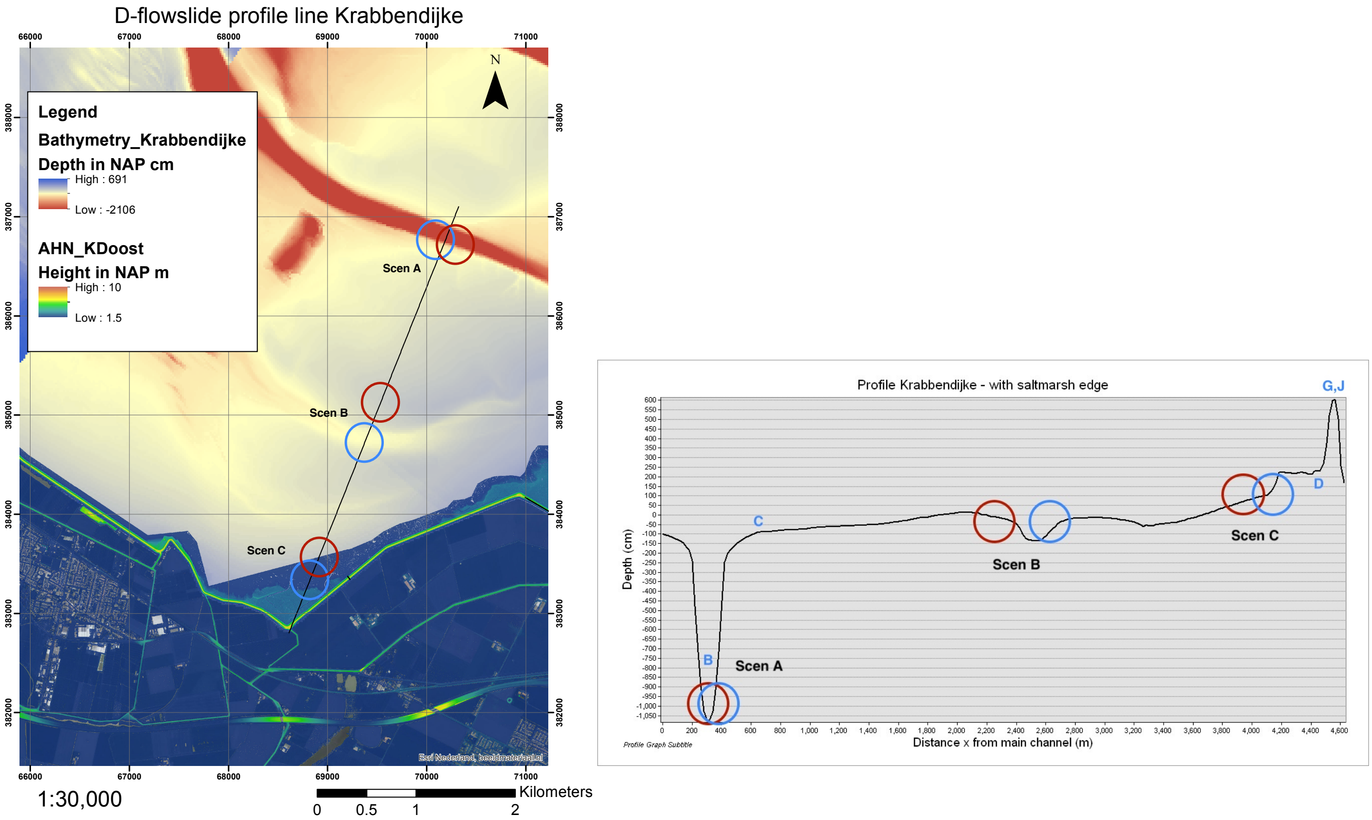

Figure 35: Bathymetry profile line of location Krabbendijke with 3 possible scenarios (A, B & C) of the channel location with salt marsh (red circles) and without salt marsh (blue circles). The position of characteristic points in this Figure correspond to scenario A. With, B (Bottom river channel), C (Insert River channel), D (Dike toe at river), G (Dike top at river) and J (Dike top at polder).

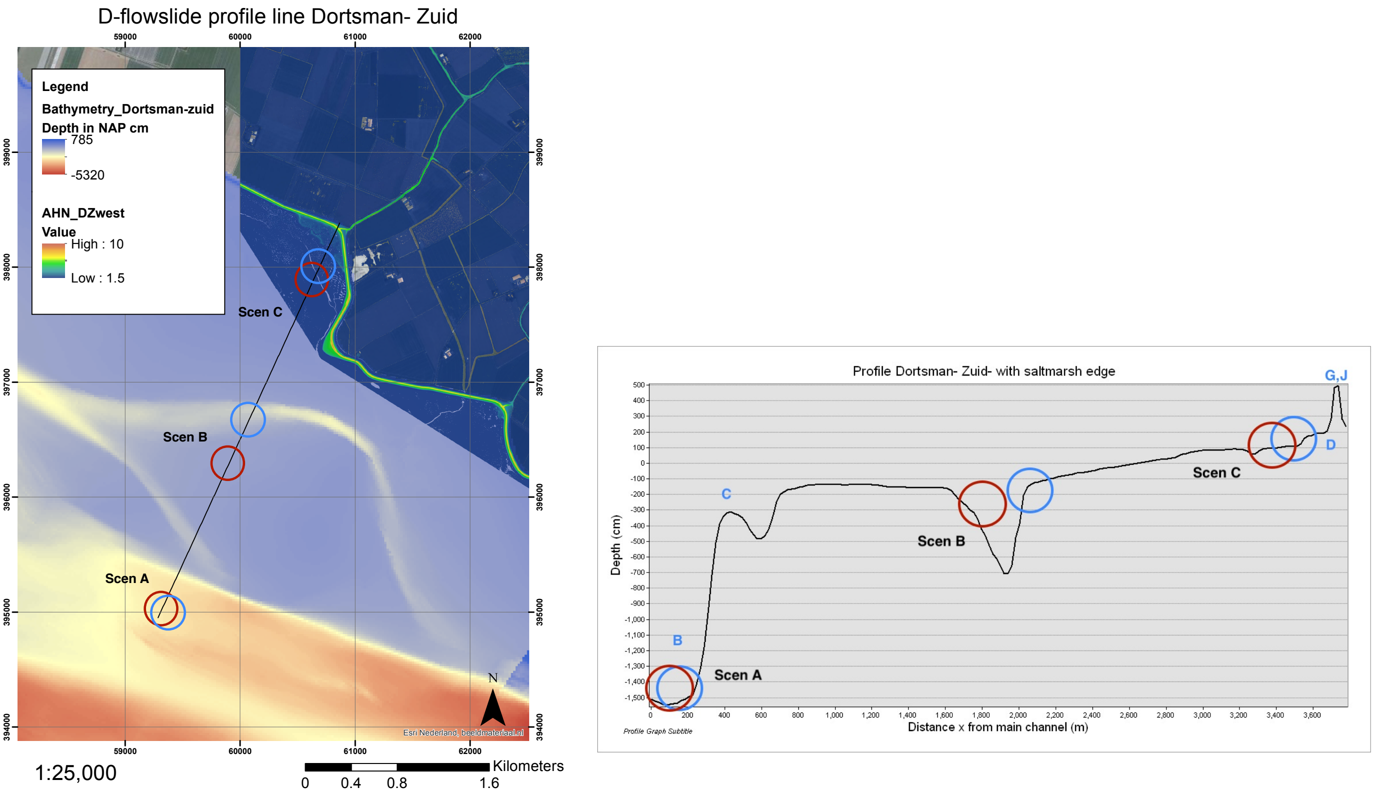

Figure 36: Bathymetry profile line of location Dortsman- Zuid with 3 possible scenarios (A, B & C) of the channel location with salt marsh (red circles) and without salt marsh (blue circles). The position of characteristic points in this Figure correspond to scenario A. With, B (Bottom river channel), C (Insert River channel), D (Dike toe at river), G (Dike top at river) and J (Dike top at polder).

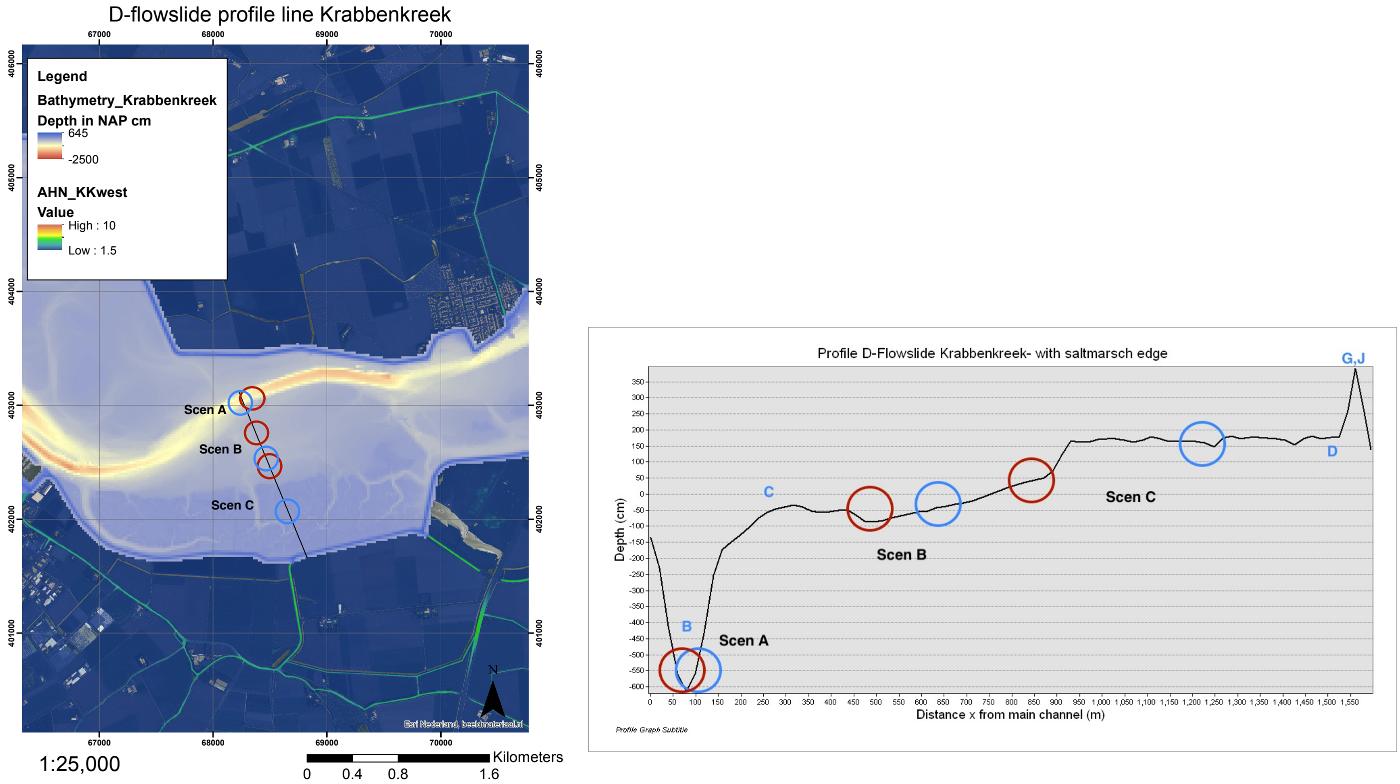

Figure 37: Bathymetry profile line of location Krabbenkreek with 3 possible scenarios (A, B & C) of the channel location with salt marsh (red circles) and without salt marsh (blue circles). The position of characteristic points in this Figure correspond to scenario A. With, B (Bottom river channel), C (Insert River channel), D (Dike toe at river), G (Dike top at river) and J (Dike top at polder).

For the three scenarios per location different increment sizes of distance x from the main location of the channel were used. These increment steps are summarized in Table 7. For location Krabbendijke and Dortsman-Zuid however, an altered increment size was necessary for scenario C of the mudflat profile. With the original increment size x, characteristic point C, 'insert river channel' was located at the inland side of the dike toe, point D, 'dike toe at riverside'. This resulted in the occurrence of a model error as the insert river channel can't lie inland of the die toe. Therefore, the new point D was chosen one meter higher than the value of point C.

Table 7: Different increment sizes x from the original location of the channel. For scenario B and C the channel was relocated to a position nearer to the foreland area for the salt marsh profile and within the foreland area for the mudflat profile.

	Applied dimensions within bathymetry plots in meters	
Krabbendijke	width saltmarsh	350
	increment size x saltmarsh profile	1800
	increment size x mutflat profile	2000
	mudfalt profile scenario c	1912
Dortsman- Zuid	width saltmarsh	220
	increment size x saltmarsh profile	1600
	increment size x mutflat profile	1750
	mudfalt profile scenario c	1620.1
Krabbenkreek	width saltmarsh	600
	increment size x saltmarsh profile	400
	increment size x mutflat profile	600

4. Results and interpretations

In this chapter, results of this study and a general interpretation are presented. Firstly shallow subsurface data and the interpretation towards shallow subsurface stability will be presented in section 4.1 in both a vertical and lateral manner to observe changes within the salt marsh and mudflat systems of the 3 locations (L1, L2, L3). Within all profile graphs sampling locations are plotted on the x-axis with an increasing number corresponding to an increasing distance from the dike. The prefix SM stands for salt marsh sample and MF for mudflat sample. Locations of the dike (grey structure), salt marsh (green bar) and mudflat (yellow bar) are represented in the small illustration underneath the Figures. The following section (4.2.1) will represent the data gathered for the deeper subsurface and the interpretation of deep subsurface geology, based on field-data and extended with Dinoloket lithology data (subsurface model GeoTOP v1.3 ;TNO-GSN, Dinoloket, 2018) to a depth of 35 meters. In the last section (4.2.2) outcomes of different scenario's with different probabilities of flow slide occurrence will be presented together with an interpretation.

4.1 Stability of the shallow subsurface

4.1.1 Shear strength and resistance to penetration

Shear strength of the surface of the foreshores' topsoil is a first indication of soil stability and the resistance to erosion. Shear strength (τ), given in kPa kN^{-2} m^{-2}, is plotted for different locations over the length of combined mudflat-salt marsh and mudflat profiles. Measurements were solely performed within a topsoil layer without vegetation. The salt marsh vegetation edge is therefore visible in the Figure below with a shear strength value of zero. It can be observed, that the mudflat of Dortsman–Zuid has the lowest shear stress along the profile. Furthermore, a general decreasing shear strength can be observed with distance from the dike side for location Dortsman-Zuid. For Krabbendijke and Krabbenkreek such a general trend of shear strength decrease with distance from the dike cannot be concluded.

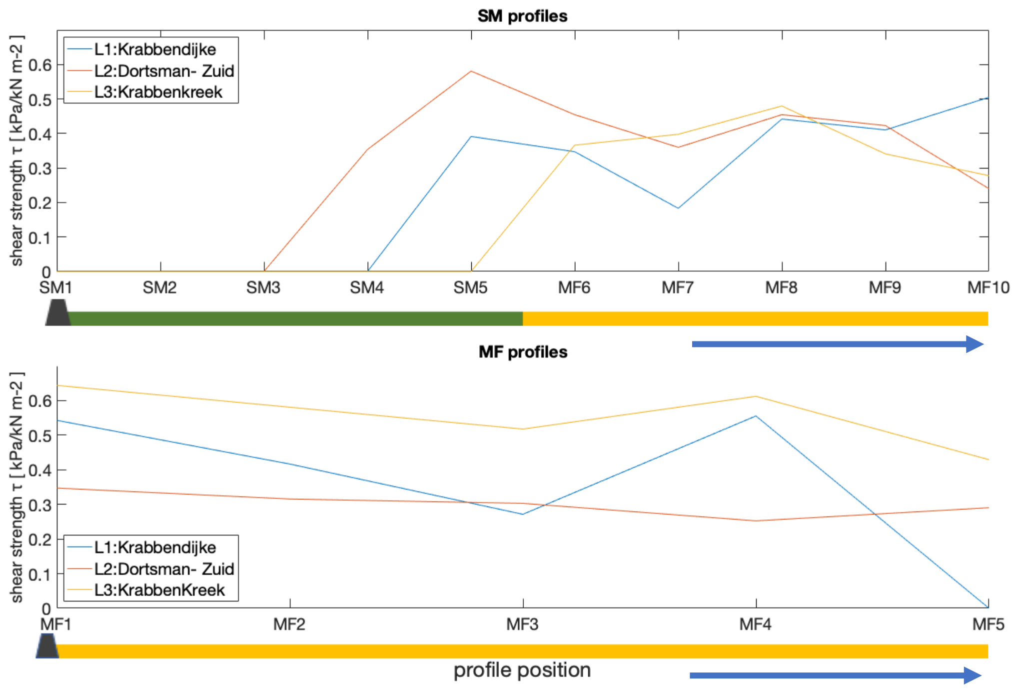

Figure 38: Shear strength for the different mudflat-salt marsh profiles (SM) and mudflat profiles (MF) for the different locations; Krabbendijke (L1, blue), Dortsman-Zuid (L2, red), and Krabbenkreek (L3, yellow). On the x-axis the different sample locations are indicated with their corresponding sub-environment (SM: salt marsh or MF: mudflat) and number increasing with distance from dike towards the waterside, indicated with the arrow and the bar illustration.

Stability of the shallow subsurface, and therefore resistance to erosion, can be expressed in resistance to penetration, indicating in situ strength of the topsoil (MPa). This resistance is plotted for the three combined salt marsh-mudflat profiles and mudflats profiles in a 2D contour plot for all locations (L1, L2, L3). From these plots it is visible, that resistance to penetration is less on the location at the salt marsh compared to the one at the mudflat. This is due to the clayey character of the salt marshes with layers of vegetation and a high water content, versus the firmly compressed sand of the mudflats with disturbance layers of shells, spread over respectively large subsurface areas (section 4.1.2). The salt marsh at the location of Dortsman-Zuid has the lowest values of resistance to penetration.

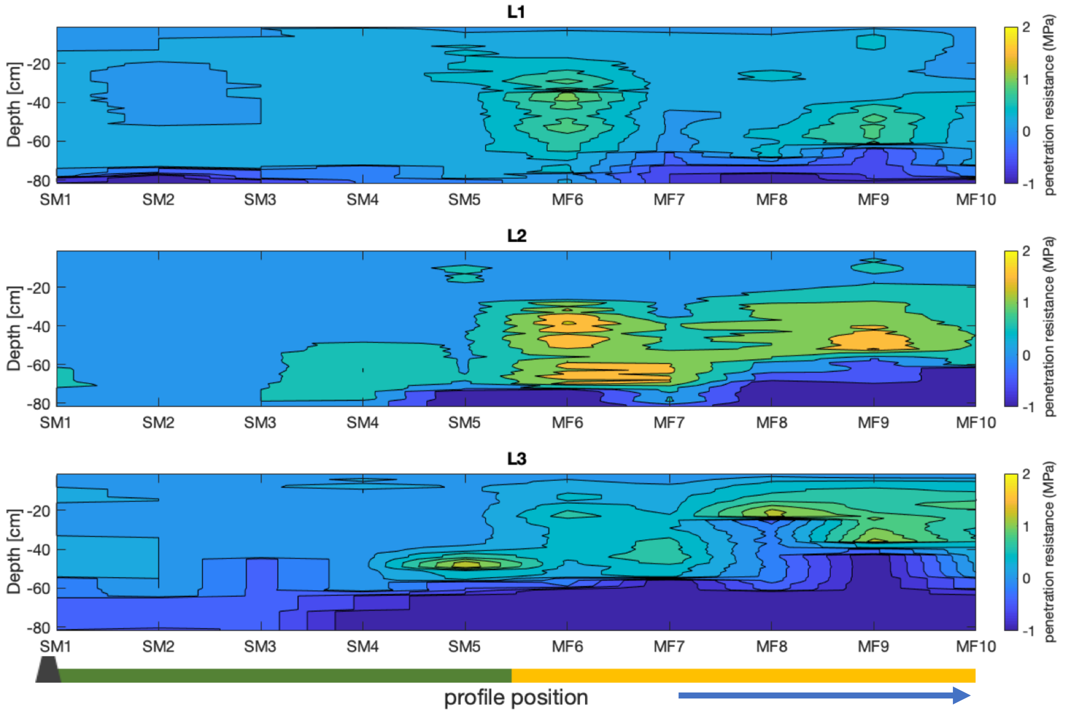

Figure 39: Resistance to penetration given in MPa per cm depth of the salt marsh- mudflat profiles for different locations; Krabbendijke (L1), Dortsman-Zuid (L2), and Krabbenkreek (L3). On the x-axis different sample locations are indicated with their corresponding sub-environment (SM: salt marsh or MF: mudflat). Distance from the dike is increasing to the right shown in the bar illustration, arrow indicates the direction to the waterside.

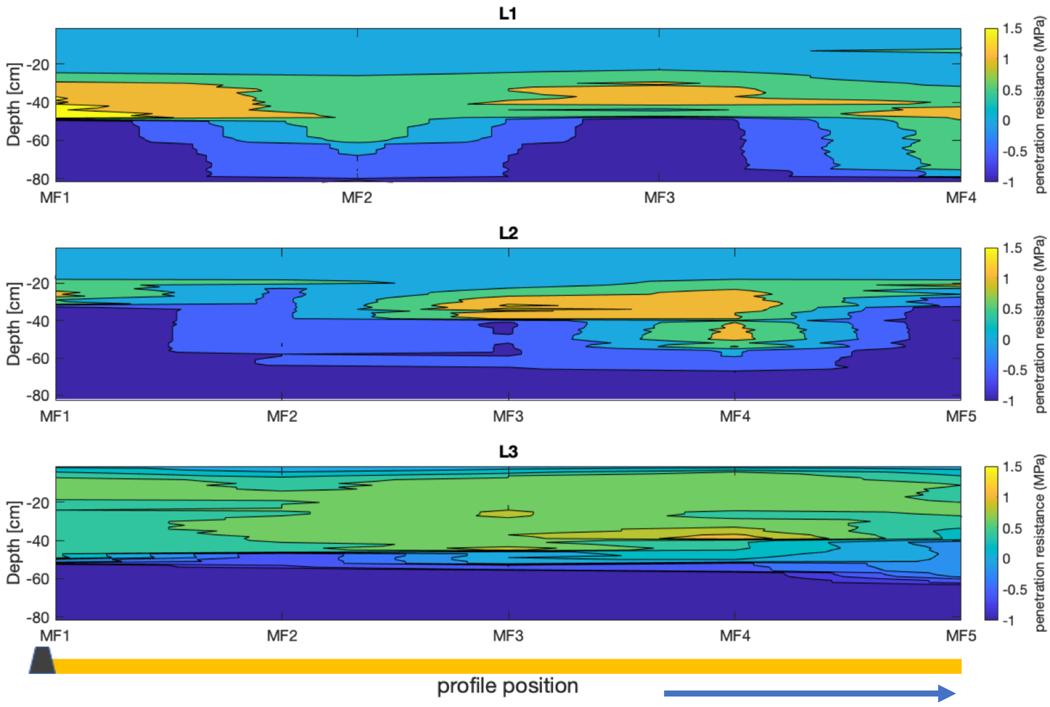

Figure 40: Resistance to penetration given in MPa per cm of the mudflat profiles (MF) for different locations; Krabbendijke (L1), Dortsman-Zuid (L2), and Krabbenkreek (L3). On the x-axis the different sample locations are indicated with their corresponding sub-environment (SM: salt marsh or MF: mudflat) Distance from the dike is increasing to the right shown in the bar illustration, arrow indicates the direction to the waterside.

4.1.2 Stability parameters of the shallow subsoil

The following parameters were visualized in depth and with distance from the dike using Excel and Matlab in a 2D manner for both the mudflat-salt marsh profiles and the mudflat profiles of the 3 locations, Krabbendijke (L1), Dortsman-Zuid (L2) and Krabbenkreek (L3). Soil parameters are plotted one by one for all locations.

Table 8: Parameters visualized per location.

Parameters visualized:
Dry bulk density
Moisture content (%)
Root/ shell density (%)
Silt percentage (%)
Sand percentage (%)
D50 sediment
D modus sediment

4.1.2a Bulk density

When analysing the filled contour graph, representing the bulk density of the 'salt marsh-mudflat' profile for location L1, Krabbendijke, it can be observed that overall dry bulk density increases with distance to the dike (Fig. 41). However, the trend of dry bulk density did not change for each of the sample locations in depth. Comparing dry bulk density to other soil parameters, it can be observed that in the case of L1, Krabbendijke, dry bulk density, g/cm^3 is positively correlated to the D50 (grainsize distribution) over the whole profile (Fig. 52). Moreover, comparing bulk density with gravimetric moisture content (Fig. 43) and silt content (Fig. 47), an inverse correlation can be detected.

When analysing the salt marsh – mudflat profile for location L2, Dortsman-Zuid it can be observed that dry bulk density follows another pattern related to distance and depth than for location Krabbendijke. Dortsman Zuid shows a similar increasing trend with distance from the dike. However, this increasing trend shows higher values for dry bulk density. When comparing dry bulk density to the D50 (Fig. 52), again a clear positive correlation can be observed. Also inverse correlations of bulk density with moisture content combined with shell and root content can be observed for the profile of Dortsman-Zuid (Fig. 43 & 47).

When analysing the salt marsh-mudflat profile for location L3, Krabbenkreek it can be observed that bulk density follows a similar pattern in relation to distance and depth as for location Dortsman-Zuid. A similar increasing trend is present with a clear transition in magnitude at the transition zone from salt marsh to mudflat. When comparing bulk density to the D50 again a clear positive correlation can be observed (Fig. 52). Again inverse correlations of bulk density with moisture content in combination with shell and root particles can be observed for the profile of Krabbenkreek (Fig 43 & 47). For all 3 study sites/areas dry bulk density thus increases with distance from the dike for the salt marsh – mudflat profiles. For the mudflat profiles this trend is not so clear. In all profiles dry bulk density of the shallow subsurface (until 30 cm depth) increases with increased D50 and a decreased silt percentage, moisture content, root and shell content. For the salt marsh with a more silty clayey character, sediment is less densely packed due to high moisture and root content. This is also found at mudflat stretches with high shell content.

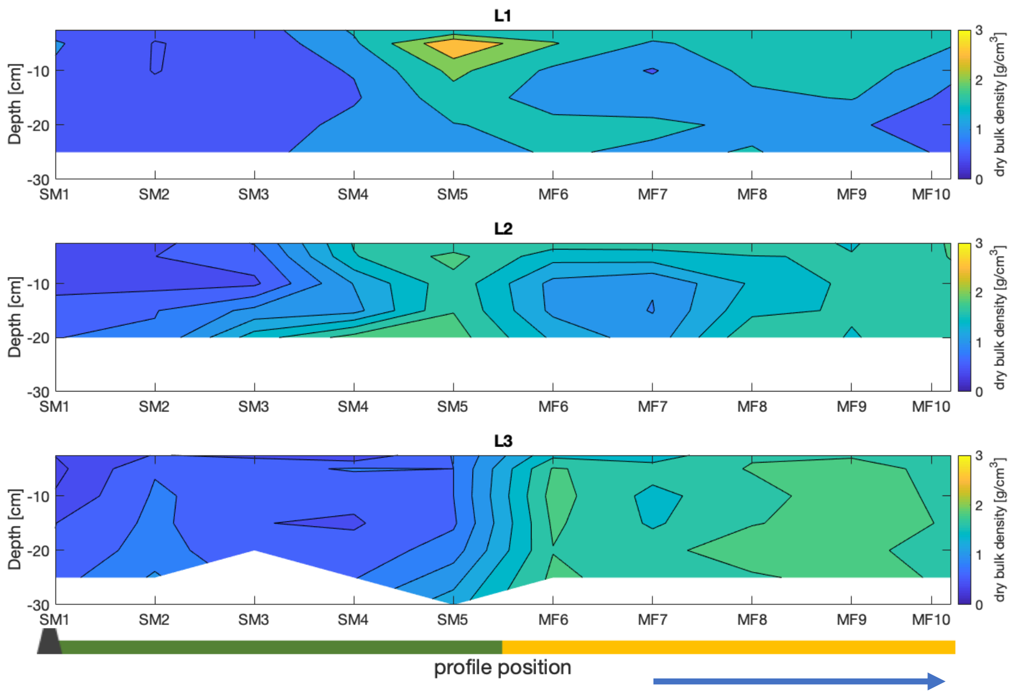

Figure 41: Filled contour plot of dry bulk density for the salt marsh- mudflat profiles of L1 (Krabbendijke), L2 (Dortsman-Zuid) and L3 (Krabbenkreek). With the first salt marsh sample (SM1) being closest to the dike and the last mudflat sample being closest to the channel (MF10). Location of dike, salt marsh and mudflat are indicated in illustration below, the arrow shows the direction of the waterside.

When analysing filled contour plots for mudflat profiles of location L1; Krabbendijke, location L2; Dortsman-Zuid and location L3; Krabbenkreek, it can be observed that the aforementioned correlations of bulk density and soil parameters such as D50, relative sand and silt percentage, and the moisture content apply also to mudflat profiles with distance from the dike (Fig. 42, 44, 49, 54). Furthermore, for deeper lain layers of L1 and L2, a reduced dry bulk density was found for the salt marsh samples closest to the dike (MF1 and MF2) (Fig. 42).

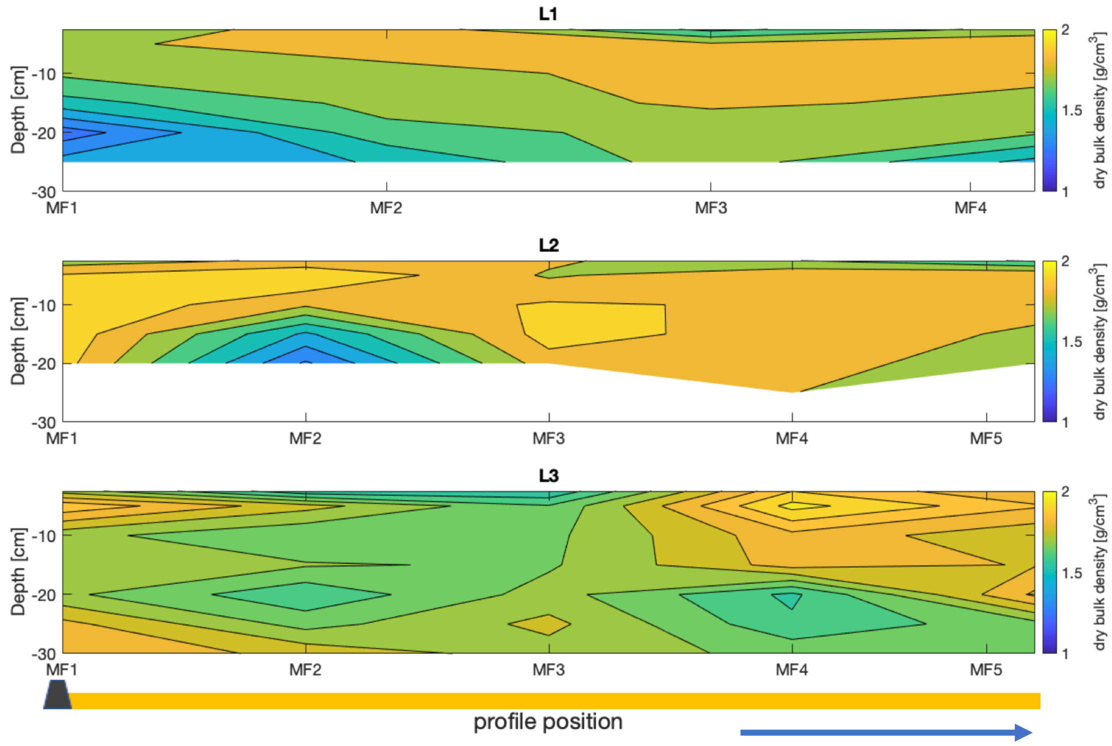

Figure 42: Filled contour plot of dry bulk density for the mudflat profiles of L1 (Krabbendijke), L2 (Dortsman-Zuid) and L3 (Krabbenkreek). With the first mudflat sample (MF1) being closest to the dike and the last mudflat sample being closest to the channel (MF4/MF5). Location of dike, salt marsh and mudflat are indicated in illustration below, the arrow shows the direction of the waterside.

4.1.2b Moisture content

Moisture content for the salt marsh- mudflat profile for location L1, Krabbendijke showed 2 relative highs (Fig. 43). The first can be found for the first salt marsh (SM1) closest to the dike after which it drops towards the transition zone of salt marsh and mudflat. However, close to the waterside of the channel, moisture content shows the second high for the mudflat samples M9 and M10 of the profile (Fig. 43). The moisture content for the salt marsh- mudflat profile for L2, Dortsman-Zuid shows higher values for the salt marsh samples SM1, SM2 and SM3 (Fig. 43). This higher moisture content is reduced with distance from the dike. Also, the moisture profile for location 3 shows a higher moisture content for the salt marsh samples. Again, this moisture content is reduced with distance from the dike.

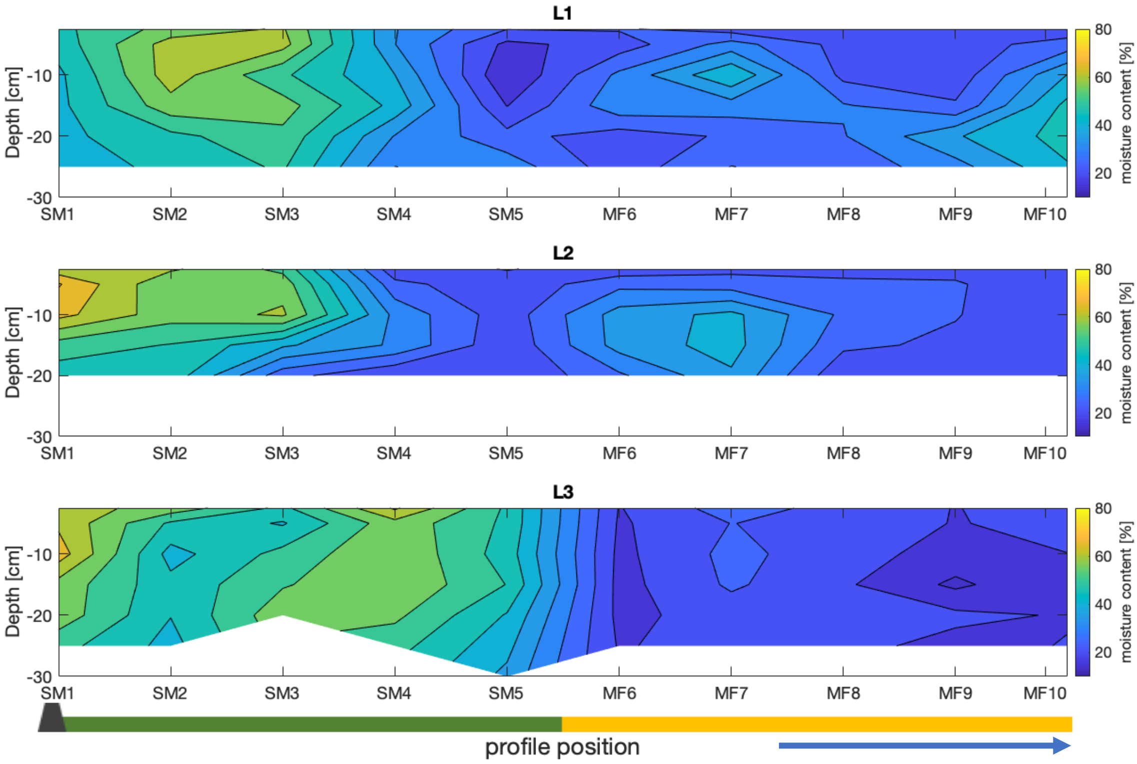

Figure 43: Filled contour plot of moisture content for the salt marsh- mudflat profiles of L1 (Krabbendijke), L2 (Dortsman-Zuid) and L3 (Krabbenkreek). With the first salt marsh sample (SM1) being closest to the dike and the last mudflat sample being closest to the channel (MF10). Location of dike, salt marsh and mudflat are indicated in illustration below, the arrow shows the direction of the waterside.

Moisture content for the mudflat profile of L1 was found to be highest both close to the dike and the waterside side in the deeper sediment layers. The moisture content for the mudflat profile of L2 for was again found to be higher close to the dike and the waterside in the deeper layers. The moisture content for the mudflat profile of L3 was however found highest for the sample locations MF2 and MF4 for the top and middle layer (Fig. 44).

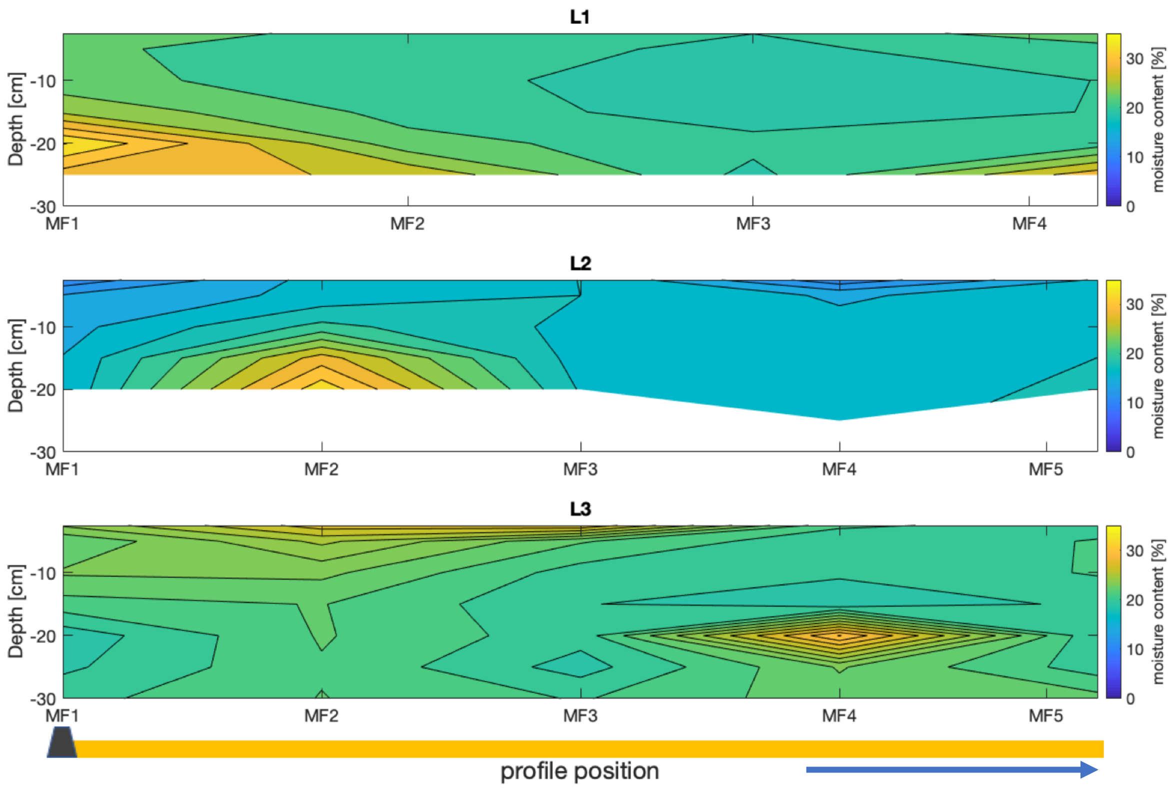

Figure 44: Filled contour plot of moisture content for the mudflat profiles of L1 (Krabbendijke), L2 (Dortsman-Zuid) and L3 (Krabbenkreek). With the first mudflat sample (MF1) being closest to the dike and the last mudflat sample being closest to the channel (MF4/MF5). Location of dike, salt marsh and mudflat are indicated in illustration below, the arrow shows the direction of the waterside.

4.1.2c Shell and root content

When analysing shell and root content for the salt marsh- mudflat profile of L1, it is clear that a small inverse correlation can be found with bulk density (Fig. 41 & Fig. 45). Furthermore, an increase of root content (only measured for the salt marsh) was found towards the transition zone. Moreover, the root content strongly decreased with depth. A high shell content was observed primarily in the most waterside sample (MF10) and mostly present in the upper (Fig. 45).

From analysing root and shell density for L2, it can be observed that a decrease of root content (only measured for the salt marsh) was found towards the transition zone. However, for salt marsh sample locations at the dike side, roots were present throughout all depths. For Dortsman-Zuid it could be observed that almost no shells were found throughout the shallow subsurface (Fig. 45). Analysing root and shell density for L3 an increase of root content (only measured for the salt marsh) was found towards the transition zone. However, for salt marsh sample locations at the dike side, roots had a higher density in shallow layers. At Krabbenkreek shells were found in low densities within the deeper layers (Fig 45).

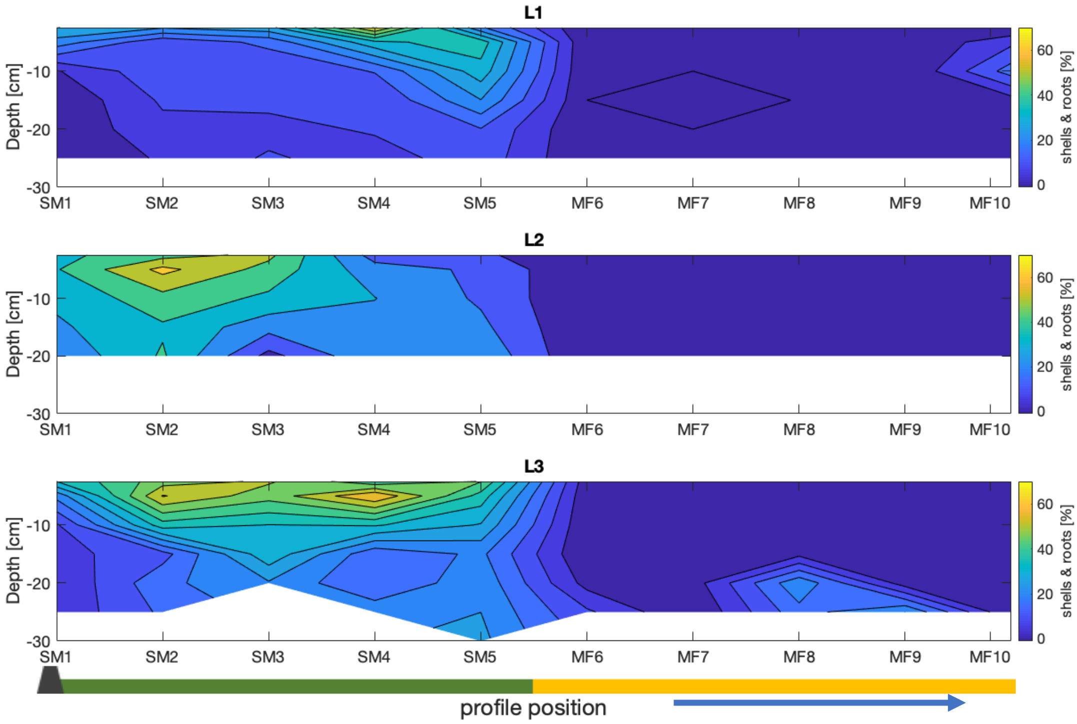

Figure 45: Filled contour plot of shell and root content for the salt marsh- mudflat profiles of L1 (Krabbendijke), L2 (Dortsman-Zuid) and L3 (Krabbenkreek). With the first salt marsh sample (SM1) being closest to the dike and the last mudflat sample being closest to the channel(MF10). Location of dike, salt marsh and mudflat are indicated in illustration below, the arrow shows the direction of the waterside.

A high amount of shell content in the mudflat profile of L1 was found within the lowest stretch of 25 cm depth increasing towards the sample locations at the waterside. For the shell content of the mudflat profile of L2 a high amount was found within the lowest layer of 25 cm depth for the dike side sample location only (MF2). For the shell content of the mudflat profile of L3 again a high amount was found within the lowest layer of 25 cm depth for the dike side sample (MF1) (Fig. 46).

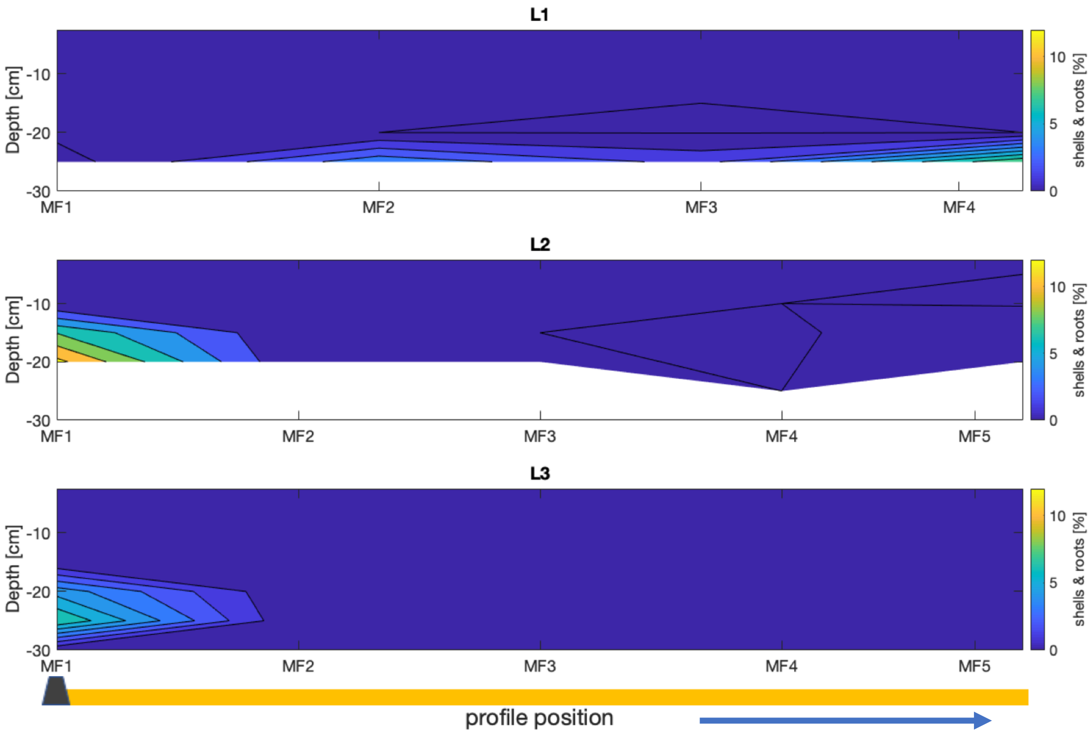

Figure 46: Filled contour plot of shell and root content for the mudflat profiles of L1 (Krabbendijke), L2 (Dortsman-Zuid) and L3 (Krabbenkreek). With the first mudflat sample (MF1) being closest to the dike and the last mudflat sample being closest to the channel (MF4/MF5). Location of dike, salt marsh and mudflat are indicated in illustration below, the arrow shows the direction of the waterside.

4.1.2d Silt and sand percentage

When analysing the sedimentary characteristics of the salt marsh-mudflat profile of L1, silt appeared to be the dominating litho-class for the saltmarsh samples. A strong decrease of silt with a corresponding increase in sand was found up till the transition zone of salt marsh and mudflat (Fig. 47 & 48). However, closer to the waterside silt content increased again with corresponding sand decrease in deeper layers of the mudflat samples.

The analysis of salt marsh samples on the sedimentary characteristics of the saltmarsh-mudflat profile from L2 shows, that silt remained to be the dominating litho-class (Fig. 47). A strong decrease of silt with a corresponding sand increase was found up till the waterside of the mudflat (Fig. 48). A little increase of silt was however present for the deeper layers around mudflat sample MF7, just beyond the transition zone of salt marsh to mudflat.

For the salt marsh- mudflat profile from L3 again silt remained to be the dominating litho-class with a corresponding decrease of silt at the transition zone from salt marsh to mudflat (Fig. 46). Furthermore, the mudflat stretch of L3 shows the highest sand concentration compared to the mudflat stretches of L1 and L2 (Fig. 49).

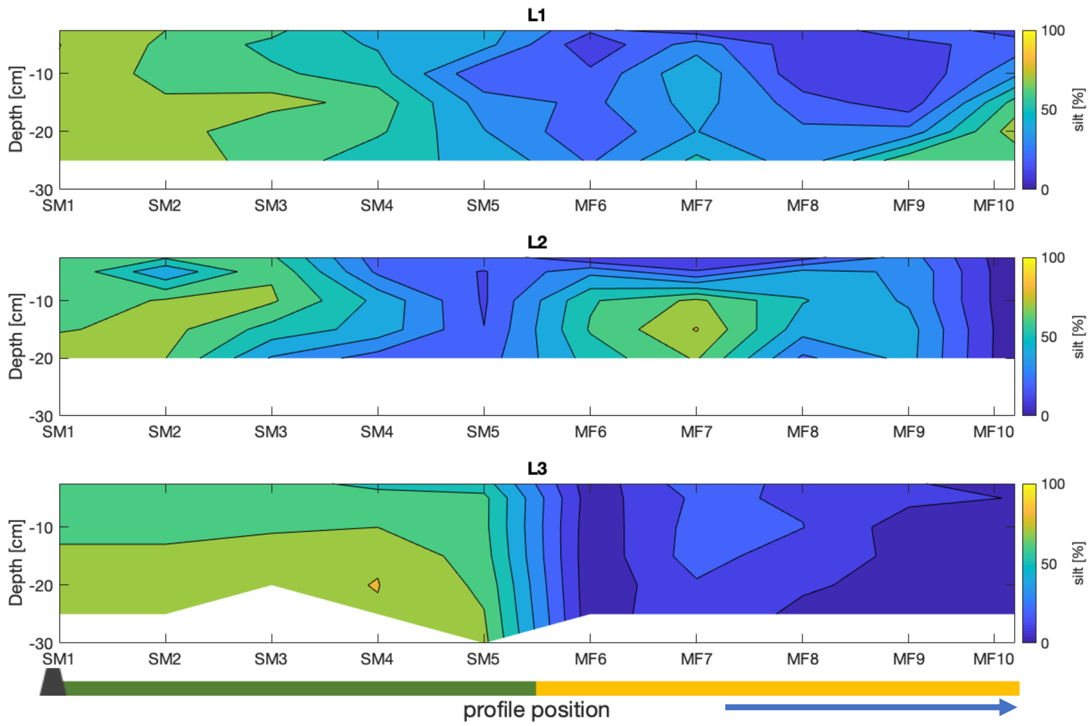

Figure 47: Filled contour plot of relative silt percentage for the salt marsh- mudflat profiles of L1 (Krabbendijke), L2 (Dortsman-Zuid) and L3 (Krabbenkreek). With the first salt marsh sample (SM1) being closest to the dike and the last mudflat sample being closest to the channel (MF10). Location of dike, salt marsh and mudflat are indicated in illustration below, the arrow shows the direction of the waterside.

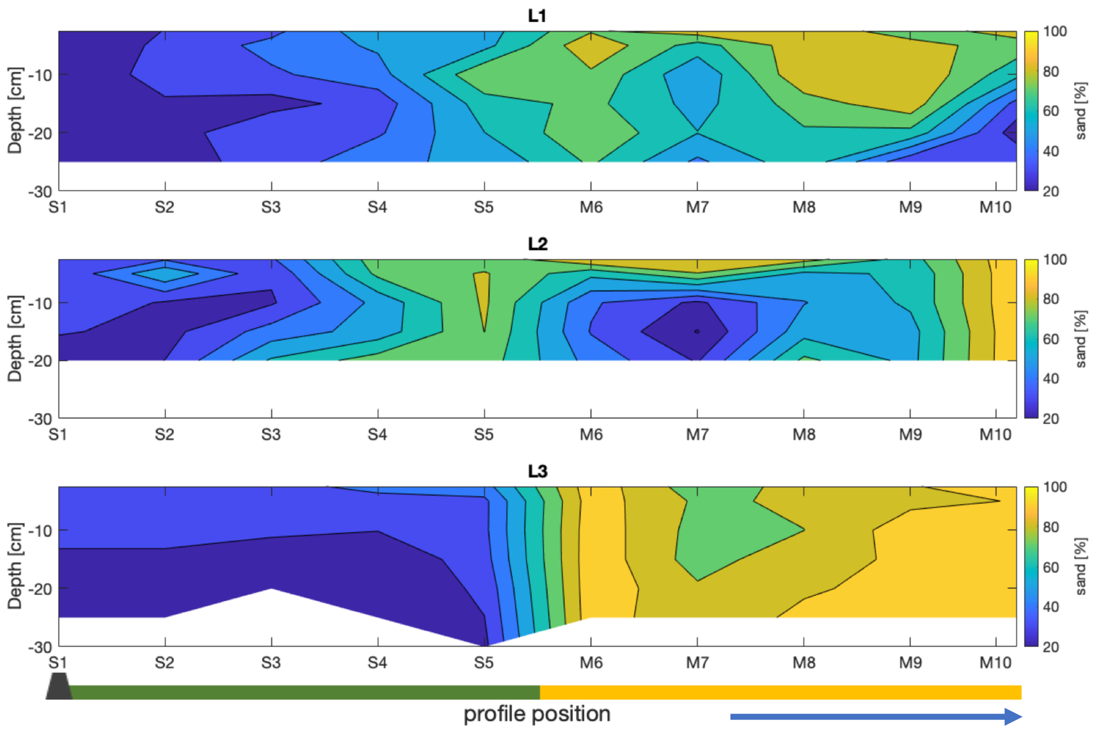

Figure 48: Filled contour plot of relative sand percentage for the salt marsh- mudflat profiles of L1 (Krabbendijke), L2 (Dortsman-Zuid) and L3 (Krabbenkreek). With the first salt marsh sample (SM1) being closest to the dike and the last mudflat sample being closest to the channel (MF10). Location of dike, salt marsh and mudflat are indicated in illustration below, the arrow shows the direction of the waterside.

Considering sedimentary characteristics of the mudflat profile for L1, sand was the dominating litho-class for the whole profile with 2 increased stretches of silt at the deeper mudflat layers closest to the dike and furthest to the waterside (Fig. 49 & 50). Along the mudflat profile for L2, again sand was found to be the dominating litho-class. Close to the dike silt content increased in deeper surface layers, similar to the MF1 and MF2 of location 1 Krabbendijke. For the mudflat profile of L3 it can be observed, that silt was present throughout all of the profile. However, sand stayed the dominating litho-class.

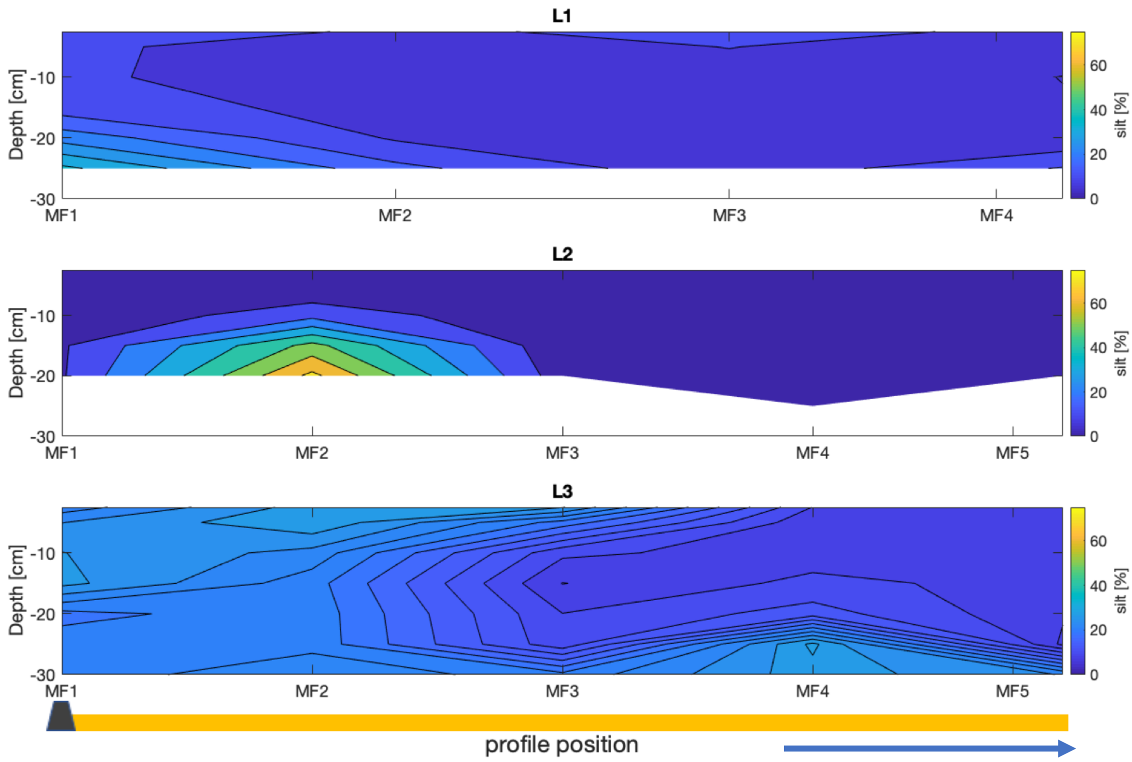

Figure 49: Filled contour plot of relative silt percentage for the mudflat profiles of L1 (Krabbendijke), L2 (Dortsman-Zuid) and L3 (Krabbenkreek). With the first mudflat sample (MF1) being closest to the dike and the last mudflat sample being closest to the channel (MF4/MF5). Location of dike, salt marsh and mudflat are indicated in illustration below, the arrow shows the direction of the waterside.

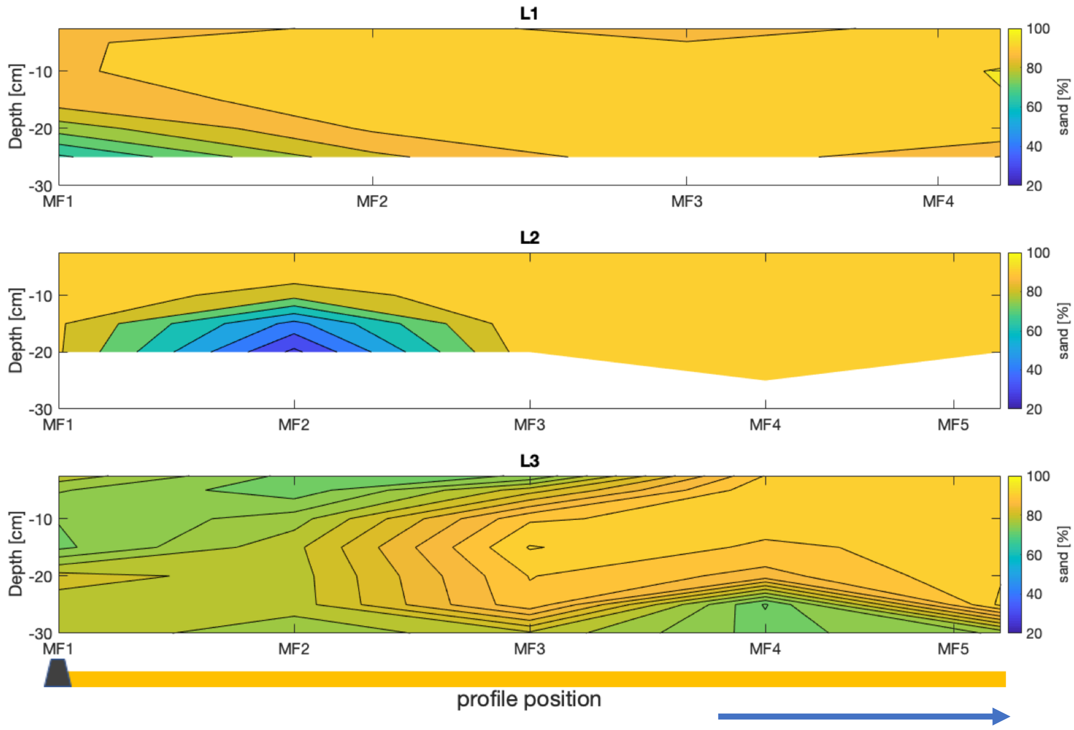

Figure 50: Filled contour plot of relative sand percentage for the mudflat profiles of L1 (Krabbendijke), L2 (Dortsman-Zuid) and L3 (Krabbenkreek). With the first mudflat sample (MF1) being closest to the dike and the last mudflat sample being closest to the channel (MF4/MF5). Location of dike, salt marsh and mudflat are indicated in illustration below, the arrow shows the direction of the waterside.

4.1.2e Modus and D50

For the salt marsh-mudflat profile of location 1, average grainsize (modus) was close to the D50 value. However, apart from the peak at the transition zone, the modus showed lower values. For location 2 and 3 average grainsize was shaped similarly over distance and depth to the D50 value, although the modus shows lower values (Fig. 51 & 52).

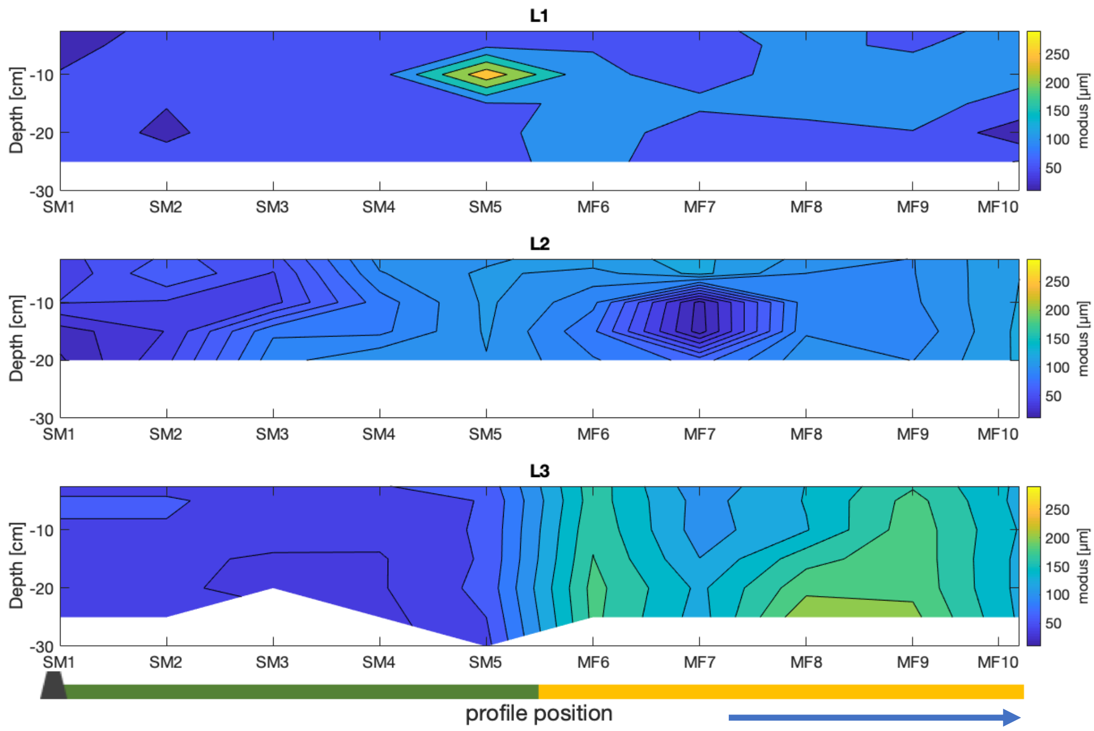

Figure 51: Filled contour plot of the average grainsize (modus) for the salt marsh- mudflat profiles of L1 (Krabbendijke), L2 (Dortsman-Zuid) and L3 (Krabbenkreek). With the first salt marsh sample (SM1) being closest to the dike and the last mudflat sample being closest to the channel (MF10). Location of dike, salt marsh and mudflat are indicated in illustration below, the arrow shows the direction of the waterside.

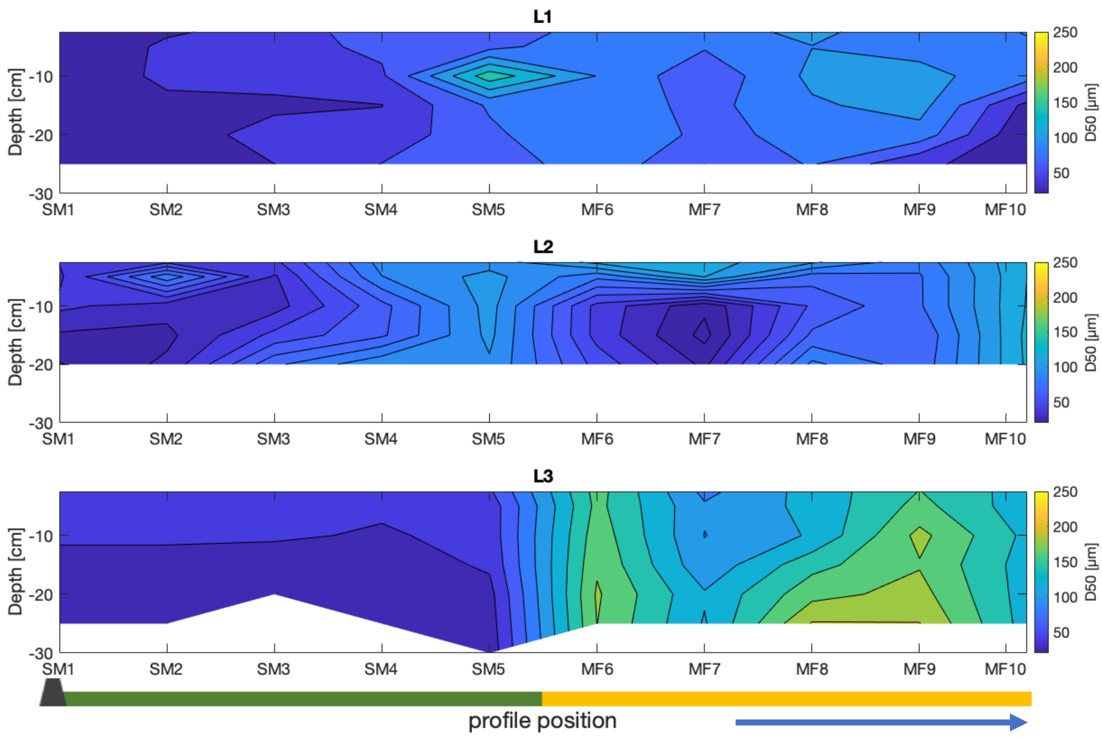

Figure 52: Filled contour plot of D50 for the salt marsh- mudflat profiles of L1 (Krabbendijke), L2 (Dortsman-Zuid) and L3 (Krabbenkreek). With the first salt marsh sample (SM1) being closest to the dike and the last mudflat sample being closest to the channel (MF10). Location of dike, salt marsh and mudflat are indicated in illustration below, the arrow shows the direction of the waterside.

For the mudflat profiles of locations 1, 2 and 3the path of the average grain size (modus) shapes similarly to the path of D50 however the average grainsize (modus) shows lower values. Furthermore various grainsize paths are found for each location In case of location 1 and 3, the average grainsize(modus) and D50 increases towards the waterside. In case of location 2 greater values for the average grainsizes and the modus were found at the dike side (Fig. 53 & 54).

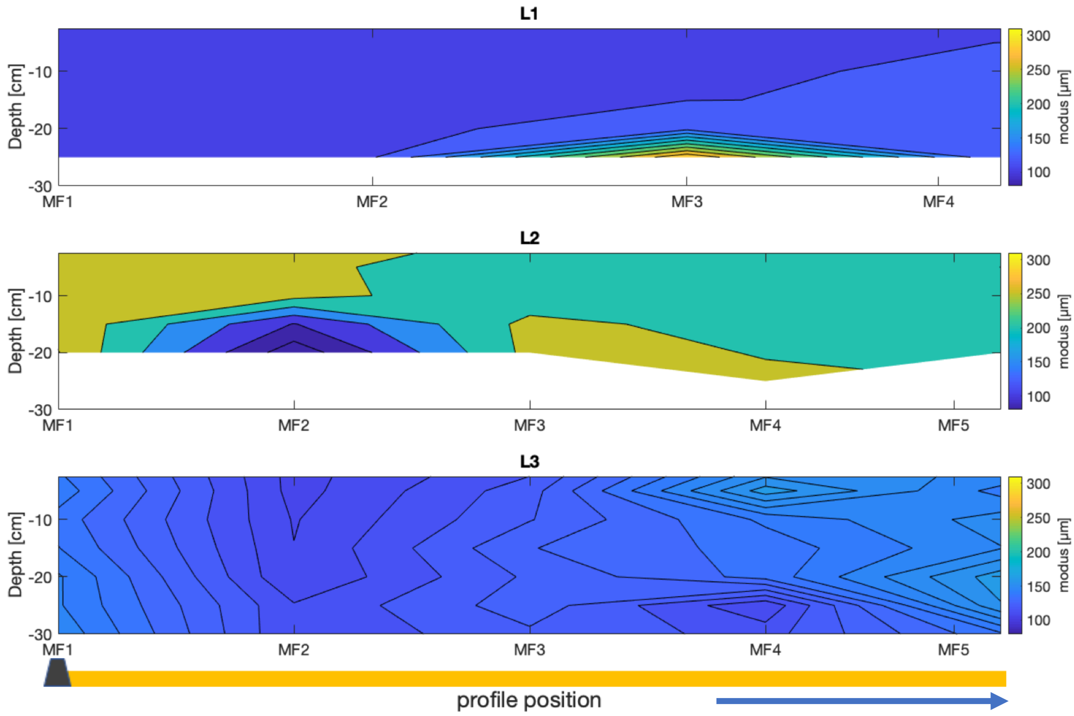

Figure 53: Filled contour plot of average grainsize (modus) for the mudflat profiles of L1 (Krabbendijke), L2 (Dortsman-Zuid) and L3 (Krabbenkreek). With the first mudflat sample (MF1) being closest to the dike and the last mudflat sample being closest to the channel (MF4/MF5). Location of dike, salt marsh and mudflat are indicated in illustration below, the arrow shows the direction of the waterside.

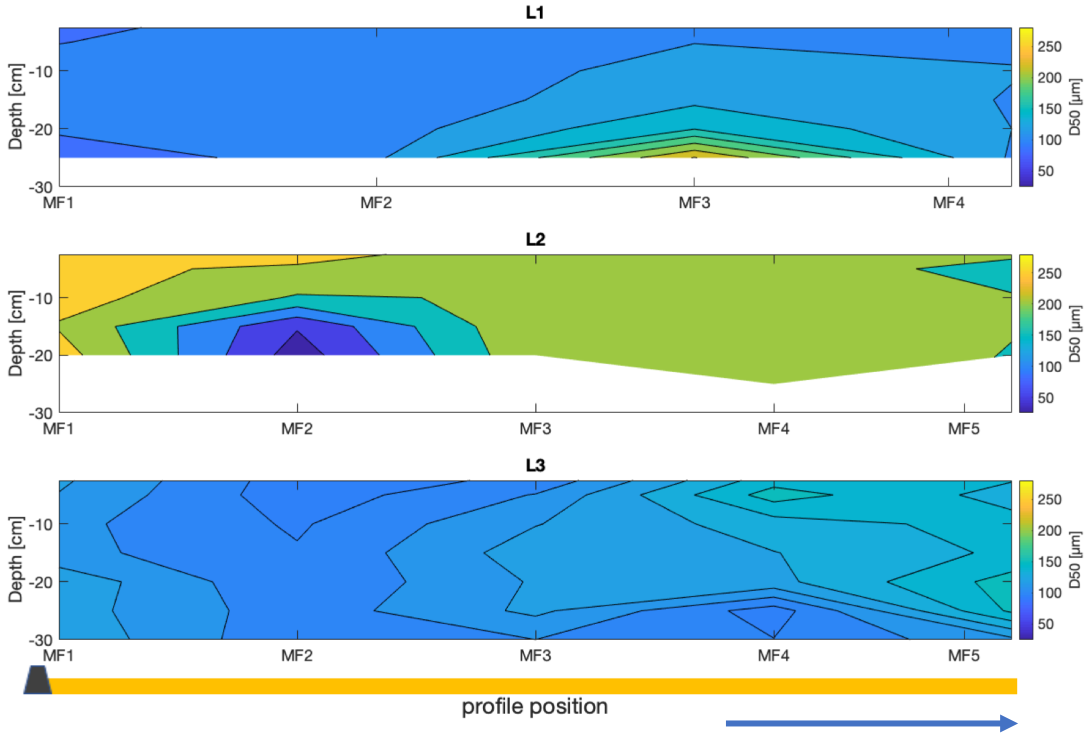

Figure 54: Filled contour plot of D50 for the mudflat profiles of L1 (Krabbendijke), L2 (Dortsman-Zuid) and L3 (Krabbenkreek). With the first mudflat sample (MF1) being closest to the dike and the last mudflat sample being closest to the channel (MF4/MF5). Location of dike, salt marsh and mudflat are indicated in illustration below, the arrow shows the direction of the waterside.

4.1.3 Cross correlations

Additionally to the observed relations of bulk density with different soil parameters within the contour surface plots, in Figure 55, 56, 57 and 58, the relation of bulk density with different soil parameters is shown for the top 2.5 cm samples of the three locations.

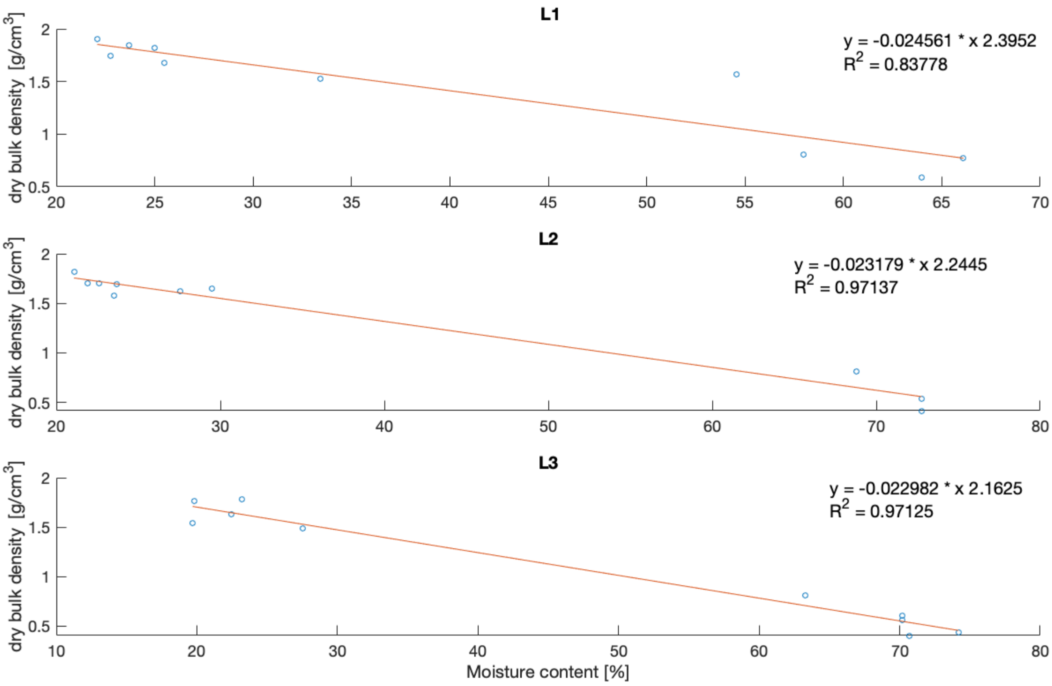

Figure 55: Relation and correlation of bulk density with the gravimetric moisture content for L1 (Krabbendijke), L2 (Dortsman-Zuid) and L3 (Krabbenkreek).

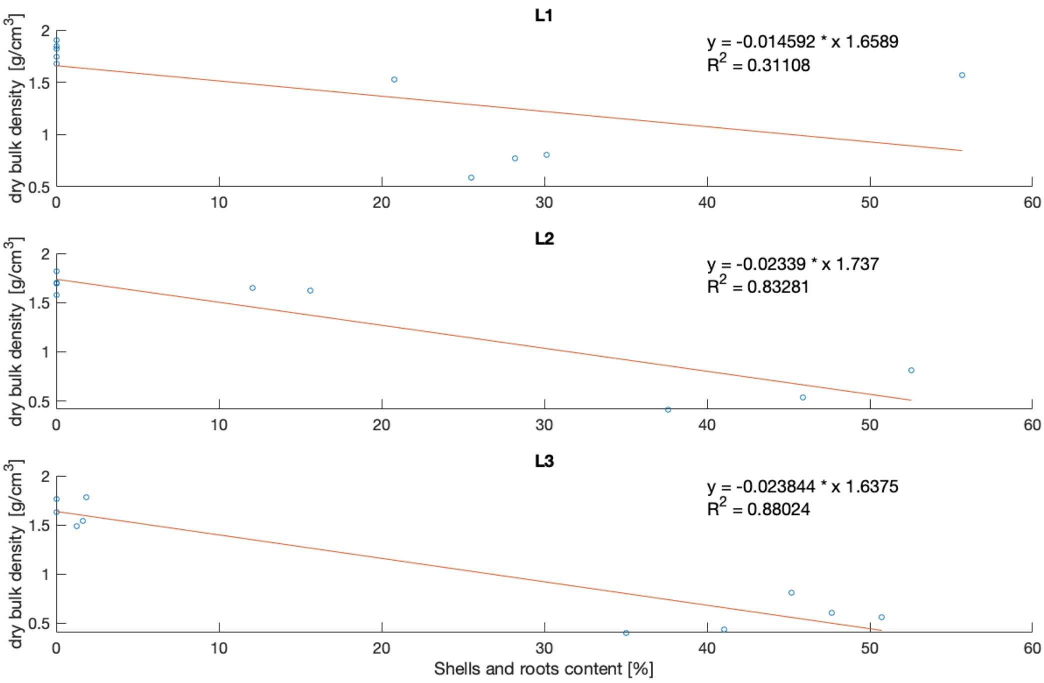

Figure 56: Relation and correlation of bulk density with the shells and root content for L1 (Krabbendijke), L2 (Dortsman-Zuid) and L3 (Krabbenkreek).

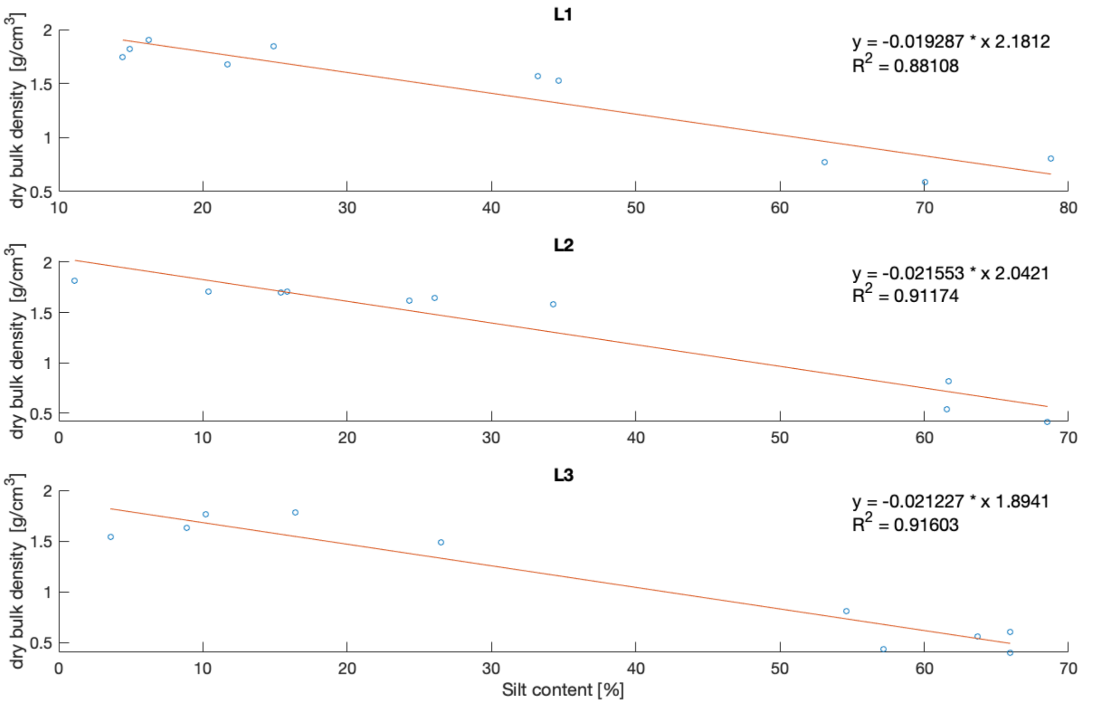

Figure 57: Relation and correlation of bulk density with the silt content for L1 (Krabbendijke), L2 (Dortsman-Zuid) and L3 (Krabbenkreek).

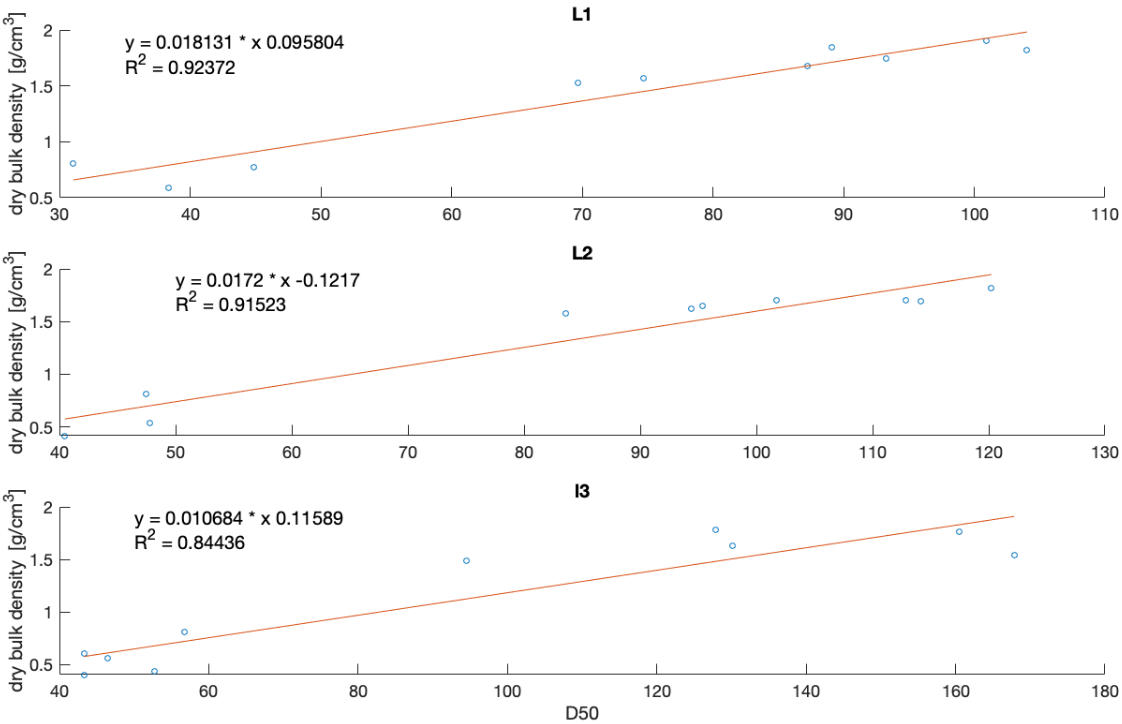

Figure 58: Relation and correlation of bulk density with the D50 for L1 (Krabbendijke), L2 (Dortsman-Zuid) and L3 (Krabbenkreek).

When analysing cross correlations of dry bulk density with gravimetric moisture content, shell and root content, silt content and D50 for the three locations different results are found. For location 1 D50 and the silt content show the highest correlation with bulk density with R^2 values of 0.92 and 0.88. This is followed by a third high correlation of bulk density with moisture content. Shells and root content do not show a high correlation; 0.31 with bulk density.
For location 2 it can be observed, that moisture content shows the highest correlation with bulk density with an R^2 value of 0.97. The inverse correlation with D50 and silt shows in this case very similar values of R^2 of 0.915 and 0.911. A third high inverse correlation is found for shells and roots of $R^2 = 0.83$.
At location 3 moisture content shows the highest correlation with bulk density with an R^2 value of 0.97. The inverse correlation with silt shows the second highest value of R^2 of 0.91. At Krabbenkreek shell and root content and D50 show the lowest R^2 of 0.88 and 0.84.

4.2 Deep subsurface stability

4.2.1 Deep lithology

For all 3 locations 1 deeper core was taken on the salt marsh and described visually for its lithological properties; grainsize and organic matter content. This succession was used to interpret the geology of the deeper surface to a depth of 5 meters. Furthermore, this geological succession was used to assess the probability of flow- slides. For deeper layers lithology was extrapolated with the GeoTOP v1.3 model (TNO-GSN, Dinoloket, 2018). In Figure 59, 60 and 61 the cored lithology and the modelled lithology of location 1, 2 and 3 are shown respectively.

For all locations comparable geological layers were found in the subsurface up till +/- 5 meters depth. These are deposits from the Walcheren Member of the Naaldwijk Fm., consisting of fine sandy inlet fills and silty clayey salt marsh deposits with a thin lamination of clay, loam and sand. At all locations plant remains of mainly reed and halophyte plants species were found in the upper 1.5-meter approximately. Within the peat layers found at Krabbendijke and Dortsman-Zuid pieces of wood and reed were found. For all locations fining upward successions were present in the sand layers from 2 meters and deeper representing tidal channel deposits with an upward decrease in fluid velocity within a channel (coarser sediments at base of channel).

Furthermore, horizontal mm laminae are present within the sandy deposits, which are characterized by an alternation of sand and thin silt interventions, representing the change of flow direction induced by the tide. For the three locations the grainsize of the sandy layers (D50), which was visually determined in the field, varied between 75 to 300 µm. Averaging this value results in an overall fine to medium sand category for Krabbendijke, Dortsman-Zuid and Krabbenkreek (fine D50 < 200 µm and medium 200 < D50 < 500 µm, Deltares 2018) More detailed descriptions of the coring's are added in the Appendix 5.

The Walcheren Member is for location 1, Krabbendijke, underlain by the Holland peat layer containing pieces of wood and reed up to a depth of -5,5 meter. The Holland peat layer is underlain by The Wormer and Zandvoort Member of the Naaldwijk Fm. followed by the Basal peat layer of the Nieuwkoop Fm. at a depth of 7.5 meter. Within the deeper subsurface coarser marine sands of the Eem Fm. and the Boxtel Fm. consisting of cover sands and loss, were present.

At location 2, Dortsman-Zuid, again the Holland peat layer was found at approximately 5 meters depth, which is directly underlain by the Wormer and Zandvoort Member of the Naaldwijk Fm.. Underneath are deposits of the Boxtel and Eem Fm. being found. For both locations 1 & 2 this succession is underlain by fluvial deposits of the Peize and Waarle Fm. consisting of varying grainsize sand deposits alternating with silt and clay – layers at a depth of 35 meters

In case of location 3, Krabbenkreek, the Walcheren Member of the Naaldwijk Fm. is directly underlain by the the Peize and Waarle Fm..

D15 and D50 values for every litho-class in the subsurface were averaged per location based on cored lab analysed grainsize data of the Malvern (Table 9). Data used for calculations in D-Flow Slide are indicated in Table 9 and 10. Grainsize of the non-sandy layers was directly used. Grainsizes of the sandy layers were adjusted and fitted to the corresponding grainsize category of medium sand for the sandy layers (Table 10) for the different locations.

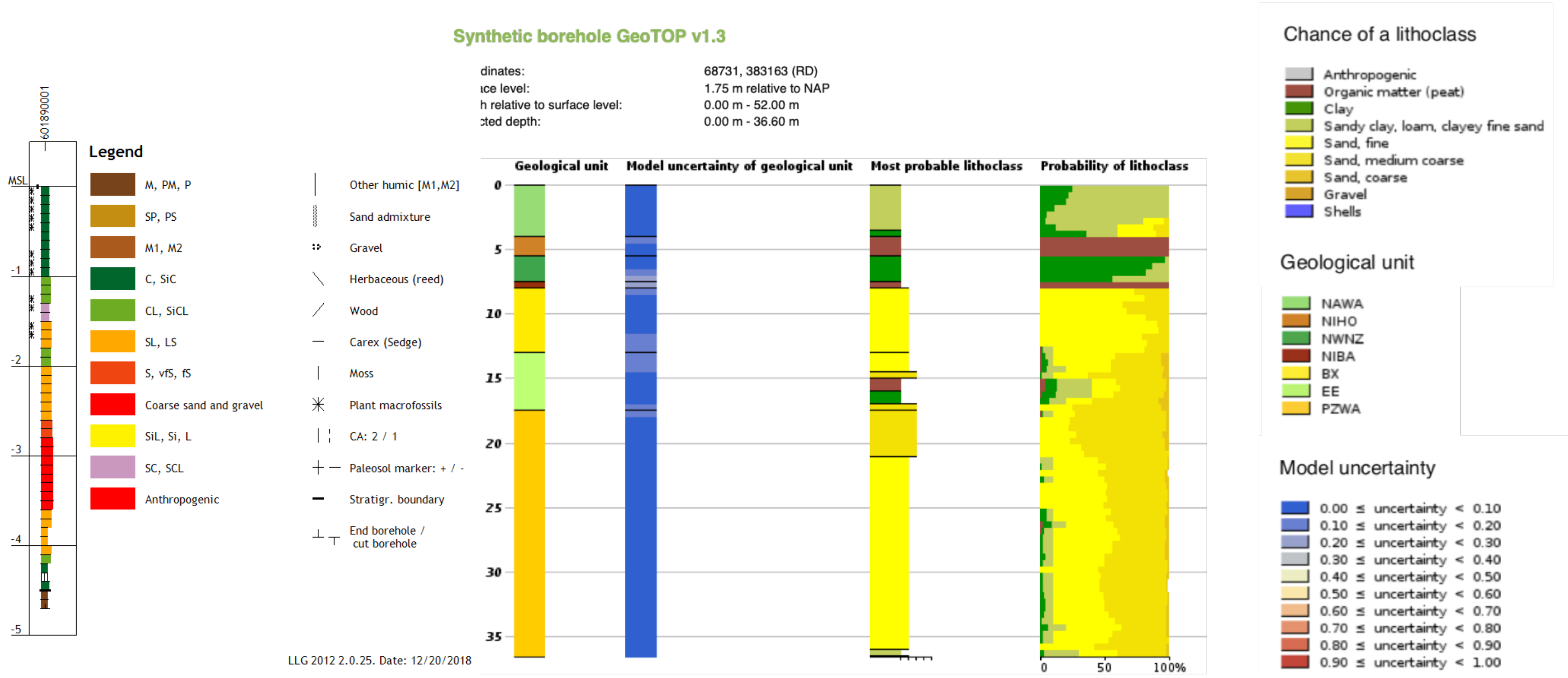

Figure 59: Lithology of Location 1 Krabbendijke) for top +/- 5 meter depth on the left and visual extrapolation through DINO-loket subsurface model GeoTOP v1.3. Lithology given presents geological units (described in the background); NAWA (Naaldwijk Fm., Walcheren Member), NIHO (Nieuwkoop Fm., Hollandveen), NIBA (Nieuwkoop Fm Basisveen), NWNZ (Naaldwijk Fm., Wormer and Zandvoort Member), BX (Boxtel Fm.), EE (Eem Fm.), PZWA (Peize and Waarle Fm.). Drillings are both visualized from the surface to scale the two successions similarly.

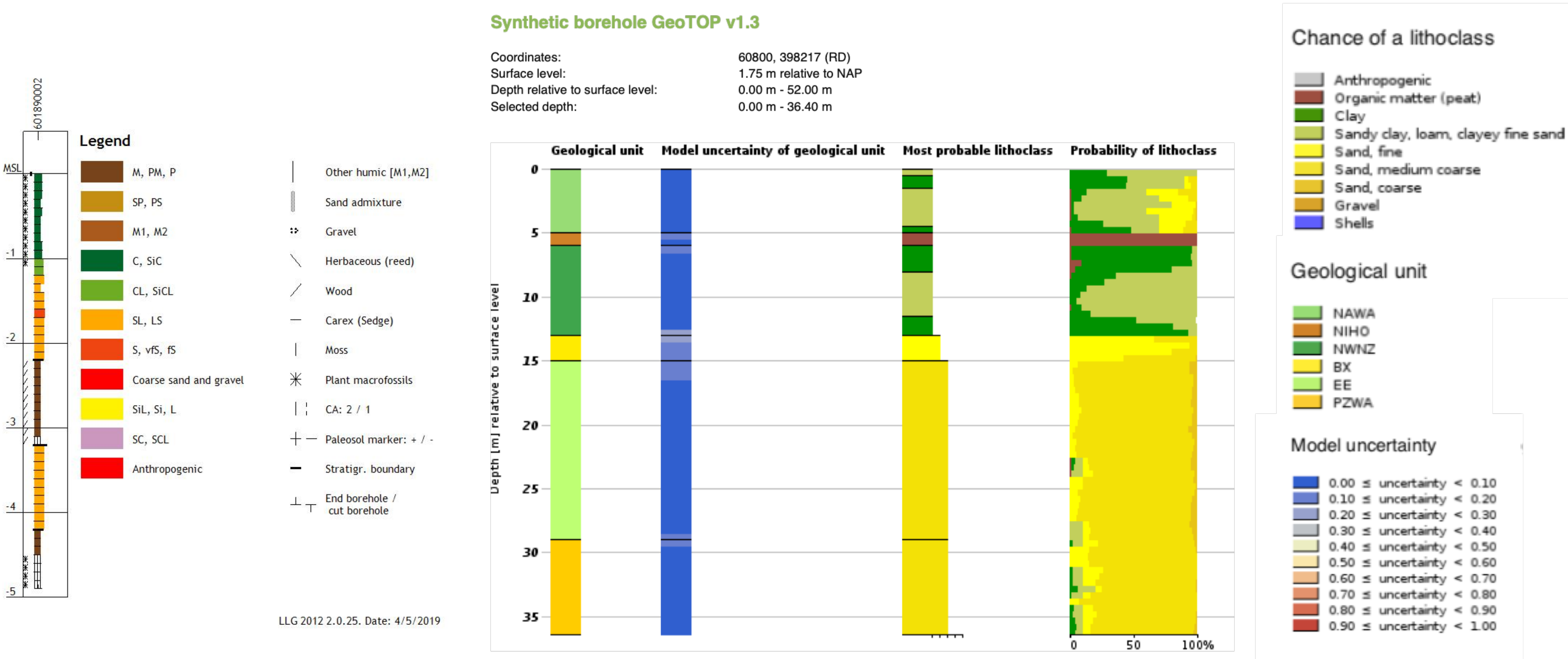

Figure 60: Lithology of Location 2 Dortsman-Zuid for top +- 5 meter depth on the left and visual extrapolation through DINO-loket subsurface model GeoTOP v1.3. Lithology given presents geological units (described in the background); NAWA (Naaldwijk Fm., Walcheren Member), NIHO (Nieuwkoop Fm., Hollandveen), NIBA(Nieuwkoop Fm Basisveen), NWNZ (Naaldwijk Fm., Wormer and Zandvoort Member), BX (Boxtel Fm.), EE (Eem Fm.), PZWA (Peize and Waarle Fm.). Drillings are both visualized from the surface to scale the two successions similarly.

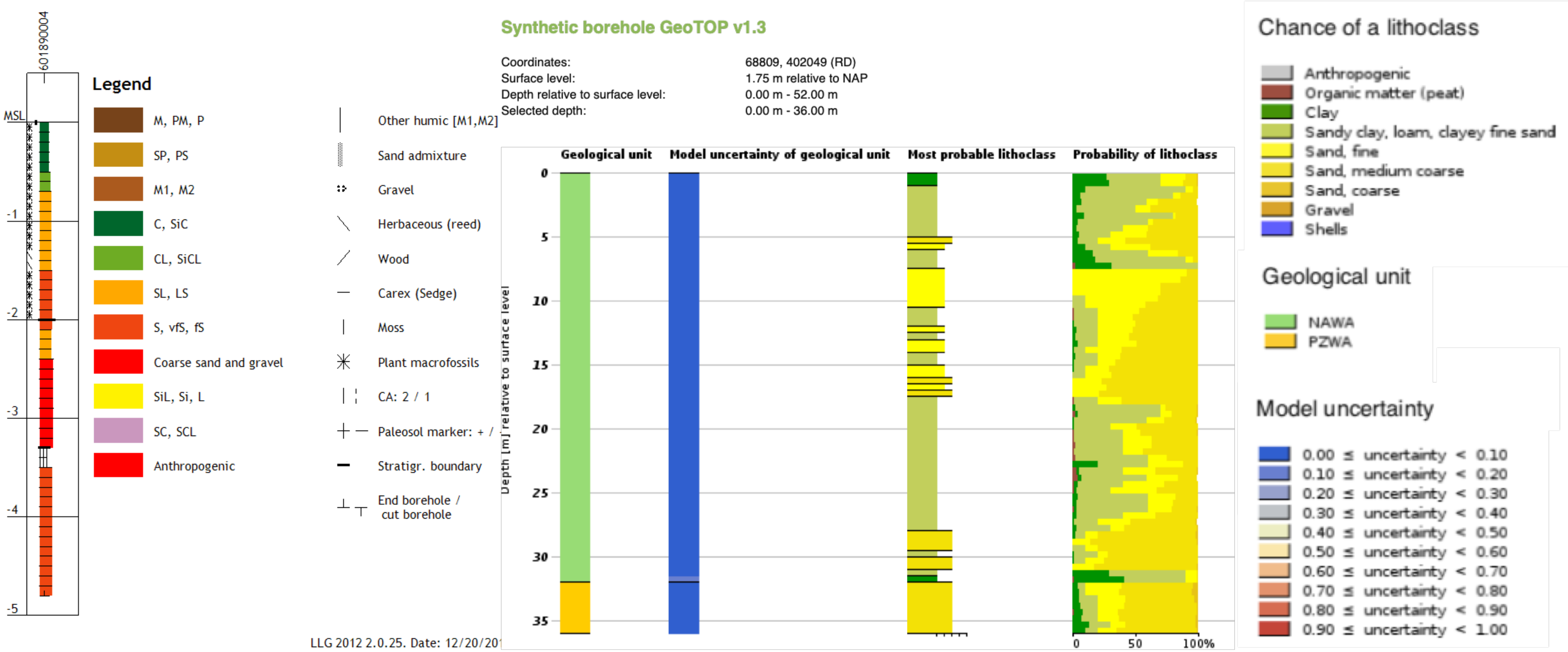

Figure 61: Lithology of Location 3 Krabbenkreek for top +- 5 meter depth on the left and visual extrapolation through DINO-loket subsurface model GeoTOP v1.3. Lithology given presents geological units (described in the background); NAWA (Naaldwijk Fm., Walcheren Member), NIHO (Nieuwkoop Fm., Hollandveen), NIBA (Nieuwkoop Fm Basisveen), NWNZ (Naaldwijk Fm., Wormer and Zandvoort Member), BX (Boxtel Fm.), EE (Eem Fm.), PZWA (Peize and Waarle Fm.). Drillings are both visualized from the surface to scale the two successions similarly.

Table 9: Values of D50 and D15 determined as averages from lab analysed data from cored sediment samples for the 3 locations of Krabbendijke, Dortsman-Zuid and Krabbenkreek.

Krabbendijke	D50	D15	Dortsman-Zuid	D50	D15	Krabbenkreek	D50	D15
peat	18.38	2.94	peat	18.38	2.94	peat	18.38	2.94
fine silty clay	18.38	2.94	fine silty caly	18.38	2.94	fine silty caly	18.38	2.94
silty clay	33.95	4.552143	SiC	38.77167	7.15375	SiC	35.7975	8.2875
silty clay loam	30.09591	3.569167	SiCL	34.4325	5.83875	SiCL	18.715	4.47
sandy loam	45.05083	4.63	SL	51.59594	8.0025	SL	92.66177	14.97938
loamy sand	82.6065	21.796	LS	64.89278	10.87375	LS	125	305
fine sand	123.085	25.2525	FS	96.8	15.36	FS	135.0718	96.50488
medium sand	134.885	56.26375	MS	20	25	MS	170.87	144.52

Table 10: Values of D50 and D15 determined as minimum and maximum within the sand size category of medium sand chosen within D-Flow Slide program version 18.1.1 for the 3 locations of Krabbendijke, Dortsman-Zuid and Krabbenkreek.

description	color	soil type	Krabbendijke				Dortsman-Zuid				Krabbenkreek			
			min D15	min D50	max D15	max D50	min D15	min D50	max D15	max D50	min D15	min D50	max D15	max D50
medium sand, NAWA	DarkGray	Sand	110	210	250	500	110	210	250	500	110	210	250	500
fine sand, NAWA	DarkGray	Sand	110	210	250	500	110	210	250	500	110	210	250	500
fine sand, BX	LemonChiffon	Sand	110	210	250	500	110	210	250	500	110	210	250	500
fine sand, PZWA	WhiteSmoke	Sand	110	210	250	500	110	210	250	500	110	210	250	500
fine sand, EE	WhiteSmoke	Sand	110	210	250	500	110	210	250	500	110	210	250	500
medium sand, EE	Gainsboro	Sand	110	210	250	500	110	210	250	500	110	210	250	500
medium sand, PZWA	Gainsboro	Sand	110	210	250	500	110	210	250	500	110	210	250	500
peat, NIBA	DarkGoldenrod	Peat	40	50	40	50	40	50	40	50	40	50	40	50
peat,NIHO	RosyBrown	Peat	40	50	40	50	40	50	40	50	40	50	40	50
peat, EE	RosyBrown	Peat	40	50	40	50	40	50	40	50	40	50	40	50
silty clay loam, NAWA/NWNZ	DarkGray	Loam	30	30.1	30	30.1	30	30.1	30	30.1	30	30.1	30	30.1
sandy loam, NAWA	DarkGray	Loam	40	45.05	40	45.05	40	51.59	40	51.59	40	92.66	40	92.66
loamy sand, NAWA	DarkGray	Sand	40	82.6	40	82.6	40	64.89	40	64.89	40	125	40	125
fine silty clay,NAWA	DarkGray	Clay	40	50	40	50	40	50	40	50	40	50	40	50
silty clay, NAWA/NWNZ	DarkGray	Clay	30	33.95	30	33.95	30	33.95	30	33.95	30	35.79	30	35.79
silty clay, EE	RosyBrown	Clay	30	35	30	35	30	35	30	35	40	50	40	50

4.2.2 Flow- slide outcomes

Within the D-Flow Slide 18.1.1 program the global and detailed test were applied to the inserted data from the 3 locations within the Eastern Scheldt; Krabbendijke, Dortsman-Zuid and Krabbenkreek. This data was tested for its probability of Flow-slide per year for the scenarios (Figure 63, Table 11) and this is visualised in Figure 64. Supplementing output of the program is summarised in Table 12.

Table 11: Scenarios with different channel locations, grainsizes for profiles with and without salt marsh tested for the probability of flow slide occurrence per year.

Code	Scenario A,B & C for saltmarsh profile (location channel)
SMminKD	Saltmarsh profile, minimum grainsize, Krabbendijke
SMmaxKD	Saltmarsh profile, maximum grainsize, Krabbendijke
SMminDZ	Saltmarsh profile, minimum grainsize, Dortsman-Zuid
SMmaxDZ	Saltmarsh profile, maximum grainsize, Dortsman-Zuid
SMminKK	Saltmarsh profile, minimum grainsize, Krabbenkreek
SMmaxKK	Saltmarsh profile, maximum grainsize, Krabbenkreek
	Scenario A,B & C for mudflat profile (location channel)
MFminKD	Mudflat profile, minimum grainsize, Krabbendijke
MFmaxKD	Mudflat profile, maximum grainsize, Krabbendijke
MFminDZ	Mudflat profile, minimum grainsize, Dortsman-Zuid
MFmaxDZ	Mudflat profile, maximum grainsize, Dortsman-Zuid
MFminKK	Mudflat profile, minimum grainsize, Krabbenkreek
MFmaxKK	Mudflat profile, maximum grainsize, Krabbenkreek

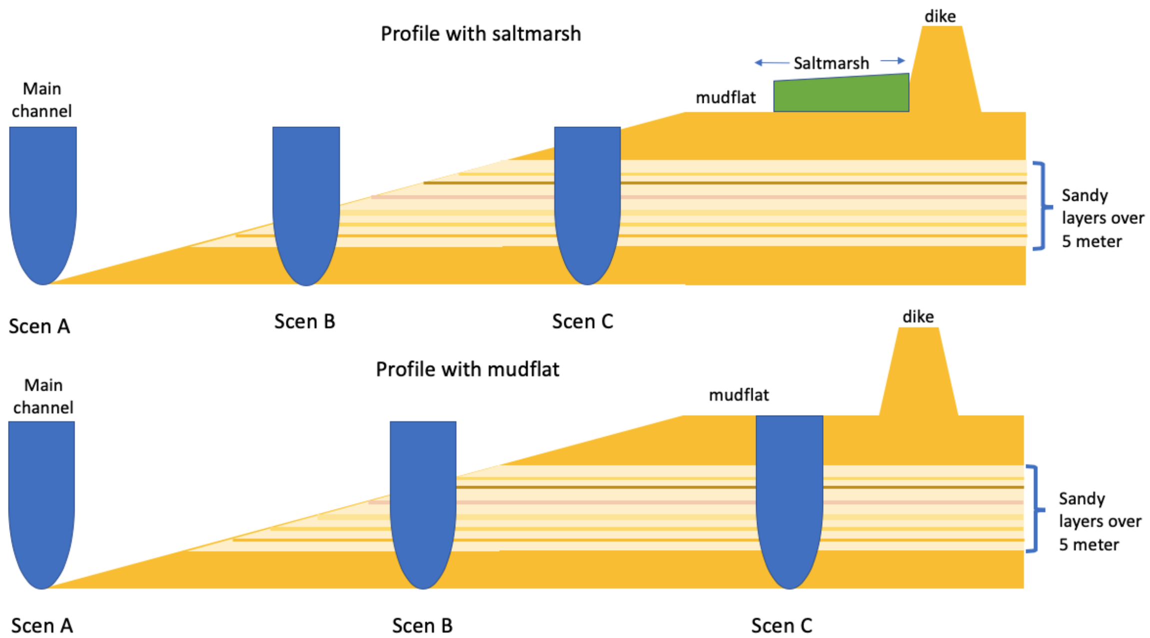

Figure 63: Scenarios visualised for profiles with and without mudflat and the different locations of the channel drawn respectively.

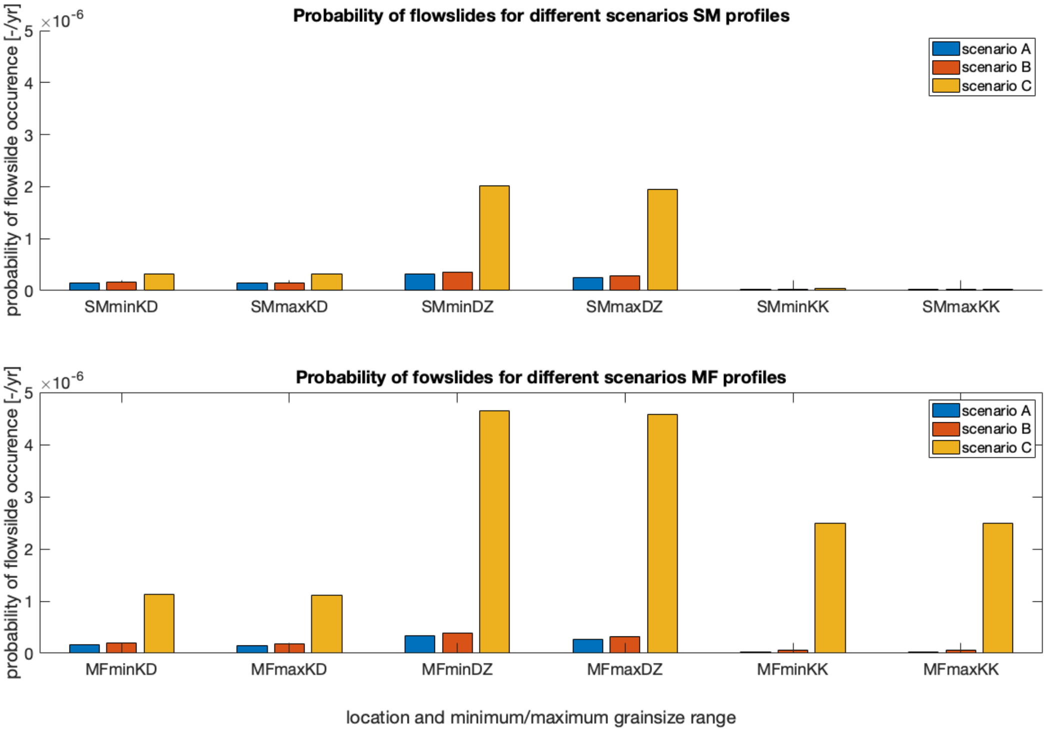

Figure 64: Results from the D-Flow Slide 18.1.1 program, plotted for the different scenarios' probability of flow-slide. For the locations Krabbendijke (KD), Dortsman-Zuid (DZ) and Krabbenkreek (KK) the different scenarios of the channels position A (original position channel), B (intermediate position channel), C (channel closest to the dike) are plotted for the minimum and maximum grainsize ranges. In the upper plot the profiles with salt marsh are shown, in the lower plot the profiles with only a mudflat present are shown.

Table 12: Supplementary raw data from the detailed check in D- flow slide, locations Krabbendijke, Dortsman-Zuid and Krabbenkreek for scenario C here the channel lies closest to the dike.

Location specific calculated output	Krabbendijke	Dortsman- Zuid	Krabbenkreek
Global check results			
Succeeded	Yes	Yes	Yes
Global check step 1a			
Depth channel	-10.75	-15.45	-6.14
Marge [m]	19.460	24.720	11.620
Slope [m]	15	15	15
Assessment level [m]	-7.507	-11.350	-4.203
Would liquefaction flow slide lead to damage on levee?	No	No	No
Global check step 1b			
Criterion on slope protection met (less then 1:2.5)?	Not available	Not available	Not available
Global check step 1c			
Artificial and non-densified sandy foreland?	No	No	No
Global check step 1d			
Average slope over 5 meter (1:..) [-]	30.319	27.913	40.103
Liquefaction flow slide possible based on criterium ‘steepest slope over 5 meter’?	No	No	No
Global check step 1e			
Total channel slope (1:..) [-]	30.319	27.913	40.103
Is breach flow slide possible?	Yes	No	No
Liquefaction flow slide possible based on averaged geometry?	Yes	No	No

It becomes quite clear from analysing results from D-Flow Slide (Figure 64, Table 12), that a chance of occurrence for a flow side to occur is almost non-existing for all locations; Krabbendijke, Dortsman-Zuid and Krabbenkreek. This is mostly due to a gentle under water slope (slope between point B, bottom river channel and point C, insert river channel). In all 3 cases embankments are characterised with such gentle slopes, that occurrence of flow slides is almost neglectable, independent of how loosely the sand is packed. Only for slopes steeper then 1:10, flow slides become a real problem (van den Ham, pers. Comm. Dec. 2018). Furthermore, for all locations the channel is located approximately 3 km from the dike. This indicates, that if a Flow-slide would occur for a 10 meter deep channel, the liquefied sandy sediment would displace with an slope angle of 1:15 (related to cot gamma in Figure 20, Chapter 2) and this would lead to a retrogression length L of foreland with approximately 75 meters (van den Ham, pers. comm. Dec. 2018). This area of displacement would not have an effect on the dike, located 2.925 meters away from the displacement.

However, when analysing differences for various scenarios, it becomes clear that different parameters do affect the occurrence rate per year. Firstly, for 'mudflat only' profiles with locations of channels closer to the dike for scenario A, B and C, which lie within the original 'salt marsh position', a higher flow-slide probability per year versus the flow slide probability of the salt marsh-mudflat profiles is observed. Furthermore, it can be observed, that a lower grainsize range increases the flow – slide probability for both mudflat and salt marsh profiles for all scenarios. When comparing results per location it is very clear, that location Krabbenkreek has the lowest probability of flow slide probability due to a long stretch of salt marsh (Table 12) and the therefore great distances between the channel and dike. Moreover, location Krabbenkreek is characterised by the most shallow channel depth (Table 12). Test questions for all locations on the occurrence of Flow-slide of both the global and detailed checks are summarized (Table 12) and found to be negative. However, the model outcome suggests breach flow is possible at Krabbendijke. This could be due to different characteristic surface line points. This could be due to a great alternation of lithological different layers in the subsurface. As was mentioned in Chapter 2, the presence of for example peat layers can significantly contribute in triggering a breach flow slide.

5. Discussion

5.1 Stability of the shallow subsurface

5.1.1 Shear strength and resistance to penetration

Shear strength measurements were solely performed within the topsoil layer without vegetation. It can be observed, that the mudflat of Dortsman-Zuid has the lowest shear strength along the profile (Fig. 37). This could be due to a higher moisture content within the topsoil sediment (Fig. 46). Sand with higher moisture content can lead to instability of grains due to an over-water pressure (Chapter 2, section 2.3.1). Furthermore, a general decreasing shear strength can be observed with distance from the dike for location Dortsman-Zuid coinciding with an increasing moisture content closer to the waterfront at the sediment top (Figure 38). As shear strength was not further extrapolated over the whole system, including the vegetated part, no clear lateral change was found for the entire salt marsh-mudflat profile. For a better understanding of the variability in topsoil strength, it is recommended to take shear vane measurements for entire profiles in future studies. To a further extent, interesting trends could be found coupling topsoil strength to the in-situ soil characteristics and resistance to penetration.

For all three locations it was found, that resistance of penetration was less on salt marshes than for mudflats. This is due to the clayey character of salt marshes with vegetation holding a greater water content, versus the firmly compressed sand of the mudflats with disturbance layers of shells, which are spread over respectively large subsurface areas (section 4.1.2). The location of Dortsman-Zuid has the lowest values of resistance to penetration for its salt marsh. This could be related to the high moisture content. For a better understanding of the in situ stability of the shallow subsurface, interesting trends could be found coupling resistance to penetration to sediment characteristics, such as grainsize, moisture content and root/shell content.

5.1.2 Dry bulk density and clarifying factors

A similar increasing trend in dry bulk density is found for all three locations over the horizontal stretch of the salt marsh – mudflat profiles. This implies, that silty clayey salt marsh sediment is less densely packed, compared to mudflat sediments, due to high moisture and root content. The same assumption can be made for siltier mudflat stretches with high shell content. However, as no particle density or particle volume was determined for the different shallow subsurface layers, the corresponding void ratio (e) and porosity (Φ) of the samples (Equation 12, Equation 13 and Equation 14) could not be determined.

$\Phi = Vp/Vs$ with Φ = porosity, Vp = volume of pores and Vg = volume of ground (12)

$e = Vp/Vg.$ with e = void ratio, Vp = Volume of pores and Vg = volume of grains (13)

$$e = \Phi /(1 - n) \text{ and } \Phi = e/(1 + e) \quad (14)$$

$$RD = \frac{emax - e}{emax - emin} \quad (15)$$

With this void ratio value (e) the relative density (Equation 15) can be calculated where e_{max} is the maximum attainable value of the void ratio and e_{min} the minimum attainable value of the void ratio e. The minimum and maximum values for e can be obtained with laboratory compression and disperse test applied to the sediment. A low value of the relative density (e.g. RD< 0.5) indicates that a sediment is loosely packed and can easily be compressed (Verruijt, 2001).

With the relative density values the stability of the shallow soil profiles of the three locations can be quantified more precisely and effectively linked to the compression status of the sediment.

When comparing moisture content for the three locations, it can be observed that this is highest around salt marsh stretches and at the waterside of the mudflats. This could be due to the silty clay character of the salt marsh. As higher suction exists in clayey soils, a greater volume of water content can be held. This is due to a different nature of water binding forces, a higher porosity and a larger variety of pore sizes for clay compared to, for example well sorted sand (Hendriks, 2010; Rawls, W.J. Gish, T.J. Brakensiek, 1986). The higher porosity of silty clay can be related to a more unstable character in the saturated state. However as the salt marsh is vegetated, erosion rates are slowed down at the salt marsh edge. In the study of Lo et al. (2017) it was found, that presence of *Spartina* spp is shown to reduce erosion across salt marsh area by 80 % for sandy soils and 17 % for silty soils. Moreover, the *Spartina* biomass in the upper 30 cm soil layer enhanced erosion resistance.

When vegetation was absent, resistance against erosion was found to be positively related to silt content, with mean erosion being 72 % lower in silty vs sandy soils. This could be due to the liquefying character of sand when saturated (section 2.3.1).

For mudflat profiles a decreasing dry bulk density was found, when shell density increased. This indicates that presence of shells makes the soil less densely packed and more susceptible to erosion. However, when taking resistance to penetration into account, a different function of shells becomes apparent, as shell banks increase resistance to penetration. For a further understanding of shells functioning towards subsoil stability, mescocosm tests could be applied at mudflats with and without shell banks present in varying amounts, to test resilience to erosion by artificially imitated wave attenuation (Lo et al., 2017).

5.2 Deep subsurface stability

5.2.1 Lithology and interpretation

In all the coring's of the three locations; Krabbendijke, Dortsman-Zuid and Krabbenkreek, young Holocene tidal deposits were found representing different energetic sub environments of a tidal estuary system. A gradual transition with depth was found in layers of clay, silt and sand representing rapidly alternated channel deposits overlain with floodplain deposits forming salt marshes. For all three locations a fining upward trend was visible and mm lamination with thin alternation of clay layers was present within the sand layers of the subsurface. These rapidly deposited, and therefore loosely packed, sediments and the presence of mm clay lamination can be linked to susceptibility to flow slides for all locations (2.3).

Despite the similar composition up till 5 meters depth for all three locations a different structure was found for the deeper subsurface. For location 1, Krabbendijke, the most variable alternation of lithology was found. With presence of two peat layers, Krabbendijke could be more susceptible to the occurrence of breach flow slides (section 2.3.5). During this study the lithology of cores was only mapped manually for approximately the first 5 meters. Variation of deeper lithology and possible stratification was visually extrapolated from the subsurface model GeoTOP 1.3v. This might deviate slightly from what would have been found manually.

5.2.2 Grain size determination

Grainsize values of D15 and D50 are based on averages of the Malvern grainsize measurements. However, no calcium carbonate or organic matter was removed from the samples prior to the measurements. This could have caused an underestimation of the grainsizes found for the different litho-classes within the Malvern output, as small organic and calcium carbonate material was taken into account within the measurements. This explains the higher grainsize values determined visually with sand classes cf. the USDA soil classification (Soil Survey Staff (SSS), 2010) compared to the lower sand grainsizes determined with the Malvern (Table 9).
For the D-Flow Slide program, only medium size sand category (200 < D50 < 500 µm and 100 < D15 < 250 µm) could be used, when applying the global and detailed check. However, most of the found values based on fieldwork belonged to the fine sand category (D50 < 200 µm and D15 < 100 µm). Therefore, the ranges of grainsizes for the different layers of sand were described in a more global manner by which the outcome of the program may have been compromised.

5.2.3 D- Flow Slide outcomes

The D-Flow Slide program only takes the sandy layers present over a height of 5 meters into account in the calculation of the static liquefaction probability. In the cores taken for this study sand starts to appear in the deeper subsurface at around 2-3 meters depth. For breach flow slide probability only grainsizes of sand layers present are taken into account. This means, that variance of litho-classes (peat, clay, silt, sand) within the deeper subsurface and the fine stratification within the layers is not well represented in the global and detailed tests of the program D- flow slide. The fine alternation of different litho-classes and presence of a fine mm lamination of sand and clay respectively, could have a major effect on in situ shear strength, the state of sediment compression and water retention capacity. This would suggest that adding new parameters into the D- flow slide program might result in a better representation of a more detailed lithological succession.

The different scenarios used are based on a channel with a single point of river bottom depth and river insert channel, that is moving in lateral position to the adjacent dike at equal distance steps alternating the bathymetry profile of the original salt marsh. However, this is not truly realistic scenario, as the channel would probably move to positions where already a shallow channel path is present and it would have alternating river bottom depth and river insert channel points. Furthermore, the bathymetry pathway within the mudflat stretch would have had different values for all characteristic surface line points.

For a closer understanding of the relation between different types of foreshores with various geometry characteristics and geological stratification within the deeper subsurface, locations with different deposition environments and different hydrological and geomorphological settings should be tested and compared with the D- Flow Slide program.

Also, in the D-Flow Slide program a third step of analysis is possible if the detailed check is not passed, applying the advanced models SLIQ2D and HMBreach (Deltares, 2018). In this study this third step in the assessment could not be included due to insufficient input data. However, performing this last step could have given a better perspective on the independent importance of the various soil parameters.

6. Conclusion

Towards understanding stability of foreshores in the Eastern Scheldt, 3 locations, with different energetic conditions and susceptibility to the occurrence of flow slides, were studied for various sub-environments within the foreshore.
From this study it is shown, that a high moisture content and a lower relative density of sediment can negatively influence resistance to erosion of shallow subsurface due to a lower consolidation of grains. The presence of shells consolidated the subsurface, therewith increasing resistance to penetration.
The studies salt marshes consisted of generally silty clayey sediments versus mudflats, which contained mainly sand. Vegetation was found within all salt marsh samples and not within the mudflat samples for all locations. Shearvane was measured only for mudflat stretches of the profiles and this was found to be highest for the topsoil of location Dortsman-Zuid. Resistance to penetration was highest for sandy soils of mudflats for all three locations, especially in disturbance layers of shells and consolidated sands indicating a solidification of the subsurface. Furthermore, high water content was found for salt marsh samples and mudflat samples closest to the waterfront.

For the deeper subsurface, stability in terms of probability of liquefaction flow slide, was determined mainly by the geometry of the channel- foreshore system. The slope from bottom river channel to insert river channel should be less then 1:10 for a static liquefaction flow slide to occur. Also, distance from channel to dike should lie within the area of sediment displacement, which takes place with a slope angle of 1:15, for a static liquefaction flow slide to influence the dike. Furthermore, for a static liquefaction flow slide to occur, at least 5 meters of sand should be present in the subsurface. For breach flow slide to occur, a sufficiently large zone of sand or silt, a proportional high and steep slope, fine grainsizes and the presence of disturbance layers increase the possibility of breach flow- slide at the waterfront edge.

With the application of the D-Flow Slide program 18.1.1 no significant probability was found for static liquefaction flow slide to occur for locations Krabbendijke, Dortsman-Zuid and Krabbenkreek due to gentle slopes and the large distance between channel and dike edge.
However, a larger probability to flow slides was found for the ‘mudflat only’ profiles as the location of the channel could come closer the dike. For location Krabbendijke a positive outcome was found for the possibility of breach flow slide. This could be due to presence of disturbing peat layers in the subsurface.
More research on the relations among shallow and deeper in situ soil characteristics is needed for a better understanding of foreshore stability. Moreover, boundary conditions for foreshores with different deeper subsurface characteristics and various hydrological and morphological settings should be tested towards its sensitivity of flow slide mechanisms.

7. References

Balke, Thorsten Stock, Martin Jensen, Kai Bouma, Tjeerd J. Kleyer, M. (2016). A global analysis of the seaward salt marsh extent: The importance of tidal range. *Water Resources Research*, *52*(51), 5974–5997. https://doi.org/10.1002/2016WR018977.Received

Bannink, B. A., & ten Brinke, W. B. M. (2008). Dutch dikes, and risk hikes–a thematic policy evaluation of risks of flooding in The Netherlands. In M. van Alphen, J., van Beek, E., Taal (Ed.) (p. 325). Nijmegen, The Netherlands: CRC Press.

Been, K., & Jefferies, M. G. (1986). Discussion: A state parameter for sands. *Géotechnique*. https://doi.org/10.1680/geot.1986.36.1.123

Bijker, W. E. (2002). The Oosterschelde Storm Surge Barrier: A Test Case for Dutch Water Technology, Management, and Politics. *Technology and Culture*, *43*(3), 569–584. https://doi.org/10.1353/tech.2002.0104

[Bosch, J.H.A.], [2003]. [Peize Formation]. In: Lithostratigrafische Nomenclator van de Ondiepe Ondergrond. Retrieved [27/03/2019] from [https://www.dinoloket.nl/formatie-van-peize].

Bouma, T. J., van Belzen, J., Balke, T., van Dalen, J., Klaassen, P., Hartog, A. M., … Herman, P. M. J. (2016). Short-term mudflat dynamics drive long-term cyclic salt marsh dynamics. *Limnology and Oceanography*, *61*(6), 2261–2275. https://doi.org/10.1002/lno.10374

Bouma, T. J., van Belzen, J., Balke, T., Zhu, Z., Airoldi, L., Blight, A. J., … Herman, P. M. J. (2014). Identifying knowledge gaps hampering application of intertidal habitats in coastal protection: Opportunities & steps to take. *Coastal Engineering*, *87*, 147–157. https://doi.org/10.1016/j.coastaleng.2013.11.014

Clarke Topp, G. Parkin, G.W. Ferre, T. P. A. (2010). Soil Water Content. In *Soil Sampling and Methods of Analysis, Second Edition*. https://doi.org/10.1201/9781420005271.ch18

Cozzoli, F., Smolders, S., Eelkema, M., Ysebaert, T., Escaravage, V., Temmerman, S., … Bouma, T. J. (2017). A modeling approach to assess coastal management effects on benthic habitat quality: A case study on coastal defense and navigability. *Estuarine, Coastal and Shelf Science*, *184*, 67–82. https://doi.org/10.1016/j.ecss.2016.10.043

Craft, C., Clough, J., Ehman, J., Jove, S., Park, R., Pennings, S., … Machmuller, M. (2009). Forecasting the effects of accelerated sea-level rise on tidal marsh ecosystem services. *Frontiers in Ecology and the Environment*, *7*(2), 73–78. https://doi.org/10.1890/070219

Dadey, K. A., Janecek, T., & Klaus, A. (2006). Dry-Bulk Density: Its Use and Determination. *Proceedings of the Ocean Drilling Program, 126 Scientific Results*, *126*, 551–554. https://doi.org/10.2973/odp.proc.sr.126.157.1992

de Groot, M.B. Stoutjesdijk, T.P. Meijers, P. Schweckendiek, T. (2007). Verwekingsvloeiing in zand. *Geotechniek*, 54–59.

De Vriend, H. J., Koningsveld, van M., Aarninkhof, S. G. J., & Baptist, M. J. (2015). Sustainable hydraulic engineering through building with nature (online first). *Journal of Hydro-Environment Research*. https://doi.org/https://doi.org/10.1016/j.jher.2014.06.004

Deltares. (2017). *D-Flow Slide 16.1.1 Slope Liquefaction and Breaching*.

Deltares. (2018). *D- Flow Slide 18.1.1 Slope liquefaction and Breaching*.

Disco, C. (2002). Remaking "nature": The ecological turn in Dutch water management. *Science Technology and Human Values*, *27*(2), 206–235. https://doi.org/10.1177/016224390202700202

Eelkema, M., Wang, Z. B., Hilba, A., & Stive, M. J. F. (2013). Morphological Effects of the Eastern Scheldt Storm Surge Barrier on the Ebb-Tidal Delta. *Coastal Engineering Journal*, *55*(03), 1350010. https://doi.org/10.1142/S0578563413500101

Eelkema, M., Wang, Z. B., & Stive, M. J. F. (2012). Impact of Back-Barrier Dams on the Development of the Ebb-Tidal Delta of the Eastern Scheldt. *Journal of Coastal Research*, *285*(6), 1591–1605.

https://doi.org/10.2112/JCOASTRES-D-11-00003.1
Eijkelkamp Agrisearch Equipment. (2010). *Penetrologger Operating Instructions*.
Feagin, R. A., Lozada-Bernard, S. M., Ravens, T. M., Moller, I., Yeager, K. M., & Baird, A. H. (2009). Does vegetation prevent wave erosion of salt marsh edges? *Proceedings of the National Academy of Sciences*, *106*(25), 10109–10113. https://doi.org/10.1073/pnas.0901297106
Fourqurean, J. W., Duarte, C. M., Kennedy, H., Marbà, N., Holmer, M., Mateo, M. A., … Serrano, O. (2012). Seagrass ecosystems as a globally significant carbon stock. *Nature Geoscience*, *5*(7), 505–509. https://doi.org/10.1038/ngeo1477
Francalanci, S., Bendoni, M., Rinaldi, M., & Solari, L. (2013). Ecomorphodynamic evolution of salt marshes: Experimental observations of bank retreat processes. *Geomorphology*, *195*, 53–65. https://doi.org/10.1016/j.geomorph.2013.04.026
Gedan, K. B., Kirwan, M. L., Wolanski, E., Barbier, E. B., & Silliman, B. R. (2011). The present and future role of coastal wetland vegetation in protecting shorelines: Answering recent challenges to the paradigm. *Climatic Change*. https://doi.org/10.1007/s10584-010-0003-7
Gedan, K. B., Silliman, B. R., & Bertness, M. D. (2009). Centuries of Human-Driven Change in Salt Marsh Ecosystems. *Annual Review of Marine Science*, *1*(1), 117–141. https://doi.org/10.1146/annurev.marine.010908.163930
Hendriks, M. R. (2010). *Introduction to physical hydrology*. Oxford university press.
Hicks, M. A., & Onisiphorou, C. (2007). Stochastic evaluation of static liquefaction in a predominantly dilative sand fill. In *Risk and Variability in Geotechnical Engineering* (pp. 68–79). Thomas Telford Publishing. https://doi.org/doi:10.1680/ravige.34860.0007
Hordijk, D. (2007). *Prognoseschor en slik ontwikkelingen Oosterschelde : Een onderdzoek ten behoeve van de versterking van steenbekledingen langs de Ossterschelde* ___ _.
Hu, Z., Yao, P., Van Der Wal, D., & Bouma, T. J. (2017). Patterns and drivers of daily bed-level dynamics on two tidal flats with contrasting wave exposure. *Scientific Reports*. https://doi.org/10.1038/s41598-017-07515-y
Jacobse, J. J., van der Zel, M., Arnold, E., & Hofstad, E. J. (2008). Toekomstprognose ontwikkeling intergetijdengebied Oosterschelde. Doorvertaling naar effecten op veiligheid en natuurwaarden, (december).
Jongeling, T. H. G. (2007). Zandhonger Oosterschelde: Maatregelen ter vergroting van doorstroomcapaciteit en zanddoorvoer stormvloedkering Oosterschelde. *WL | Delft Hydraulics*, (November).
Kanning, W. (2012). *The Weakest Link - Spatial Variability in the Piping Failure Mechanism of Dikes*. *Technische Universiteit Delft*. https://doi.org/10.4233/uuid:5fb7b121-dc00-48aa-bda2-b163f10513bf
Li, B., Cozzoli, F., Soissons, L. M., Bouma, T. J., & Chen, L. (2017). Effects of bioturbation on the erodibility of cohesive versus non-cohesive sediments along a current-velocity gradient: A case study on cockles. *Journal of Experimental Marine Biology and Ecology*. https://doi.org/10.1016/j.jembe.2017.08.002
Lo, V. B., Bouma, T. J., van Belzen, J., Van Colen, C., & Airoldi, L. (2017). Interactive effects of vegetation and sediment properties on erosion of salt marshes in the Northern Adriatic Sea. *Marine Environmental Research*, *131*, 32–42. https://doi.org/10.1016/j.marenvres.2017.09.006
Louters, T., van den Berg, J. H., & Mulder, J. P. M. (1998a). Geomorphological changes of the Oosterschelde tidal system during and after the implementation of the delta project. *Journal of Coastal Research*.
Louters, T., van den Berg, J. H., & Mulder, J. P. M. (1998b). Geomorphological changes of the Oosterschelde tidal system during and after the implementation of the delta project. *Journal of Coastal Research*, *14*(3), 1134–1151.

Nienhuis, P. H., & Smaal, A. C. (1994). The Oosterschelde estuary, a case-study of a changing ecosystem: an introduction. *Hydrobiologia*, *282–283*(1), 1–14. https://doi.org/10.1007/BF00024616

Patrick Kiden. (2006). De evolutie van de Beneden- Schelde in België en Zuidwest- Nederland na de laatste ijstijd. *Belgeo*, (3), 279–294. https://doi.org/10.4000/belgeo.12025

Rawls, W.J. Gish, T.J. Brakensiek, D. L. (1986). Estimating Soil Water Retention from Soil Physical Properties and Characteristics. In B. A. Stewart (Ed.), *Advances in Soil Science* (Vol. 4, pp. 213–230). https://doi.org/10.1007/978-1-4613-8847-0

Rijkswaterstaat. (2017). *Regeling veiligheid primaire waterkeringen*.

Rijkswaterstaat, W. V. en L. (2016). *Schematiseringshandleiding zettingsvloeiing*.

[Schokker, J,. de Lang, F.D., Weerts, H.J.T,. den Otter, C. Passchier, S.], [2005]. [Boxtel Formation]. In: Lithostratigrafische Nomenclator van de Ondiepe Ondergrond. Retrieved [27/03/2019] from [https://www.dinoloket.nl/formatie-van-boxtel].

Soil Survey Staff (SSS). (2010). *Keys to Soil Taxonomy, 2010*. *Change*. https://doi.org/10.1109/TIP.2005.854494

Stark, J., Plancke, Y., Ides, S., Meire, P., & Temmerman, S. (2016). Coastal flood protection by a combined nature-based and engineering approach: Modeling the effects of marsh geometry and surrounding dikes. *Estuarine, Coastal and Shelf Science*, *175*, 34–45. https://doi.org/10.1016/j.ecss.2016.03.027

Stouthamer, E. Cohen, K.M. Hoek, W. Z. (2015). *De vorming van het land: geologie en geomorfologie* (7th ed.). Utrecht: copyright 2015 Perspectief Uitgevers, Utrecht.

Stoutjesdijk, T.P. De Groot, M.B. Lindenberg, J. (1998). Flow-slide prediction method: influence on slope geometry. *Can Geotech*, *35*(1), 43–54.

Stoutjesdijk, T., de Groot, M., & Lindenberg, J. (1995). Engineering Approach to Coastal Flow Slides. *Coastal Engineering 1994*, 3350–3359. https://doi.org/doi:10.1061/9780784400890.242

TAW. (1999). Leidraad Zee- en Meerdijken.

Temmerman, S., De Vries, M. B., & Bouma, T. J. (2012). Coastal marsh die-off and reduced attenuation of coastal floods: A model analysis. *Global and Planetary Change*. https://doi.org/10.1016/j.gloplacha.2012.06.001

Temmerman, S., Meire, P., Bouma, T. J., Herman, P. M. J., Ysebaert, T., & De Vriend, H. J. (2013). Ecosystem-based coastal defence in the face of global change. *Nature*. https://doi.org/10.1038/nature12859

van de Meene, E. A. Van der Staaij, J. Teoh, L. H. (1979). *The Van der Staay suction-corer: a simple apparatus for drilling in sand below groundwater table*.

van den Ham, G A de Groot, M. B., & van der Ruyt, M. (2012). *Handreiking Toetsen Voorland Zettingsvloeiing t.b.v. het opstellen van het beheerdersoordeel (BO) in de verlengde derde toetsronde*.

van den Ham, Geeralt A. van der Ruyt, M. (2009). *SBW Buitendijkse afslagbeheer Toetsing op Zettingsvloeiing*.

van Den Ham, G. A., de Groot, M. B., & Mastbergen, D. R. (2014). A semi-empirical method to assess flow-slide probability. In *Advances in Natural and Technological Hazards Research*. https://doi.org/10.1007/978-3-319-00972-8_19

van den Ham, G. A., Mastbergen, D. R., Koelewijn, A. R., ter Brake, C. K. E., & Zomer, W. S. (2015). Eindrapport validatie-experiment zettingsvloeiing, meten aan zettingsvloeiing.

van Dijk, W. M., Mastbergen, D. R., van den Ham, G. A., Leuven, J. R. F. W., & Kleinhans, M. G. (2018). Location and probability of shoal margin collapses in a sandy estuary. *Earth Surface Processes and Landforms*. https://doi.org/10.1002/esp.4395

van Duinen, A., Bezuijen, A., van den Ham, G., & Hopman, V. (2014). Field Measurements to

Investigate Submerged Slope Failures. In S. Krastel, J.-H. Behrmann, D. Völker, M. Stipp, C. Berndt, R. Urgeles, … C. B. Harbitz (Eds.), *Submarine Mass Movements and Their Consequences: 6th International Symposium* (pp. 13–21). Cham: Springer International Publishing. https://doi.org/10.1007/978-3-319-00972-8_2

Verruijt, A. (2001). *Grondmechanica*. Delft University.

Vos, P.C. van Heeringen, R. M. (1997). Holocene geology and occupation history of the province of Zeeland. *Mededelingen Nederlands Instituut Voor Toegepaste Geowetenschappen TNO*, (59), 5–109.

Wang, H., van der Wal, D., Li, X., van Belzen, J., Herman, P. M. J., Hu, Z., … Bouma, T. J. (2017). Zooming in and out: Scale dependence of extrinsic and intrinsic factors affecting salt marsh erosion. *Journal of Geophysical Research: Earth Surface*, *122*(7), 1455–1470. https://doi.org/10.1002/2016JF004193

Waterschap Scheldestromen. (2016). *Waterkeringenbeheerplan*.

[Weerts, H.J.T. & Busschers, F.S.], [2003]. [Nieuwkoop Formation]. In: Lithostratigrafische Nomenclator van de Ondiepe Ondergrond. Retrieved [27/03/2019] from [https://www.dinoloket.nl/formatie-van-nieuwkoop].

Wesselink, A., Warner, J., Syed, M. A., Chan, F., Tran, D. D., Huq, H., ... & Wester, P. (2015). Trends in flood risk management in deltas around the world: Are we going ‘soft’? *International Journal of Water Governance*, *4*(4), 25–46. https://doi.org/10.7564/15-IJWG90

[Westerhoff, W.E &. Weerts, H.J.T], [2003]. [Waarle Formation]. In: Lithostratigrafische Nomenclator van de Ondiepe Ondergrond. Retrieved [27/03/2019] from [[https://www.dinoloket.nl/formatie-van-waalre].

Wilderom, N. H. (1979). *Resultaten van het vooroeveronderzoek langs de Zeeuwse stromen.*

8. APPENDIX 1

To understand the mechanism of static liquefaction for water saturated sand and silt layers a general understanding of the relation between shear stress changes and the related deformation of the soil skeleton is required. This relation can be illustrated best by examples of triaxial test on dry sands and water-saturated sands.

When constant vertical stress (σ'_v) is applied to dry sand shear strain (τ) will increase. This will lead to contraction, decreasing the volume strain ($\varepsilon_{vol<0}$) of the sand after which dilatancy, will magnify the volume strain of the sand, $\varepsilon_{vol}>0$ (Fig. 65).

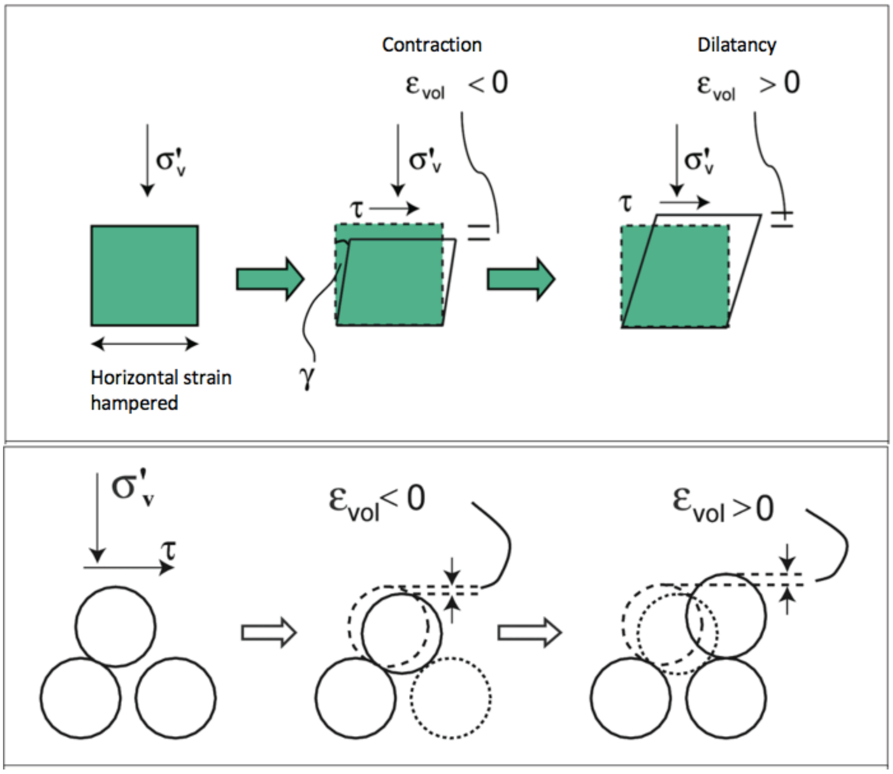

Figure 65: Changes to volume(ε_{vol}) of sand with constant vertical stress(σ'_v) and vertical shear strain(τ). First contraction will reduce the volume (ε_{vol}<0) after which the volume will increase again (ε_{vol}>0) with dilatancy (adapted from: de Groot et al., 2007).

With shear strain, grains first fill up the cavities in the soil skeleton and afterwards roll over on top of other grains. When applying an all-round external stress (deviator stress, q), to a sand particle with internal isotropic particle stress (p'), the phase of dilatancy will end to a steady state will be reached with shear strain (γ) still increasing but all other parameters staying constant (volume, deviator stress and isotropic stress) shown in Figure 66.

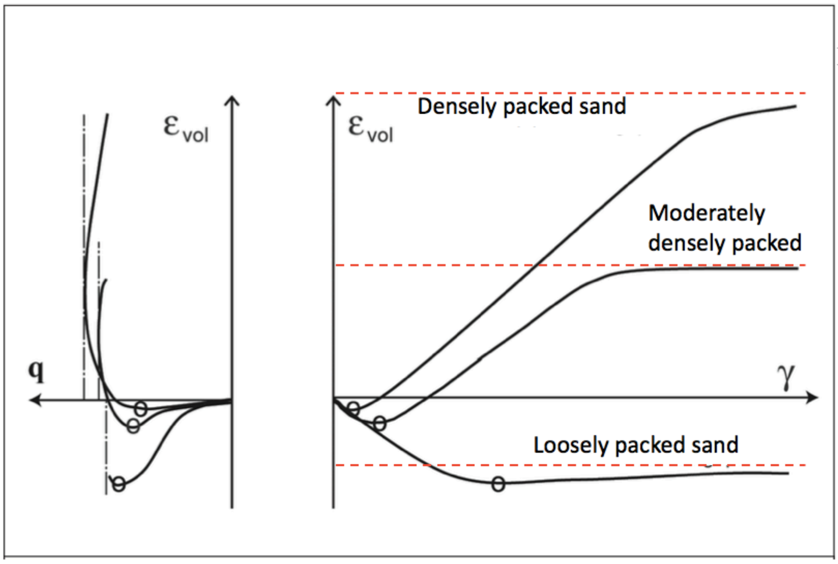

Figure 66: different shear strain trajectories for variously packed sand bodies. Discontinued red line indicates the steady state where internal isotropic particle stress (p'), external deviator stress (q, σ'$_v$), the volume strain (ε_v) stays constant while shear strain (γ) increases (adapted from: de Groot, et al., 2007).

Contrary to dry sand, for a saturated sand body the volume cannot change as was described for the example above. Instead a water overpressure is being generated by which the soil skeleton experiences both contraction and dilatancy averaging out to a zero-volume change (Figure 67). This principle can be understood through the following equation:

$$p = p' + u \qquad \text{or} \qquad p' = p - u \ [\text{kN/m}^2 \text{ or kPa}] \qquad (16)$$

Here, water pressure u is the difference between the total stress of the soil (p) and isotropic grain stress (p'). the soil stress increases with growing external deviator stress (q). The grain stress (p') shows a contrary signal and first decreases after which it increases to the steady state value. From this equation and Figure 15 it follows that the less dense the sand body is packed the higher the water over pressure within the soil structure becomes with increasing deviator stress (q).

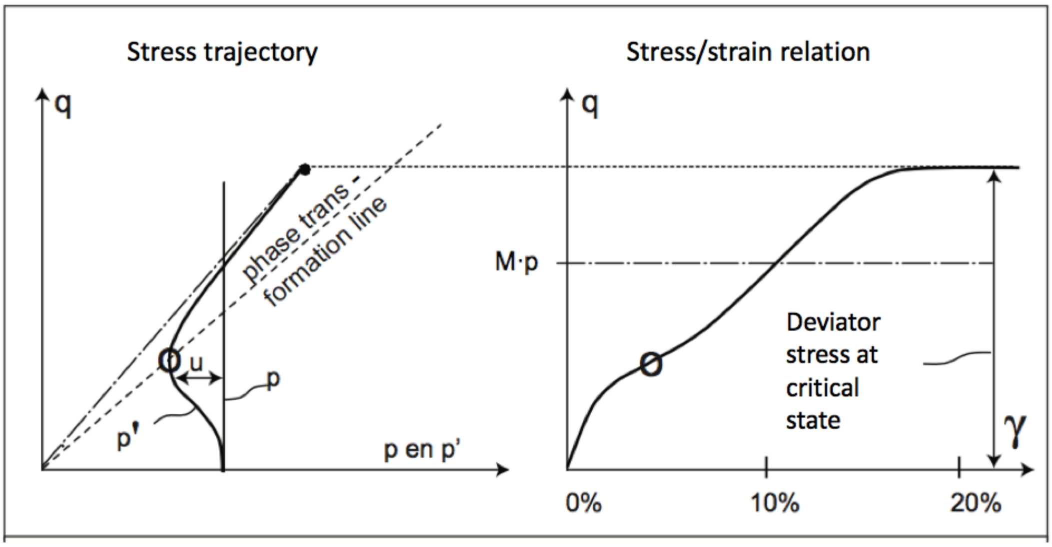

Figure 67: Left: An increasing water overpressure u develops when the deviator stress (q) applied to a saturated sand body, increases. Volume change is zero for a saturated sand body in contrary to the situation of dry sand. Therefore the total ground stress (p) stays unchanged and the grain stress p' decreases simultaneously until the phase transformation line. Right: the Deviator stress (q) stays constant at the critical state with shear strain(γ) still increasing (adapted from: de Groot et al., 2007).

A special phenomenon occurs within the shear trajectory of loosely packed sand, as the deviator stress (q) reaches an intermediate maximum indicated with the red star. From this maximum, it decreases to a moment of maximum contraction ('phase transformation'), which is indicated with a 0 and then reduces to negative values. Here the shear strain is still small but the deviator stress has almost reached its maximum. This proportion of contraction and dilatancy is strongly related to both density and stress state of the soil structure. When comparing the path of the deviator stress with different sand body densities it appears that for denser soil structures this intermediate maximum is no longer reached. The moment of this intermediate maximum is called the wet critical density. Soils with a higher initial ground stress (p) or a low initial density (Figure 68 & Figure 69) often lie beneath the distinction line of the wet critical density, indicated with the discontinued red line in Figure 68.

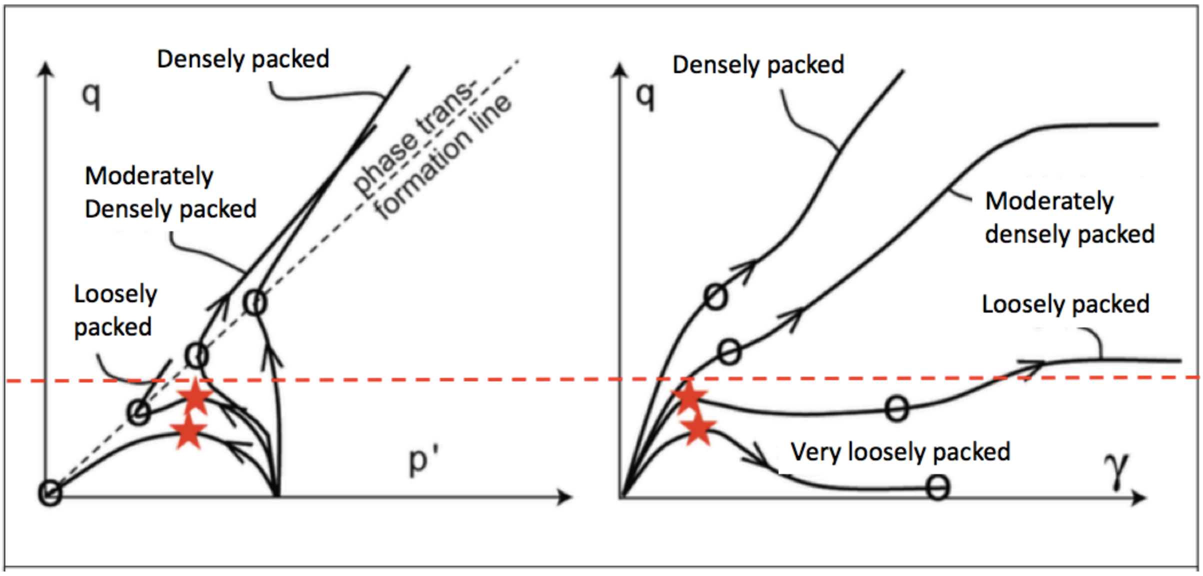

Figure 68: Intermediate maximum of deviator stress(q) for loosely packed sand (indicated with the red star), decrease to a moment of maximum contraction ('phase transformation') indicated with a 0 and boundary of wet critical density (indicated with the discontinued red line) (adapted from: de Groot et al., 2007).

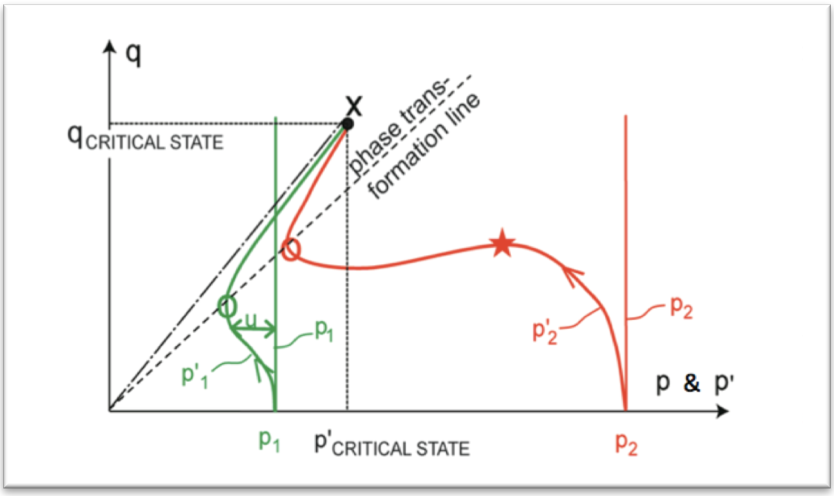

Figure 69: Higher initial ground stress (p) results in a density below the wet critical density (adapted from: de Groot et al., 2007).

For every type of sand a unique relation exists between the density of the sand body/ void ratio and the critical state values of deviator stress (q) and grain stress (p'). This relation is called the critical state line (de Groot et al.,2007 and is illustrated in Figure 70 with the stress trajectories of Figure 69. The difference between the in situ void ratio and the void ratio at the steady state/ critical state is named the state parameter (ψ) (Been & Jefferies, 1986). The larger the state parameter is (positive value) the more sensitive the sand is for static liquefaction.

With a high ground stress (p), the grain stress (p') should subsequently decrease to the steady/ critical state. This implies a generation of water overpressure (u) causing instability of the sand. This process of instability is illustrated in Figure 71, where the body of sand is not in a balanced state at the intermediate maximum of q at point A and jumps to a new state at point B. As the net ground stress is unchanged and p' decreases, the water over pressure develops in the same split second accompanied with high shear strain causing the instability. In point A, known as the meta- stability point of the soil, only a small trigger could lead to the liquefaction.

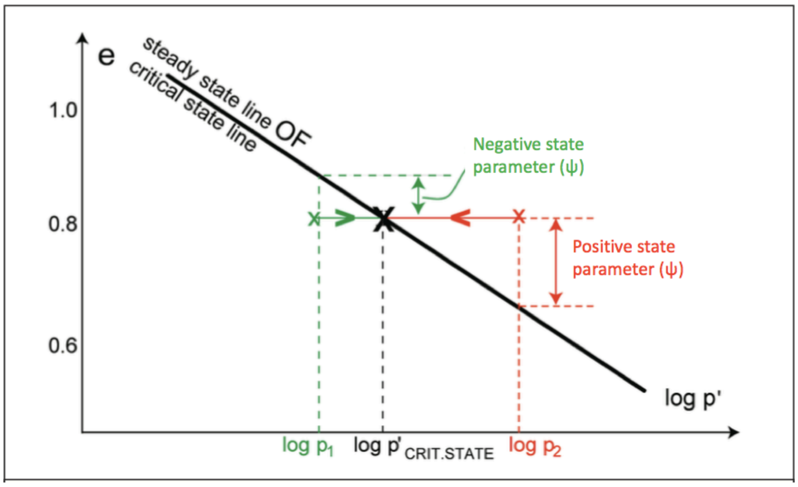

Figure 70: The difference to the in-situ void ratio and the void ratio at the steady state/ critical state is known as the state parameter (ψ). A positive value for ψ implies sensitivity to liquefaction (adapted from: de Groot et al., 2007).

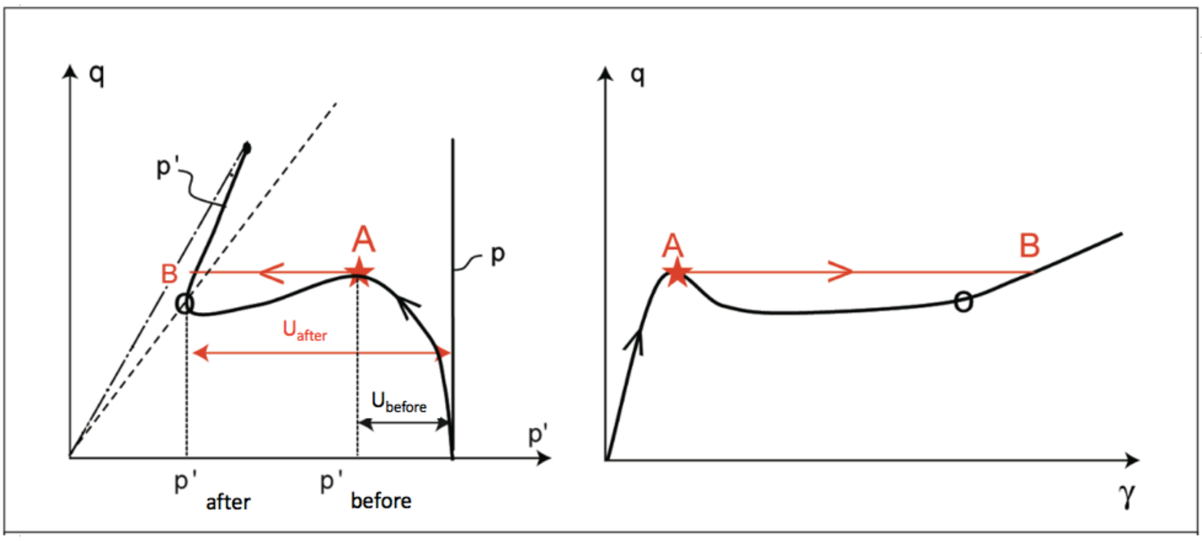

Figure 71: A sudden shift from the point of metastability (A) to point of phase transformation (B) (adapted from: de Groot et al., 2007).

9. APPENDIX 2

Together with the empirical data from historical cases a semi empirical method has been developed to quantify the influence of site characteristics on flow slide probability based on empirical data (Rijkswaterstaat, 2016; van den Ham, de Groot & van der Ruyt, 2012; van den Ham, Mastbergen, Koelewijn, ter Brake, & Zomer, 2015; van Den Ham et al., 2014). This method tweaks the flow slide probability with a mean slope as starting point and quantifies the influence of local deviations using the empirical data. As most of the flow slides encompass both mechanisms of static liquefaction and breaching the probability of flow slides can be written as :

$$P(ZV) = 0.5 \cdot P\,(ZVliquefaction) + 0.5 \cdot P\,(ZVbreachflow) \tag{17}$$

Within this equation, the occurrence of liquefaction is dependent on (1) the stress state, expressed by the fictious slope height, H_R (shown in Figure 72). Here the height of the above water part of the slope is also included and the average of the underwater slope and an average under-water slope angle (cotanα_R) to simulate the most unfavourable situation of water overpressure during the assessment.

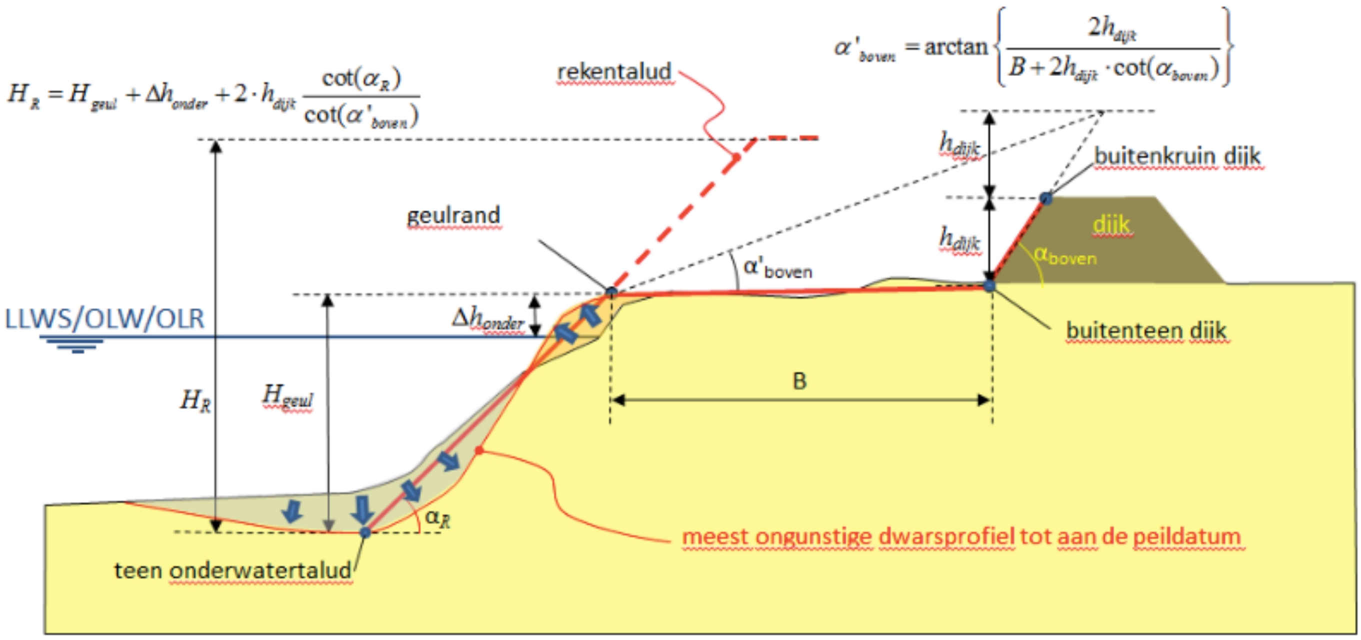

Figure 72: determination of H_R in its most unfavourable situation during the assessment period. In this figure: Hgeul is depth of the channel [m], Δh_{onder} is the height of the slope above the water level during extreme low water: "niveau van geulrand" – "niveau LLWS/OLW/OLR" [m], h_{dijk} height of the levee with respect to the outer toe of the levee [m], B is the width of the foreland. In case of a so-called "schaardijk", B = 0 [m], cot(α) is the cotangent of the slope α [-], α_R is the slope angle of the schematized fictitious under water profile [degrees], α_{boven} is the slope of the outer slope of the levee [degrees] and α'_{boven} is the slope between incision of channel and the fictitious outer crest of the levee with a height of 2.h_{dijk} In case of a "schaardijk", α'boven = αboven [degrees] (Deltares 2017).

Furthermore, the probability of liquefaction depends on (2) the packing of the liquefiable layer expressed in relative density (I_D) of the subsoil (Equation 3) or the state parameter (ψ). The thickness of the layer is set to be 5 meters as this is the minimal thickness of the layer to be vulnerable to liquefaction. For the occurrence of breach flow, the medium grain size (D_{50}) and the presence of clay layers are included as important parameters too (van den Ham et al., 2014). This leads to the following two equations for both the probability of static liquefaction and breaching:

$$P\left(ZV_{liquefaction}\right) = f1(H_R) \cdot f2(\text{cotan}\alpha_\text{R}) \cdot f3(\text{density}) \tag{18}$$

$$P\left(ZV_{breaching}\right) = f4(H_{RB}) \cdot f2(\text{cotan}\alpha_\text{R}) \cdot f5(D_{50}) \cdot f6(claylayers) \tag{19}$$

Based on additional analytical calculations performed by (Stoutjesdijk, De Groot, Lindenberg, 1998) with the liquefaction programme SLIQ2D these probability equations could be further defined. As was earlier discussed, the frequency of flow slides increases when the relative density of the sand body decreases. When the relative density decreases with 10 % this corresponds with an increase of the state parameter (ψ) of 0.05 (van den Ham et al., 2014). However, the size of the metastable area also increases if the slope height is enlarged with a factor three (from 5 to 15 m) or with an increase of slope angle by a factor of 1.5 (from 1:6 to 1:4). These factorial relations lead to the following (van den Ham., 2014; van Dijk, Mastbergen, van den Ham, Leuven, & Kleinhans, 2018) :

$$P\left(ZV_{liquefaction}\right) = \left(\frac{(H_R)}{24}\right)^{2.5} \cdot \left(\frac{5}{(\text{cotan}\alpha_\text{R})}\right)^{5.7} \cdot \left(\frac{1}{10}\right)^{-10(0.05+\psi)} \tag{20}$$

In Figure 73 the effect of H_R, the slope angle cotan αR and the relative density is shown to be related to the frequency of metastability as calculated with SLIQ2D (Stoutjesdijk, De Groot, Lindenberg, 1998).

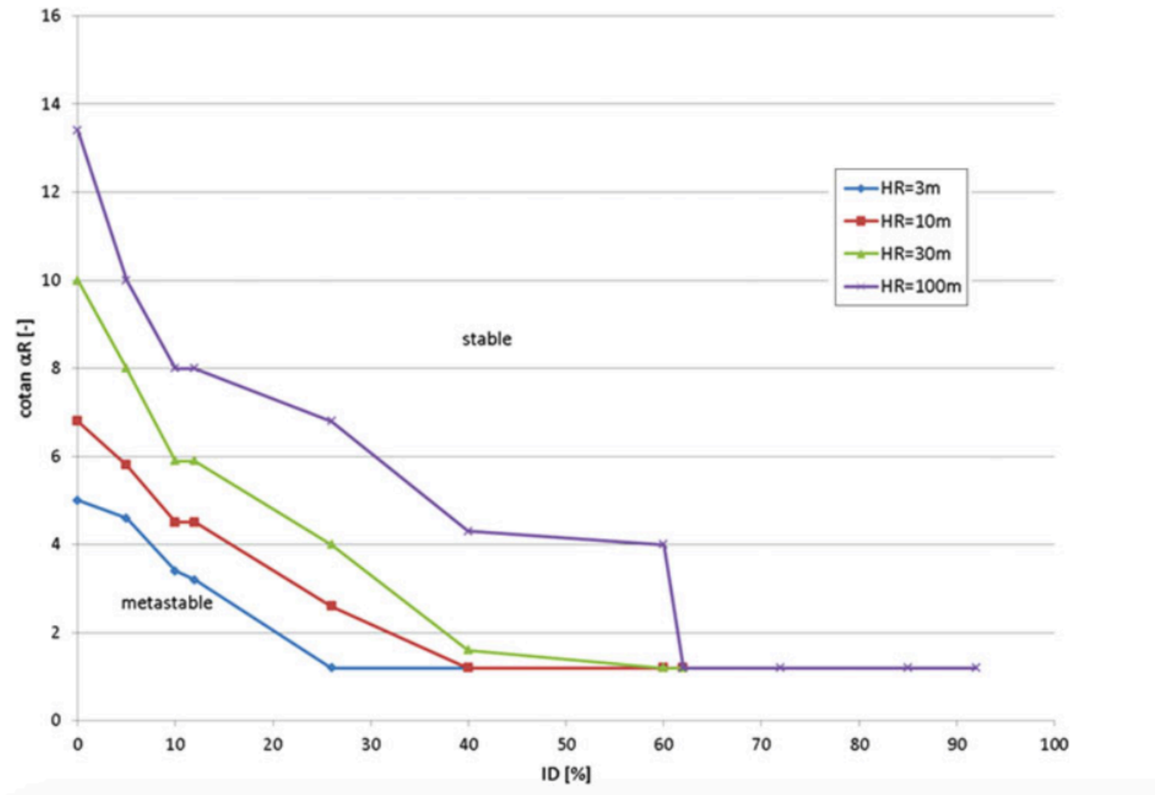

Figure 73: relation of H_R, the slope angle cotanαR and the relative density influences the frequency of meta stability as calculated with SLIQ2D (Stoutjesdijk, De Groot, Lindenberg, 1998)

With the similar analytical programme to SLIQ2D, HMBreach the sensitivity of sandy slopes to an initial breach was investigated for different slopes and grainsizes (Figure 74). It was shown that for a decrease in grainsize from 200 µm to 125 µm and a reduce of slope angle of cotan 4 to cotan 6 led to a critical value to which a self-accelerating turbulent sand-water mixture flow is initiated (sand transport, sz). Herby f5 can be expressed as (van den Ham et al., 2014):

$$f5(D_{50}) = \left(\frac{2\cdot 10^{-4}}{D_{50}}\right)^{E} \; where \; \frac{f5(1.25\cdot 10^{-4})}{f5(2\cdot 10^{-4})} = \frac{f2(6)}{f2(4)} \; or \; \left(\frac{1.25\cdot 10^{-4}}{2\cdot 10^{-4}}\right)^{E} = \left(\frac{6}{4}\right)^{5.7} \qquad (21)$$

and E is then found to be 5.

In a similar matter f4 is found to be $f4(H_{RB}) = \left(\frac{H_{RB}}{24}\right)^{D}$ where D is 5 is found (Deltares, 2017; van den Ham, 2014).

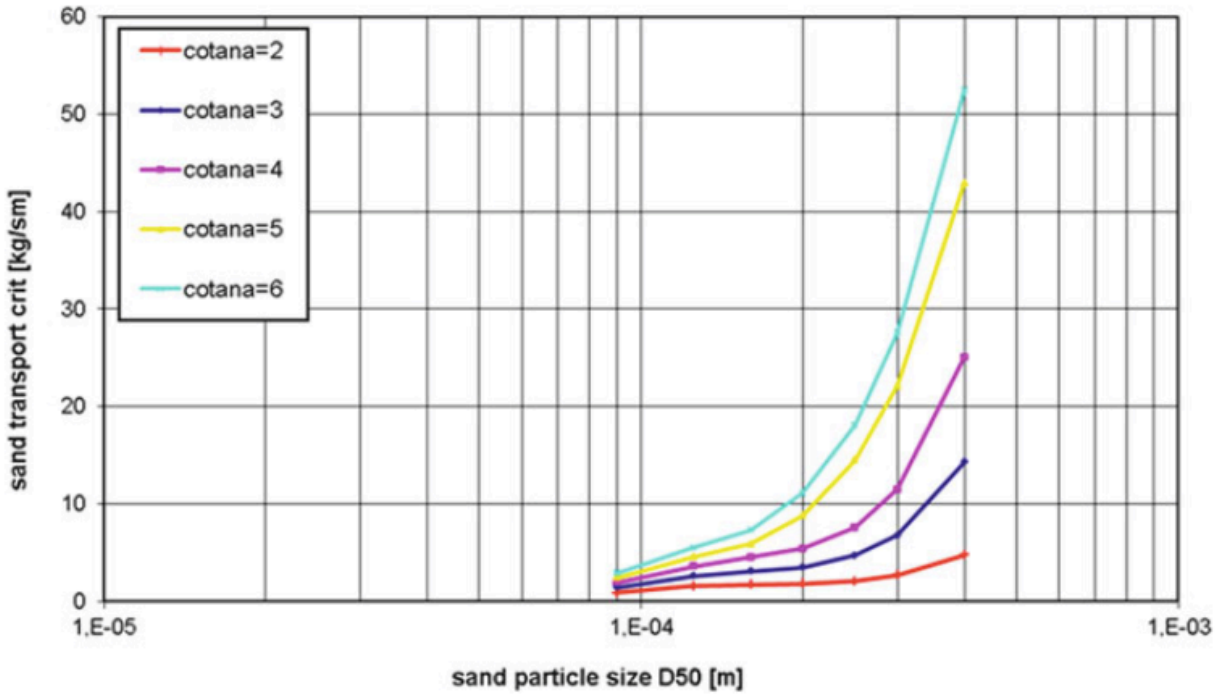

Figure 74: relation of grainsize, slope - angle and critical sand transport (kg/sm) (van den Ham et al., 2014).

The presence of cohesive layers from clayey or peaty material increases the probability of a trigger to occur. When an upwards moving breach reaches these layers, a sudden dilation of the vertical breach can arise. This leads to an increase of erosion and sand displacement. This effect however only occurs with cohesive layers' present with an individual thickness larger than 0.5 meters. When the thickness of the layer exceeds 5 meter the layer has an opposing effect to the initiation of the breach. With this knowledge f6 can be expressed as a single constant. Here F may vary from 1/3 (no clay layers) to 3 (many clay layers). For Zeeland's alternation of clay layers within the sand successions of young Holocene depositional age, F= 1 holds representing the median. This results in the following equation for P (ZVbreach). As for all the flow slides documented by Wilderom, it could not be determined which sub mechanism was main responsible; it could be considered that half of the total was due to static liquefaction and half due to breaching. This then leads to the total probability of P (ZVliquefaction) and P(ZVbreach) taken together.

$$P(ZV) = \left(\frac{5}{(\mathrm{cotan}\alpha_R)}\right)^{5.7} \left\{0.5 \cdot \left(\frac{(H_R)}{24}\right)^{2.5} \cdot \left(\frac{1}{10}\right)^{-10(0.05+\psi)} + 0.5 \cdot \left(\frac{(H_R)}{24}\right)^{5} \left(\frac{2 \cdot 10^{-4}}{D_{50}}\right)^{5} \cdot Fcohesivelayers\right\} \cdot 0.02\ km^{-1} \cdot year^{-1} \qquad (22)$$

10. APPENDIX 3a

Global check (retrieved from **https://publicwiki.deltares.nl/display/GEO/Background+-+Global+check**)

The global check as implemented in **D-Flow Slide** comprises the following steps, which can also be found in Toetsmethode zettingsvloeiing (version 2, 22 febr. 2016).

Step 1a : Would flow slide lead to damage on levee (i.e. is the "schadelijksheidscriterium" met)?
The damage criterion ("schadelijksheidscriterium" in Dutch) is met if at the so-called assessment level ("beoordelingsniveau") the actual slope lies landward of the so-called assessment profile ("signaleringsprofiel"), see Figure below, which is adopted from Toetsmethode zettingsvloeiing (version 2, 22 febr. 2016).

1) Determination of the assessment profile
The required margin (the horizontal part from the "invloedslijn" of the dike) depends on the presence of a revetment and is determined by the relation:

- in case **no** revetment: $M = 2\ H_{geul}$
- in case a revetment: $M = \text{Max}\ [\ M_{bestorting} - L_{influence};\ 2\ H_{onbest})\ ]$ (see also figure below)

where:
H_{geul} is the channel depth
H_{onbest} is the depth of the channel below the top revetment.
$M_{bestorting}$ is the horizontal projection of the length of the top revetment starting at the outer dike toe
$L_{influence}$ is the length of the influence zone from the outer dike toe

The influence zone is defined as follows: if this zone is damaged by an indirect failure mode, for example a flow slide, the safety of the dike drops below the required safety level, considering all direct failure modes. At surface level the influence zone is confined by influence lines (in Dutch: "invloedslijnen").

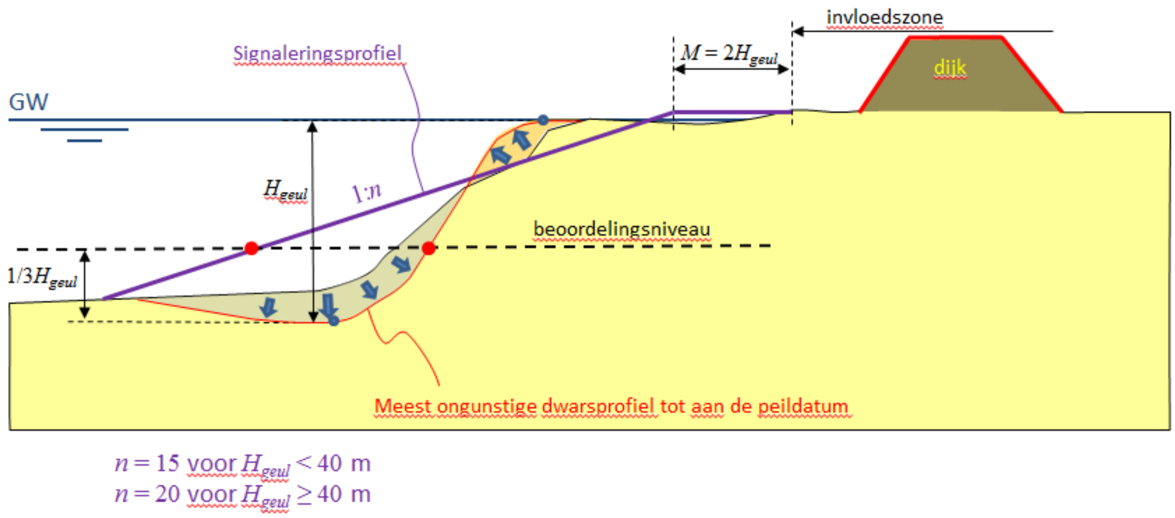

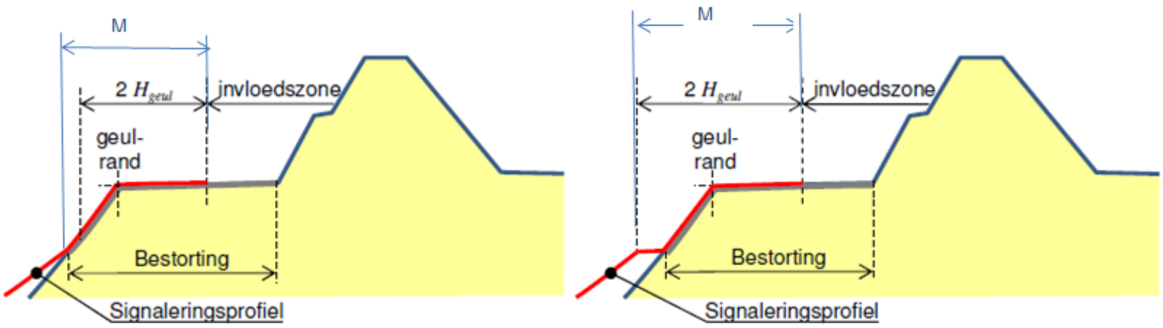

Schadelijksheidscriterium - Determination of the observation profile ("signaleringsprofiel") when a top revetement is present

In case no slope protection is present, this margin is thus equal twice the fictive channel depth (M = 2 H), assuming that entire submerged consists of sand that is sensitive to liquefaction and/or breach flow. The inclined part of the observation profile in line with the horizontal portion. The inclination of the slope depends on the channel depth:

- 1:15 if the fictive channel depth is less than 40 m ($H < 40$ m)
- 1:20 if the fictive channel depth is more than 40 m ($H \geq 40$ m)

2) Determination of the assessment level

The assessment level is the lower boundary of the liquefiable sand layer, but has a minimum and maximum of H/3 and H/2 above the bottom of the channel respectively.

3) Comparison of the observation profile with the existing profile at the assessment level

S_{sign} is the intersection point between the observation profile (from the foreshore) and the assessment level and S_{ZV} is the intersection point between the existing profile and the assessment level.

If the liquefaction point S_{ZV} is situated landwards of the observation point S_{sign} (so as in figure above), the criteria is met, so go to step 1c.
If the liquefaction point S_{ZV} is not situated landwards of the observation point S_{sign}, the criteria is not met, which means that the Global check PASSES.

Step 1b: Criterion on slope protection met (<1:2,5)?
The slope directly in front of the toe of the dike or outer boundary of the slope protection, may not cut a 1:2.5 slope that starts at the toe of the dike or outer boundary of the slope protection respectively.
This check should be performed only if the damage criterion (step 1a) is not met (i.e. a flow slide does not lead to damage). The result of this check will not result in a "failure" in the safety assessment, but only indicates that the slope protection may become unstable.
As this check has no influence on the final answer, it is therefore not performed and the answer is always "Not available".

Step 1c: Artificially underwater installed and non-compacted sandy foreland ?
The nature of the submerged slope is given as input by the user in the "General parameters" window.
In case of non-natural deposited slopes, both Global and Overall checks FAIL and it should immediately be switched to the Advanced methods.
In case of natural deposited slopes, go to step 1d.

Step 1d: Is flow slide possible based on the occurrence criterion of "the steepest slope over 5 m"?
If the previous step (step 1c) has not been passed, a check on the first of two occurrence criteria ("optredingscriteria") must be performed.
A flow slide can occur if the following condition is met: the average slope is steeper than or equal to 1:4, over a height of at least 5 m.

If this occurrence criterion is met, both Global and Overall checks FAIL and it should be switched to Advanced methods.
If this occurrence criterion not met, go to step 1e.

Step 1e: Is flow slide possible based on the occurrence criterion based on average geometry?
If the previous step (step 1d) has not been passed, a check on the second occurrence criterion must be performed.
A flow slide can occur if one of the two following conditions is met:

- Liquefaction is possible: the total slope (channel edge-channel bottom) is on average steeper than or equal to 1 : [7 × $(H_R/24)^{(1/3)}$], in which H_R is defined below.
- Breaching is possible: see paragraph below called "Breach flow criteria"

If the criteria of occurrence is met, the Global check FAILS and it should be switched to the Detailed method.
If the criteria of occurrence is not met, the Global and the Overall checks SUCCEED.

<u>Liquefaction flow criteria:</u>

H_R [m] is the fictitious height of the submerged slope in its most unfavourable situation during the assessment period and determined with:

$$H_R = H_{geul} + \Delta h_{onder} + 2 \cdot h_{dijk} \cdot \frac{\cot(\alpha_R)}{\cot(\alpha'_{boven})}$$

in which:

$$\alpha'_{boven} = \arctan\left\{\frac{2h_{dijk}}{B + 2h_{dijk} \cdot \cot(\alpha_{boven})}\right\}$$

$$h_{boven} = 2 \cdot h_{dijk}$$ (with h_{dijk} is dike height)

In which::
H_{geul} depth of the channel [m]
Δh_{onder} height of the slope above the water level during extreme low water: “niveau van geulrand” – “niveau LLWS/OLW/OLR” [m]
h_{dijk} height of the levee with respect to the outer toe of the levee [m]
B width of the foreland. In case of a so-called "schaardijk", $B = 0$ [m]
$\cot(\alpha)$ cotangent of the slope α [-]
α_R slope angle of the schematized fictitious under water profile [degrees]
α_{boven} slope of the outer slope of the levee [degrees]
α'_{boven} slope between incision of channel and the fictitious outer crest of the levee with a height of $2.h_{dijk}$ In case of a "schaardijk", $\alpha'_{boven} = \alpha_{boven}$ [degrees]

Other symbols in the figure below are (in Dutch):

LLWS meerjarig gemiddelde van het laagste springlaagwater ten opzichte van NAP, geldig in het kustgebied en de estuaria.
OLW Overeengekomen Laag Water ten opzichte van NAP, geldig in het benedenrivierengebied (in Waal stroomafwaarts van Tiel).
OLR Overeengekomen Lage Rivierstand ten opzichte van NAP, geldig in het bovenrivierengebied (in Waal stroomopwaarts van Tiel), hetgeen overeenkomt met de Overeengekomen Lage Afvoer bij Lobith.

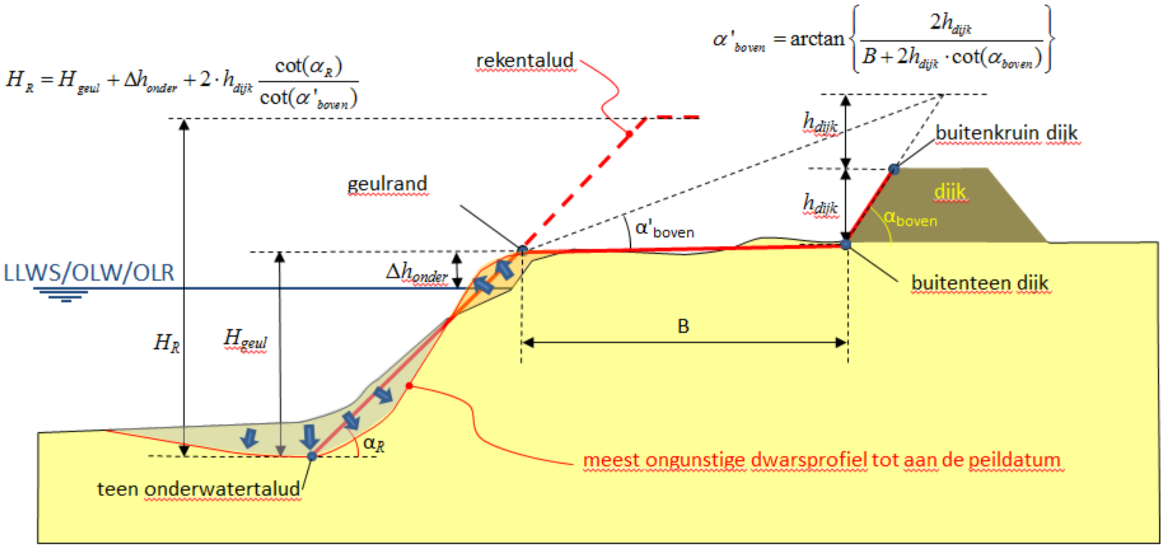

Breach flow criteria:

This criterion is adopted from step 5 of CUR Aanbeveling 113, 2008.
When considering the geometry of the slope, are there parts of the slope with a height as given in the first column of the tables below which is equal to or steeper than the slope given in the second column?
If so then the slope is sensitive to breaching. This means that the check fails and a Detailed check should be performed. In the case the slope height is larger than 40 m a Detailed check is also needed.

Different cases are considered to determine the critical slope:

- a slope with or without horizontal steps ("berms")
- the sand type:
- very fine sand with $D_{50,5m} \leq 200$ µm and $D_{15,5m} \leq 100$ µm
- medium fine sand with $200 < D_{50,5m} \leq 500$ µm and $100 < D_{15,5m} \leq 250$ µm
- coarse sand and gravel with $D_{50,5m} > 500$ µm and $D_{15,5m} > 250$ µm

where $D_{15,5m}$ and $D_{50,5m}$ are the minimum averaged values (only for sand and gravel soils) over a thickness of 5 m between the water line and the toe of the channel slope.
The type of sand (particle size) is a user-defined parameter: very fine sand, medium fine sand or coarse sand/gravel.
The program checks that the user-defined parameter is coherent with:

- the calculated diameter $D_{50;5m}$ if a Detailed check is performed
- the calculated diameter $D_{15;5m}$ and $D_{50;5m}$ if an Advanced Breach flow check is performed

In case of a incoherence, the Overall result gives a Warning message.
NOTE: In the current version of the program, it is not checked if the thickness is minimal 5 m. The average is performed over a thickness of 5 m, by not taking into account the none-sandy layers.

NOTE: In case the user-defined sand type is "very fine sand", the breach flow criteria cannot be checked. The program indicates breach flow is possible and a warning message will be given in the Overall Results window.

Table with th average and local slope

from depth [m +GL[a]]	**to depth z [m +GL[a]]**	**Average slope**			
from depth [m +GL[a]]	**to depth z [m +GL[a]]**	**Average slope**			
		Medium fine sand $D_{50} > 200$ µm and $D_{15} > 100$ µm		Coarse sand/Gravel $D_{50} > 500$ µm and $D_{15} > 250$ µm	
		Local slope	Average slope 0 - z	Local slope	Average slope 0 - z
0	-5	1:2	1:2	1:2	1:2
-5	-10	1:3	1:2.5		
-10	-15	1:4	1:3	1:3	1:2.5
-15	-20	1:5	1:3.5		
-20	-25	1:6	1:4	1:4	1:3
-25	-30	1:8	1:4.67		
-30	-35	1:10	1:5.43	1:6	1:3.75
-35	-40	1:10	1:6		

[a] In D-Flow Slide, the ground surface level (GL) (maaiveld in Dutch) is the lowest level between the water level and the top of the channel slope (called "Insert river channel").

<u>NOTE:</u>
The above table is based on Table A.4.2a from CUR113b, In D-Flowslide only "without horizontal steps" are implemented, as defined in the CUR-report.

11. APPENDIX 3b

Detailed check (**https://publicwiki.deltares.nl/display/GEO/Background+-+Detailed+check**)

The detailed check is a probabilistic check on section level ("vakniveau"). The way in which dike sections are defined are described in the Schematiseringshandleiding zettingsvloeiing. Per dike section the following steps have to be passed through subsequently, see also Rekenregels voor gedetailleerde toets:

Step 1 Determine the probability of occurrence per subsurface scenario S_i: $P(ZV|S_i)$
Step 2 Determine the probability of occurrence for all subsurface scenario's: $P(ZV|S_i)P(S_i)$ *(not supported by D-FlowSlide)*
Step 3 Determine the probability of exceedance of the maximum allowable retrogression length (inscharingslengte) given the occurrence of a flow slide: $P(L > L_{toelaatbaar}|ZV)$.
Step 4 Determine the probability of exceedance of the maximum allowable retrogression length (inscharingslengte) of the dike section: $P(L > L_{toelaatbaar})_{vak}$.
Step 5 Check if $P(L > L_{toelaatbaar})_{vak}$ is less than the allowable probability $P_{eis,vak}$. *(not supported by D-FlowSlide)*

Step 2 is not supported by D-FlowSlide. In case of more than one subsurface scenario, for each scenario $(P(L > L_{toelaatbaar})_{vak})P(S_i)$ can be calculated and then combined in $(P(L > L_{toelaatbaar})_{vak})$. In fact step 2 is done after step 4.
Also Step 5 is not supported by D-FlowSlide and should be done by hand.
Step 1
Determine the probability of occurrence per subsurface scenario $P(ZV|S_i)$
First per subsurface scenario the frequency $F(ZV|S_i)$ is calculated:

$$F(ZV|S_i) = \left(\frac{5}{cot\alpha_R}\right)^5 \left\{0.5 \cdot \left(\frac{H_R}{24}\right)^{2.5} \cdot \left(\frac{1}{10}\right)^{-10\cdot(0{,}05+\psi_{5m,kar})} + 0.5 \cdot \left(\frac{H_{geul}}{24} \right. \right.$$
$$\left. \cdot \left(\frac{2\cdot 10^{-4}}{d_{50,gemiddeld,kar}}\right)^5 \cdot F_{cohesivelayers}\right\} \cdot L_{vak} \cdot \frac{V_{lokaal}}{V_{Zeeland}} \cdot 0.($$
$$\cdot\, year^{-1} \qquad (1)$$

The frequency is transformed into a probability with:

$$P(ZV|S_i) = 1 - e^{-F(ZV|S_i)} \qquad (2)$$

A detailed description how the parameters in the equations above should be determined is given in the schematiseringshandleiding. Below a brief description is given, by subdividing the parameters referring to slope geometry, soil properties/state and dynamics of the geometry respectively:

Geometry (see figure below):
The geometry of the fictitious under water slope (*reken*talud), resulting in highest probability of failure during the assessment period (e.g. 12 years) is characterized by the fictitious slope height H_R [m] slope angle α_R [graden]:

$$H_R = H_{geul} + \Delta h_{onder} + 2 \cdot h_{dijk} \cdot \frac{\cot(\alpha_R)}{\cot(\alpha'_{boven})}$$	(3)

with

$$\alpha'_{boven} = \arctan\left\{\frac{2h_{dijk}}{B + 2h_{dijk} \cdot \cot(\alpha_{boven})}\right\}$$	(4)

in which:

H_{geul} channel depth [m]

Δh_{onder} height of the slope above the water level during extremely low tide: "niveau van geulrand" – "niveau LLWS/OLW/OLR" [m]

h_{dijk} crest height of the dike above the outer dike toe [m]

B distance between outer dike toe and top of the top of the channel bank ("geulrand"). In case of a "schaardijk": $B = 0$ [m]

α_R angle the (schematized) under water slope [degrees]

α_{boven} angle of the outer slope of the dike [degrees]

α'_{boven} fictitious slope angle of a line running from the top of the channel bank to the crest of a fictitious dike with a height equal to two times the actual dike height [degrees]. In case of a "schaardijk" $\alpha'_{boven} = \alpha_{boven}$

Other parameters in the figure (Dutch)

LLWS meerjarig gemiddelde van het laagste springlaagwater ten opzichte van NAP, geldig in het kustgebied en de estuaria.
OLW Overeengekomen Laag Water ten opzichte van NAP, geldig in het benedenrivierengebied (in Waal stroomafwaarts van Tiel).
OLR Overeengekomen Lage Rivierstand ten opzichte van NAP, geldig in het bovenrivierengebied (in Waal stroomopwaarts van Tiel), hetgeen overeenkomt met de Overeengekomen Lage Afvoer bij Lobith.

A detailed description how various bends (characteristic points) are determined is given in the schematiseringshandleiding.

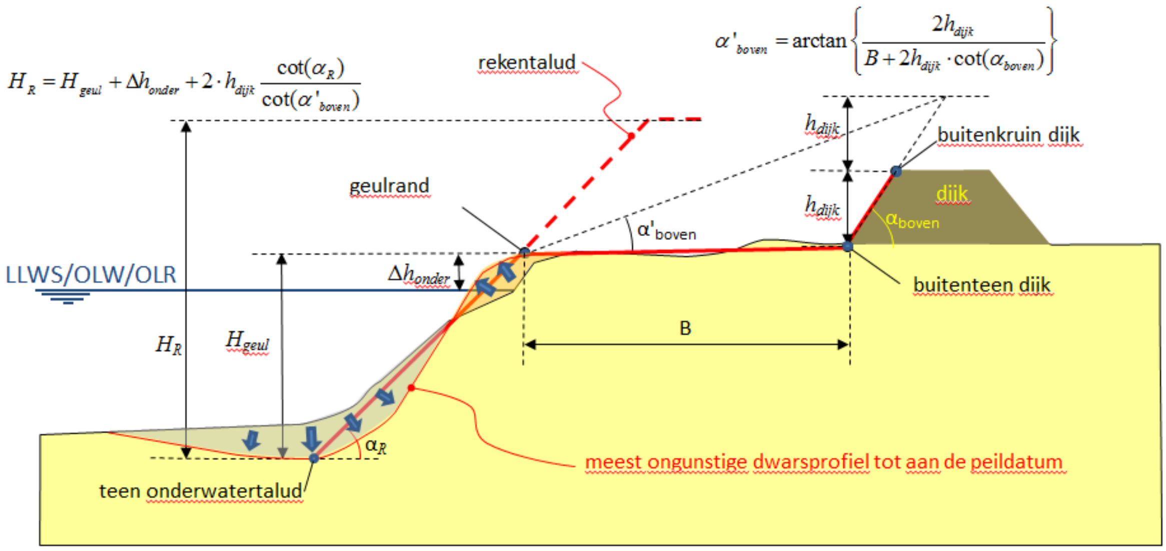

Material parameters:

$\psi_{5m,kar}$ characteristic value of ψ_{5m} [-]. ψ_{5m} is the value of the state parameter ψ averaged over a total (cumulative) thickness of 5 m of sand layers in which the state parameter is the highest (most liquefiable) and which are between the ground water level and a depth of 0,5 H_R below the channel bottom.

$d_{50,gemiddeld,kar}$ characteristic value of $d_{50,gemiddeld}$ [m]. $d_{50,gemiddeld}$ is the average value of d50 in all sand layers between the top of the channel bank and the channel bottom.

$F_{cohesivelayers}$ is a parameter expressing the influence of thin clay and peat layers (between 0.5 m and 5 m thickness) within the sand layers [-]. See table below

(0,5m < thickness of cohesive layer < 5m)	$F_{cohesivelayers}$
almost no clay of peat layers	1/3
limited number of clay of peat layers (comparable with "average" sand in Zeeland)	1
large number of clay of peat layers	3

Dynamics of the under water slope:

V_{lokaal} is a measure for the dynamics of the under water slope. This parameter is the largest value of:

– velocity of backward or forward displacement of the waterline,
– velocity of backward or forward displacement of the average under water slope
– velocity of deepening of the channel bottom multiplied with $\cot\alpha_R$.

The minimum value of V_{lokaal} is 0,001 m/year

$V_{Zeeland}$ is the average value of V_{lokaal} of the under water slopes in Zeeland, that form the basis of the equation of the probability of occurrence of flow sliding. $V_{Zeeland}$ = 1 m/year

Step 2 (not supported by D-FlowSlide)

The probabilities of occurrence per subsurface scenario are combined with:

$$P(ZV) = \sum_i P(ZV|S_i)P(S_i) \tag{5}$$

in which $P(S_i)$ is the probability of occurrence of a subsurface scenario S_i. Furthermore: $\sum_i P(S_i) = 1$.

Step 3

The method to predict the retrogression length of a flow slide is based on analysis of the pre- and post failure geometries of a large number of flow slides in Zeeland. The figure below gives the variables that D-FlowSlide uses to calculate the retrogression length.

In top-view most flow slides show a hourglass shape: a shelf-shaped scar around the erosion area, a narrow flow channel and a wide, cone-shaped sedimentation area. If schematized in 2D cross section through the centerline of the flow slide the surface area of part in which soil is removed (Area 1 in figure below) is in average approximately 1.4 times larger than the deposition area (Area 2). Generally the resulting profile roughly consists of two parts: a very gentle lower part and a much steeper upper part, see figure below.

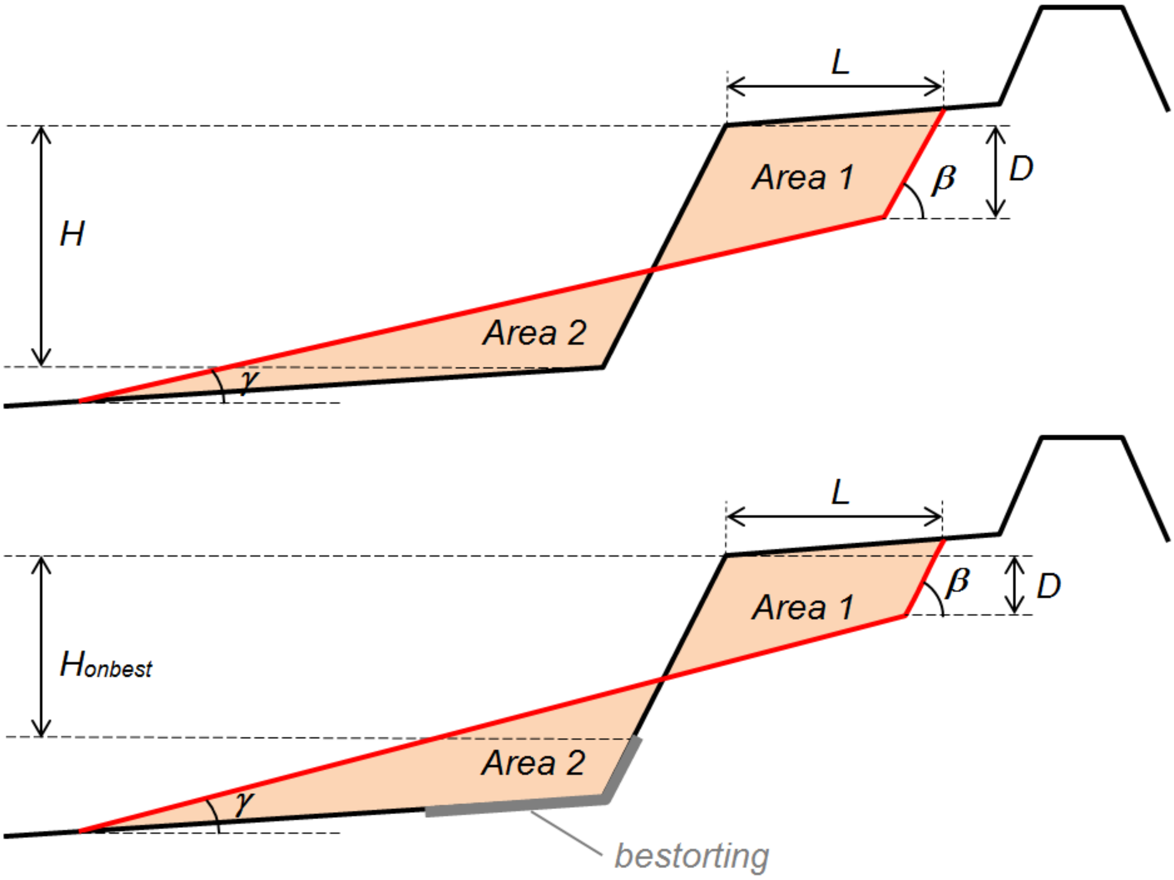

Figuur: Inscharingslengte (L) na zettingsvloeiing

The variables in the figure above are uncertain. Based on statistical analysis of ca 140 flow slides in Zeeland for each variable the expected values, standard deviation and distribution type were derived, see table below.

The standard deviation of parameters c en cotan(a) are not based on observations and were estimated.

				Underlying normal distribution	
X	**E(*X*)**	**σ(*X*)**	**Type of distribution**	**μ(*X*)**	**σ(*X*)**
cotan(γ)	16,8	7,1	Lognormal	2,82	0,38
cotan(β)	2,9	1,7	Lognormal	1,05	0,47
D/H	0,43	0,06	Normal		
c	1,4	0,1	Normal		
cotan(α)		0,05·μ(X)	Normal		

Conversion of expected value and standard deviation from average and stand deviation of the underlying normal distribution: $E(X)=\exp\left(\mu(X)\right)$ *en*

$$\sigma(X)=\exp(\mu(X)+\sigma(X))-\exp(\mu(X))$$

To determine the probability that the retrogression length L is larger than the maximum allowable retrogression length $L_{toelaatbaar}$ the following reliability function (z-function) should be solved:

$$Z=L_{toelaatbaar}-L \tag{6}$$

In D-FlowSlide the equation is solved using a FORM analysis. The probabilistic parameters are D/H, c, cotan γ and cotan β. The balance between c.Area 1 and Area 2 is solved numerically. This means that in case of a narrow channel, the retrogression length will smaller compared with a wide channel.

Note: During the different steps of the FORM analysis, the values of the four probabilistic parameters (D/H, c, cotan γ and cotan β) can lead to a damage profile outside the geometry limits. That's why the program extrapolates the geometry at both left and right sides by extending the surface line with an horizontal line (length is 1000 m) starting at the point situated at geometry limit as illustrated in figure below.

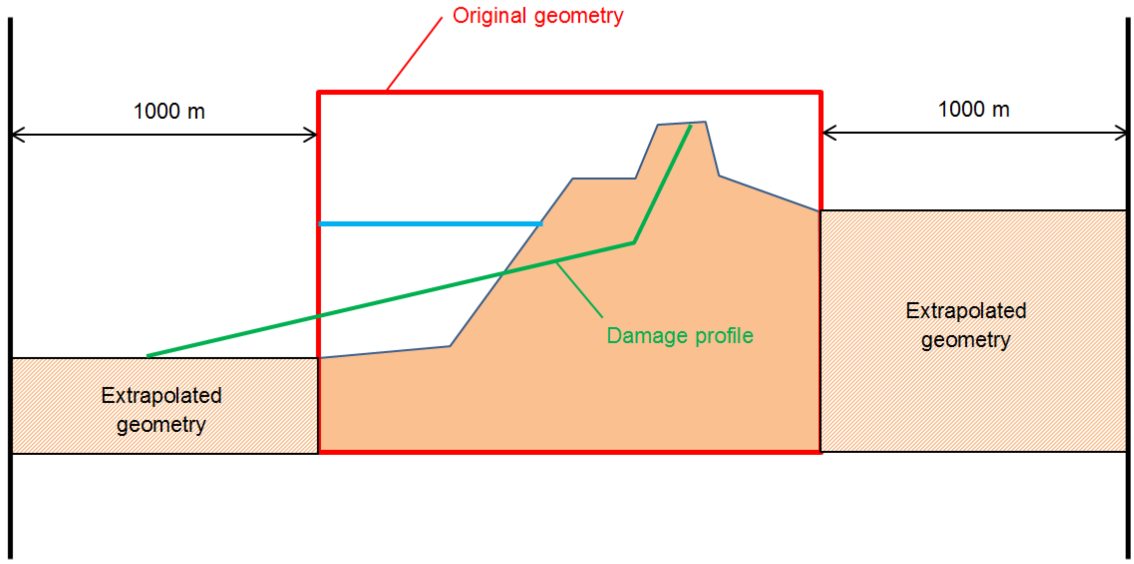
Original geometry
1000 m
1000 m
Extrapolated geometry
Damage profile
Extrapolated geometry

12. APPENDIX 4

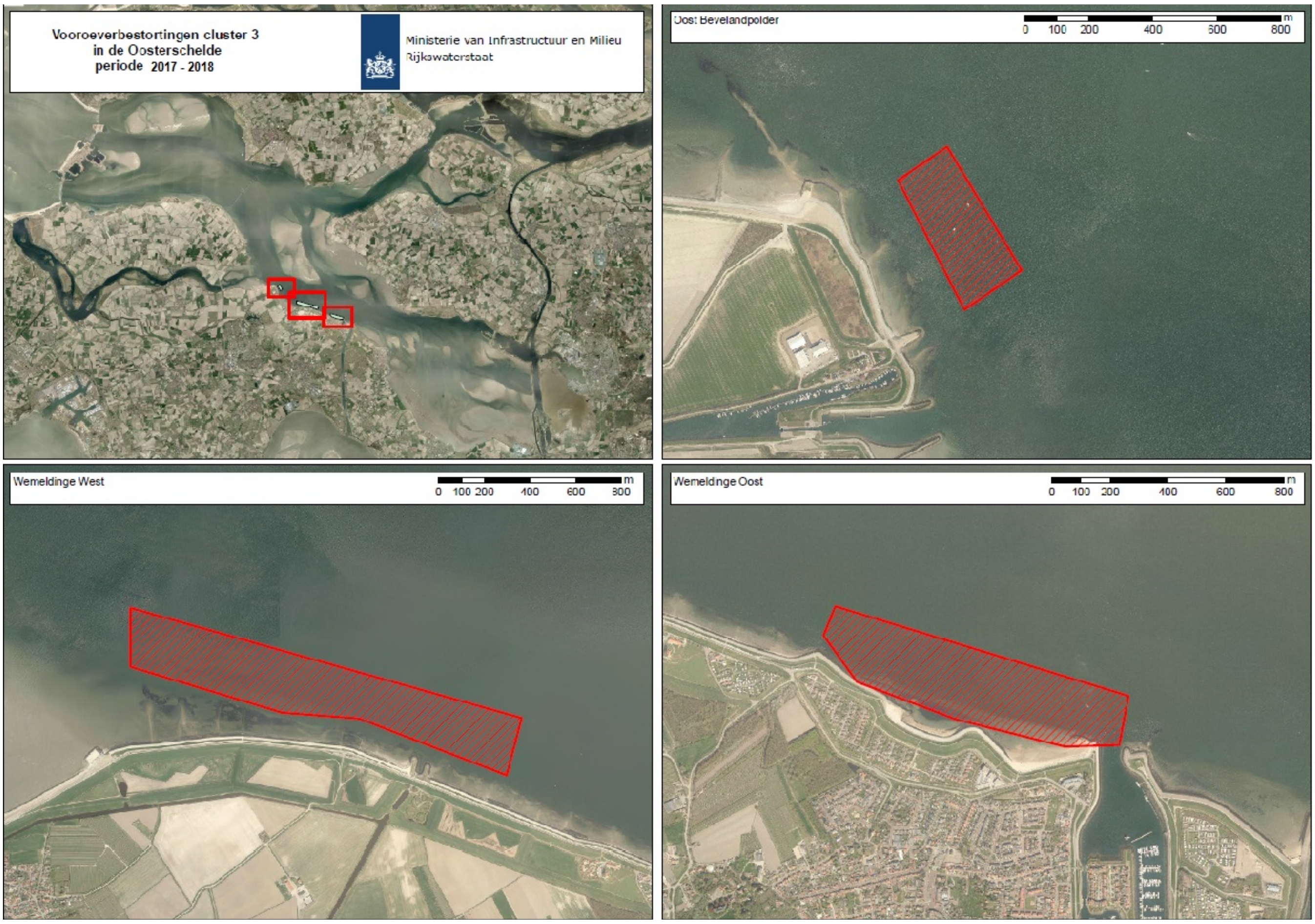

Overview revetment presence within the Eastern Scheldt

13. APPENDIX 5

Section 3.5 from Waterkeringenbeheerplan 2016-2017, Scheldestromen; Waterboard Zeeland area.

3.5 Eigen beleid en regelgeving

3.5.1 Uitgangspunten

Een van de hoofdtaken van het waterschap is het handhaven van zijn waterkeringen en van de waterveiligheid in zijn beheergebied voor nu en in de toekomst. Daarnaast heeft het waterschap de uitgangspunten om economische en recreatie belangen toe te staan als het niet in strijd is met de hoofdtaak. Om ervoor te zorgen dat de hoofdtaak gewaarborgd blijft, heeft waterschap Scheldestromen beleid en regelgeving wat bindend is voor het waterschap zelf maar ook voor anderen die in aanraking komen met de waterstaatswerken.
De volgende paragrafen beschrijven in hoofdlijnen de belangrijkste kaders waarin het waterschap als beheerder functioneert.

3.5.2 Beheersinstrumenten

Om de zorg op de waterkeringen uit te kunnen oefenen heeft het waterschap een aantal beheersinstrumenten. Hieronder zijn deze instrumenten kort toegelicht. Alle beheersinstrumenten zijn online te raadplegen, via de digitale balie van het waterschap, www.scheldestromen.nl/digitale_balie.

Keur

In de Keur zijn de geboden en verboden gesteld voor de activiteiten in, op en aan waterkeringen. Voor bepaalde werkzaamheden is in de keurzones een watervergunning vereist. In Bijlage IV: *Kaart Keurzones* staat de kaart met Keurzones. Het dagelijks bestuur is bevoegd die vergunning te verlenen. De belangrijkste functie van de zones is om het waterkerend vermogen van de waterkering te waarborgen en om ruimte te reserveren voor toekomstige dijk- en duinversterking.

Daarnaast reguleert de Keur activiteiten die een negatieve invloed hebben op de stabiliteit en sterkte van de waterkering. Hierin is niet alleen de waterkering meegenomen maar ook een beschermingszone voor de huidige waterkering en de waterkering over 200 jaar.
Figuur 3-3 laat de zone-indeling zien voor de primaire waterkering. Voor de regionale waterkering is de breedte van de beschermingszone A en B samen 50m.

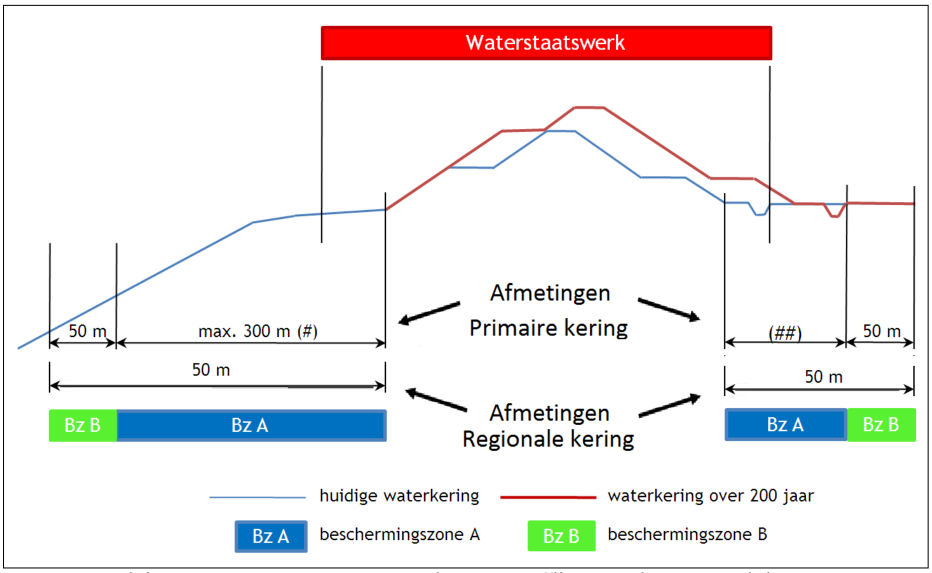

Figuur 3-3: Indeling zones voor primaire waterkeringen geïllustreerd voor een dijk

***De bepaling van de breedte van de diverse waterkeringszones is als volgt*:**

Waterstaatswerk	• Omvat de feitelijke waterkering (zoals vastgelegd in de legger); • Bij een dijk is dat het dijklichaam (de kunstmatige verhoging boven het maaiveld) inclusief de kreukelberm en de kwelsloot. Bij het ontbreken van een kwelsloot behoort een strook van 10 m landwaarts tot het waterstaatswerk. Bij inlagen behoort zowel de inlaag zelf als de inlaagdijk tot het waterstaatswerk; • Bij een duin is dit de strook van het duin dat inclusief de verwachte afslag bij de maatgevende storm als zeewering dient te worden aangemerkt. Ook hoofden, nollen en paalrijen kunnen afhankelijk van hun belang in relatie tot het waterkerend vermogen van het waterstaatswerk, behoren tot het waterstaatswerk.
Beschermingszone A	• Wordt aan beide zijden van het waterstaatswerk aangewezen; • Breedte wordt bepaald aan de hand van een aantal criteria. De beschermingszone omvat in ieder geval die gronden die technisch/fysisch (mede) een bijdrage leveren aan de stabiliteit van de waterkering, waaronder de bestortingen. Daarbij geldt echter aan de landwaartse zijde als minimum dat gronden die voor toekomstige dijkverzwaring nodig zijn (het profiel van vrije ruimte of reserveringsstroken) in ieder geval binnen de beschermingszone vallen. • (#) de maximale afstand bedraagt 300 m rekening houdend met het volgende criterium: wanneer het diepste punt van een vaargeul binnen deze afstand ligt, zal de grens van de beschermingszone A daar worden aangehouden (zie ook Nota begrenzingen). • (##) Voor de bepaling van de breedtes van de beschermingszone A wordt rekening gehouden met de stabiliteit (4x kerende hoogte tussen maaiveld en kruin) en de pipinglengte (18-25x de kerende hoogte).
Beschermingszone B	• Wordt aan beide zijden van de beschermingszone A aangewezen; • Dit betreft een erosie- c.q. invloedszone met een breedte van 50 m.

Noot: Bij regionale waterkeringen is de breedte van beschermingszone A en B samen 50 m.

Legger

De ligging van de primaire waterkeringen is vastgelegd in de legger van het waterschap (artikel 5.1 van de Waterwet). In de Waterverordening zijn de specificaties voor het stelsel van regionale keringen in de legger vastgelegd. De legger omvat naast de primaire en regionale waterkeringen, ook de ondersteunende kunstwerken. In de legger is omschreven de gewenste staat of de vereiste toestand van de waterstaatswerken. Deze toestand is vastgelegd naar richting, vorm, afmetingen en constructieve normen. De waterstaatswerken en beschermingszones zijn ook op kaart vastgelegd.

In de periode 2018-2023, is het mogelijk dat de legger aangepast en geüpdatet moet worden. Bij het toetsen van de nieuwe normering kunnen bijvoorbeeld door een strengere norm of door nieuwe inzichten voor een dijktraject, de beschermingszones aangepast worden.
Daarnaast moet de legger voor een aantal plekken gedetailleerd uitgewerkt worden. Op een aantal plekken is gebleken dat de legger niet consequent is uitgewerkt. Een voorbeeld hiervan is het havenplateau in Vlissingen, die niet binnen het waterstaatswerk valt.
Ook zullen een aantal versterkingswerken opgeleverd worden in de komende jaren. Hier behoort de legger ook aangepast te worden.

In het kader van de overstromingsrisico benadering, wil het waterschap ook de legger van de omringende en inliggende beheerders meenemen.

Beheerregister
Een belangrijke randvoorwaarde voor een goed functionerende beheerorganisatie is de vastlegging en (mogelijkheid tot) ontsluiting van de geografische en administratieve gegevens van de waterkeringen. In het beheerregister zijn zowel de actuele afmetingen en toestand, als de constructieve gegevens van de waterkeringen vastgelegd. Deze gegevens zijn in een digitale database OEI (voorheen IRIS) opgeslagen. De gegevens van de vooroever worden beheerd en opgeslagen in een aparte (Oracle) database (Zeekoe). Door de uitvoering van het project Zeeweringen en de dijkversterkingswerken (Zwakke Schakels/ HWBP2) zijn eind 2015 van nagenoeg alle dijkvakken de noodzakelijke gegevens bekend en beschikbaar. Voor de kunstwerken wordt nog een inhaalslag gemaakt om ook deze gegevens volledig en op orde te krijgen. Hieronder vallen sluizen en gemalen maar ook de locaties van de afsluiters in de waterstaatswerken in eigendom van derden en de locaties van de drainages. Daarnaast is er ook een inhaalslag te maken in het register met gebruikers en pachters.

Naast constructieve gegevens zijn binnen de GIS-omgeving aanvullende geografisch georiënteerde data opvraagbaar waarmee snelle en doeltreffende analyses uitgevoerd kunnen worden. Door beter gebruik en slim combineren van gegevens zal de beheertaak van het waterschap de komende jaren geoptimaliseerd worden.

Nota Vergunningenbeleid waterkeringen
In de Nota Vergunningenbeleid waterkeringen zijn de regels aangegeven voor het medegebruik van de ruimte in, op en om de waterkeringen in beheer bij waterschap Scheldestromen. De nota vormt het toetsingskader voor de vergunningenverlening.

Wijzigingen in het beleid van Rijk en provincie Zeeland zullen doorwerken in het vergunningenbeleid van het waterschap. Actueel is het bouwbeleid in de kustzone, waar een nationaal Kustpact eind van de zomer 2016 inzicht moet geven in hoe de toekomst ontwikkeling van de ksut eruit gaat zien. Als daar aanleiding voor is, zal de Nota Vergunningenbeleid in 2016 geheel of gedeeltelijk worden herzien.

Nota Beleid toezicht en handhaving
Toezicht en handhaving van de keur en op de verleende vergunningen is vastgelegd in de nota Beleid toezicht en handhaving. Het toezicht valt onder de verantwoordelijkheid van de opzichters. Zij melden overtredingen van de Keur of vergunningsvoorschriften aan het team Handhaving.

3.5.3 Zorgplicht
Het waterschap heeft de wettelijke taak om de primaire waterkeringen aan de veiligheidseisen te laten voldoen en voor het noodzakelijke preventieve beheer en onderhoud te zorgen. Dit valt

onder de zorgplicht. Naast het Waterkeringenbeheerplan, zal het waterschap de zorgplicht op waterkeringen uitwerken in het inspectieplan, de onderhoudsplannen en de draaiboeken. Met de controle en toezicht door de Inspectie Leefomgeving en Transport (ILT) op de implementatie van de zorgplicht van de primaire waterkeringen, zal de werkwijze veranderen.

In Bijlage VIII: *Kaderzorgplicht* staan de activiteiten en de producten waaraan de ILT het waterschap controleert en toetst. De ILT wil inzicht in de organisatie, het systeem, de processen, de kwaliteitseisen aan de medewerkers, etc. Daarnaast zal het waterschap een continu inzicht moeten hebben in de feitelijke toestand van de waterkering. Deze veranderingen in de zorgplicht zijn te lezen in paragraaf 5.4.

Een aantal plannen die benodigd zijn om te voldoen aan de zorgplicht, zijn al uitgewerkt. Met de implementatie van de methode van de ILT kunnen deze plannen gewijzigd worden. Hieronder zijn de huidige plannen van het waterschap kort toegelicht.

Inspectieplannen waterkeringen
In het Inspectieplan Waterkeringen 2015 staan de uitvoering en de inrichting van de inspecties voor de primaire en regionale waterkeringen en de kunstwerken beschreven. Het plan beschrijft het type inspecties en de uitvoeringsfrequentie. Daarnaast benoemt het de verbeter- en ontwikkelingspunten. Het inspectieplan zal in het kader van ILT geactualiseerd worden om de Plan-Do-Check-Act (PDCA) cyclus in te voeren.

Daarnaast zet het waterschap zich in voor de bestrijding van muskusratten. Muskusratten graven in de waterkeringen, waardoor de waterveiligheid in gevaar kan komen. Omdat niet alleen muskusratten een bedreiging vormen voor de waterkeringen maar ook andere dieren (mollen, vossen, konijnen) zal een bestrijdingsplan voor andere soorten dan muskus- en beverratten worden opgesteld.

Onderhoudsplannen
In 2014 heeft het ILT de pilot-controle op *Onderhoud van de primaire waterkeringen* bij waterschap Scheldestromen uitgevoerd. Er zijn drie aanbevelingen waar het waterschap komende periode mee aan de slag gaat: werken met onderhoudsbeheersysteem, opstellen onderhoudsplan en bijbehorende meerjarenplanning. Daarom zal het waterschap een plan van aanpak opstellen voor het onderhoud voor primaire waterkeringen en kunstwerken. In de periode 2016-2020 zullen deze onderhoudsplannen uitgewerkt en uitgevoerd worden.

Draaiboeken voor calamiteiten
In het geval van calamiteiten maakt het waterschap gebruik van twee draaiboeken. Het eerste draaiboek is het Draaiboek Dijkbewaking voor het bewaken van de primaire en regionale keringen tijdens zware stormvloeden. Het tweede draaiboek is het Draaiboek Schadevaring voor het handelen bij schade aan een beheerde waterkering veroorzaakt door een vaartuig. In beiden staan de dreigende situaties, de werkwijze en de stappen die doorlopen moeten worden. Daarnaast zijn de verantwoordelijken aangewezen en hun bevoegdheden vastgelegd. Beide draaiboeken vormen een onderdeel van het calamiteitenplan.

In 2016 zullen deze twee draaiboeken vervangen worden door het Deelplan Waterkering, als onderdeel van het nieuwe Crisisplan Waterschap. Hierin zal ook invulling gegeven worden aan het concept van netcentrisch werken.

14. APPENDIX 6

With the bathymetry and altimetry data of the Eastern Scheldt the following data points were found using ArcMap for the locations Krabbendijke, Dortsman- Zuid and Krabbenkreek for the different surface lines :

Table 13: Data points for different geometry scenario's for location Krabbendijke generating different surface lines within the D-Flow Slide program. Both x and z values are in meters.

Krabbendijke geometry saltmarsh	Scen A		Scen B		Scen C	
	l	z	l	z	l	z
bottom river channel	5	-10.75	5	-10.75	5	-10.75
Insert river channel	300	-1.02	300	-1.02	300	-1.02
dike toe at river	4125	2.3	2325	2.3	525	2.3
dike top at river	4265	6.401	2465	6.401	665	6.401
dike top at polder	4270	6.856	2470	6.856	670	6.856
Krabbendijke geometry mudflat	Scen A		Scen B		Scen C	
	l	z	l	z	l	z
bottom river channel	5	-10.75	5	-10.75	5	-10.75
Insert river channel	300	-1.02	300	-1.02	300	-1.02
dike toe at river	4125	1.02	2125	1.02	301	1.02
dike top at river	4265	6.401	2265	6.401	441	6.401
dike top at polder	4270	6.856	2270	6.856	446	6.856

Table 14: Data points for different geometry scenario's for location Dortsman-Zuid generating different surface lines within the D-Flow Slide program. Both x and z values are in meters.

Dortsman-zuid geometry saltmarsh	Scen A		Scen B		Scen C	
	l	z	l	z	l	z
bottom river channel	5	-15.47	5	-15.47	5	-15.47
Insert river channel	350	-3.11	350	-3.11	350	-3.11
dike toe at river	3592	2.07	1992	2.07	392	2.07
dike top at river	3654	6.5	2054	6.5	454	6.5
dike top at polder	3659.4	6.75	2059.4	6.75	459.4	6.75
Dortsman-zuid geometry mudflat	Scen A		Scen B		Scen C	
	l	z	l	z	l	z
bottom river channel	5	-15.47	5	-15.47	5	-15.47
Insert river channel	350	-3.11	350	-3.11	350	-3.11
dike toe at river	3592	1.5	1842	1.5	351	1.5
dike top at river	3654	6.5	1904	6.5	413	6.5
dike top at polder	3659.4	6.75	1909.4	6.75	418.4	6.75

Table 15: Data points for different geometry scenario's for location Krabbenkreek generating different surface lines within the D-Flow Slide program. Both x and z values are in meters.

Krabbenkreek- oost geometry saltmarsh	Scen A		Scen B		Scen C	
	l	z	l	z	l	z
bottom river channel	5	-6.14	5	-6.14	5	-6.14
Insert river channel	238	-0.33	238	-0.33	238	-0.33
dike toe at river	1445	1.76	1045	1.76	645	1.76
dike top at river	1482	5.44	1082	5.44	682	5.44
dike top at polder	1487	5.69	1087	5.69	687	5.69
Krabbenkreek- oost geometry mudflat	Scen A		Scen B		Scen C	
	l	z	l	z	l	z
bottom river channel	5	-6.14	5	-6.14	5	-6.14
Insert river channel	238	-0.33	238	-0.33	238	-0.33
dike toe at river	1445	0.64	845	0.64	245	0.64
dike top at river	1482	5.44	882	5.44	282	5.44
dike top at polder	1487	5.69	887	5.69	287	5.69

15. APPENDIX 7

Borehole description Krabbendijke

Borehole: 601890001 Names: FvG Year: 6018 Group: 90 Date: 16-1-2018

Coordinates		Elevation	Depth	MAP LEGEND CODE		
XCO	YCO	Z [m]	[cm]	Geomorphogenetical map:	SM	
68737	383154	0	470	Geological map:	Groundwaterstep:	
				Vegetation-map:	Soil map:	

Borehole on saltmarsh (SM) Krabbendijke, southeast of Yerseke, Zeeland.
tidal sequenced deposits. Silty clay deposits with sand bands alternated

Depth	Texture	Org	Plr	Color	Redox	Gravel	M50	Ca	Fe	GW	M	LKL	Strat	Remarks
10	SiC		plr	dbrgr	o				0				WDk	#
20	SiC		plr	dbrgr	o				0	GHG			WDk	
30	SiC		plr	dbrgr	or				0				WDk	piece of wood
40	SiC		plr	dbrgr	or				0				WDk	
50	SiC		plr	dbrgr	r				0	GLG			WDk	
60	SiC			dgr	r				0				WDk	
70	SiC			dgr	r				0				WDk	
80	SiC		plr	dgr	r				0				WDk	little shell rest
90	SiC		plr	dgr	r				0				WDk	sigular reed
100	SiC		plr	dgr	r				0				WDk	shell band/ singular reed
110	SiCL			dgr	r				0				WDk	shell band
120	SiCL			dgr	r				0				WDk	
130	SiCL		plr	dgr	r				0				WDk	
140	SCL		plr	dgr	r				0				WDk	=2, EP1, shell band
150	SCL			dgr	r				0				WDk	=2, EP1
160	SL		plr	dgr	r				0				WDk	=2, EP1, vf
170	SL		plr	dgr	r				0				WDk	=2, EP1, vf
180	SL			dgr	r				0				WDk	=2, EP1,vf,half bivalve
190	SiCL			dgr	r				0				WDk	EP1
200	SiCL			dgr	r				0				WDk	EP1
210	SL			dgr	r				0				WDk	=1, EP1, vf
220	LS			dgr	r				0				WDk	=1, EP1, vf
230	LS			dgr	r				0				WDk	=1, EP1, vf
240	LS			dgr	r				0				WDk	=1, EP1, vf
250	LS			dgr	r				0				WDk	=1, EP1, very fine,org band,#
260	LS			dgr	r		150-210		0				WDk	f, $
270	fS			dgr	r		150-210		0				WDk	
280	fS			dgr	r		150-210		0				WDk	shell band
290	mS			dgr	r		210-300		0				WDk	shell grit, half bivalve
300	mS			dgr	r		210-300		0				WDk	
310	mS			dgr	r		210-300		0				WDk	
320	mS			dgr	r		210-300		0				WDk	
330	mS			dgr	r		210-300		0				WDk	
340	mS			dgr	r		210-300		0				WDk	
350	mS			dgr	r		210-300		0				WDk	$
360	mS			dgr	r		210-300		0				WDk	$ new hole 60cm from first hol
370	LS			dgr	r		210-300		0				WDk	fine
380	LS			dgr	r				0				WDk	fine
390	LS	M0		dgr	r				0				WDk	fine
400	LS	M0		dgr	r				0				WDk	very fine
410	LS			dgr	r				0				WDk	$
420	SiCL			dgr	r				0				WDk	#
430	SiC	M0		dgr	r				0				WDk	
440	SiC	M1		dgr	r				0				WDk	
450	SiC			dgr	r				0				WDk	
460		PM		dbrgr	r				0				Vo	
470		P		dbrbk	r				0				Vo	END, #

End of borehole: 601890001

Borehole description Dortsman-Zuid

Borehole: 601890002	Names: FvG	Year: 6018	Group: 90	Date: 10-1-2018

Coordinates		Elevation	Depth	MAP LEGEND CODE	Geomorphogenetical map:	SM
XCO	YCO	Z [m]	[cm]	Geological map:	Groundwaterstep:	
60811	398204	1.11	490	Vegetation-map:	Soil map:	

drillhole on saltmarsh of Dortsman South, northwest of Yerseke, Zeeland.
tidal sequenced deposits alternated with peat from the Nieuwkoop formation.

Depth	Texture	Org	Plr	Color	Redox	Gravel	M50	Ca	Fe	GW	M	LKL	Strat	Remarks
10	SiC		plr	br	o				0				WDk	grasrests, #
20	SiC		plr	br	o				0				WDk	grasrests
30	SiC		plr	gr	or				1	GHG			WDk	grasrests
40	SiC	M0	plr	gr	or				1				WDk	grasrests
50	SiC		plr	gr	or				1	GLG			WDk	grasrests
60	SiC	M0	plr	gr	r				0				WDk	grasrests
70	SiC	M0	plr	gr	r				0				WDk	grasrests, shell rests
80	SiC	M0	plr	gr	r				0				WDk	grasrests, shell rests
90	SiC		plr	gr	r				0				WDk	grasrests
100	SiC		plr	gr	r				0				WDk	grasrests
110	SiCL		plr	gr	r				0				WDk	#, $
120	SiCL			gr	r				0				WDk	
130	SL			gr	r				0				WDk	f
140	SL	M0		gr	r				0				WDk	f
150	SL			gr	r				0				WDk	f
160	SL			gr	r				0				WDk	f, shell grit
170	fS			gr	r		150-210		0				WDk	f
180	LS			gr	r		105-150		0				WDk	f
190	LS			gr	r		105-150		0				WDk	f
200	LS			gr	r		105-150		0				WDk	f, shell band 1-2 cm
210	LS			gr	r		105-150		0				WDk	f, $
220	LS			gr	r		105-150		0				WDk	#, fine shell band
230		M	w	brgr	r				0				Vo	
240		M	w	brgr	r				0				Vo	
250		PM	w	brgr	r				0				Vo	
260		PM	w	brgr	r				0				Vo	
270		M	w	brgr	r				0				Vo	
280		PM	w	brgr	r				0				Vo	
290		PM	w	brgr	r				0				Vo	
300		PM	w	brgr	r				0				Vo	
310		PM	w	brgr	r				0				Vo	
320	SL	M1	w	brgr	r				0				Vo	
330	SL			gr	r				0				WCk	=1, EP1
340	SL			gr	r				0				WCk	=1, EP1
350	SL			gr	r				0				WCk	=1, EP1
360	SL			gr	r				0				WCk	
370	SL			gr	r				0				WCk	
380	SL			gr	r				0				WCk	
390	SL			gr	r				0				WCk	
400	LS			gr	r		75-105		0				WCk	f
410	LS			gr	r		75-105		0				WCk	f
420	LS			gr	r		75-105		0				WCk	f
430		P		gr	r				0				Vo	f, woodreed
440		P		dbr	r				0				Vo	f
450		P		dbr	r				0				Vo	f
460	LS	M2	plr	ywgr	r		75-105		0				Vo	f, woodrest & roots
470	LS	M2	plr	ywgr	r		75-105		0				Vo	f, color is yellow/orange
480	LS	M2	plr	ywgr	r		75-105		0				Vo	f
490	LS	M2	plr	ywgr	r		75-105		0				Vo	f

End of borehole: 601890002

Borehole description Krabbenkreek

Borehole: 601890004	Names: FvG	Year: 6018	Group: 90	Date: 9-1-2018

Coordinates		Elevation	Depth	MAP LEGEND CODE	Geomorphogenetical map:	SM
XCO	YCO	Z [m]	[cm]	Geological map:	Groundwaterstep:	
68712	402024	0	480	Vegetation-map:	Soil map:	

drillhole at SM of Krabbenkreek, northeast of Yerseke, Zeeland
Sandy and loamy sequence without peat alternations of the Nieuwkoop Formation.
Fining upwards, clear channel deposits with saltmarsh depostis on top.

Depth	Texture	Org	Plr	Color	Redox	Gravel	M50	Ca	Fe	GW	M	LKL	Strat	Remarks
10	SiC		plr	br	o				0					#, toplayer, reed
20	SiC		plr	br	o				0					reed
30	SiC		plr	br	or				1	GHG				reed
40	SiC		plr	br	or				1					reed
50	SiC		plr	drdgr	or				1				WDk	reed
60	SiCL		plr	drdgr	or				1	GLG			WDk	reed
70	SiCL		plr	drdgr	r				0				WDk	reed
80	SL		plr	drdgr	r		50-105		0				WDk	=1, EP1 /1 vf, reed
90	SL		plr	dgr	r		50-105		0				WDk	=1, EP1 vf, reed
100	SL		plr	dgr	r		50-105		0				WDk	=1, EP1 vf
110	SL		plr	dgr	r		75-150		0				WDk	=1, EP1 vf
120	SL		plr	dgr	r		75-150		0				WDk	=1, EP1 f
130	SL		plr	dgr	r		75-150		0				WDk	=1 =2 EP1 f
140	SL		h	dgr	r		75-150		0				WDk	=1 =2 EP1 f
150	SL		h	dgr	r		75-150		0				WDk	=1 =2 EP1 f
160	fS		plr	dgr	r		105-210		0				WDk	=1, EP1 f
170	fS		plr	dgr	r		105-210		0				WDk	=1, EP1 f
180	fS		plr	dgr	r		105-210		0				WDk	=1, EP1 f
190	fS		plr	dgr	r		105-210		0				WDk	=1, EP1 f
200	fS		plr	dgr	r		105-210		0				WDk	=1, EP1 f
210	fS			dgr	r		150-300		0				WDb	=1, EP1 f
220	SL			dgr	r		150-300		0				WDb	=1, EP1 f, #
230	SL			dgr	r		210-300		0				WDb	=1, EP1 f, $
240	SL			gr	r		210-300		0				WDb	f, /4
250	mS			gr	r		210-300		0				WDb	f,whole mussel 6 mm
260	mS			gr	r		210-300		0				WDb	
270	mS			gr	r		210-300		0				WDb	
280	mS			gr	r		210-300		0				WDb	
290	mS			gr	r		210-300		0				WDb	
300	mS			gr	r		210-300		0				WDb	half bivalve 5 mm
310	mS			gr	r		210-300		0				WDb	
320	mS			gr	r		210-300		0				WDb	
330	mS			gr	r		210-300		0				WDb	half bivalve 5 mm
340	fS	M2		gr	r		150-210		0				WDk	org. band +shel rest
350	fS	M2		gr	r		150-210		0				WDk	
360	fS			gr	r		150-210		0				WDk	
370	fS			gr	r		150-210		0				WDk	
380	fS			gr	r		150-210		0				WDk	
390	fS			gr	r		150-210		0				WDk	
400	fS			gr	r		150-210		0				WDk	
410	fS			gr	r		150-210		0				WDk	
420	fS			gr	r		150-210		0				WDk	
430	fS			gr	r		150-210		0				WDk	shell rest
440	fS			gr	r		150-210		0				WDk	
450	fS			gr	r		150-210		0				WDk	half bivalve
460	fS			gr	r		150-210		0				WDk	
470	fS			gr	r		150-210		0				WDk	
480	fS			gr	r		150-210		0				WDk	$

End of borehole: 601890004